# Simultaneous recording of EEG and fMRI: New approach to remove gradient and ballistocardiogram EEG-artifacts

## Dissertation

zur Erlangung des akademischen Grades

**Doktoringenieur**

**(Dr. -Ing.)**

von **Limin Sun**

geb. am 16. April 1973 in Jinzhou, Liaoning, China

genehmigt durch die Fakultät für Elektrotechnik und Informationstechnik
der Otto-von-Guericke-Universität Magdeburg

Gutachter:

Prof. Dr.-Ing. Hermann Hinrichs

Prof. Dr.-Ing. habil. Bernd Michaelis

Prof. Dr. rer. nat. habil. Herbert Witte

Promotionskolloquium am 21. Oktober 2009

# Dedications

This dissertation is dedicated to my family— my parents, my wife, and my daughter. It is impossible to finish it without their supports.

To my mother, Yan Mu, and my father, Dezhong Sun, who give me a wonderful open and help me to build the model of life. Especially, mom always encouraged me to finish this dissertation and help me release the heavy burden of life.

To my wife, Chunling Dong, who is my strength and the purpose of life.

To my daughter, Yijin who brings more fun every day.

# Acknowledgments

This thesis was completed during my work as a doctoral student. However, the credit of this work belongs to not only me but also many other people involved in making it possible.

First of all, I would like to extend my heartfelt gratitude to my perfect advisor, Prof. Dr. -Ing. Hermann Hinrichs for his encouragement and ongoing kind support. I am also greatly indebted for his taking much effort and patience in mentoring me to become a qualified researcher from the method researching to the paper writing. It is indeed his insight and wide knowledge to guide me to finish the works of this thesis.

I sincerely thank Prof. Dr. -Ing. habil. Bernd Michaelis for being the referee and for his important suggestions regarding my thesis.

I am indebted to Prof. Dr. med. Hans Jochen Heinze who is the head of the Clinic of Neurology at the Otto-von-Guericke-University Magdeburg for giving me this chance.

I thank all colleagues in the center of Advanced Imaging who educated me in the technique of magnetic resonance imaging and in operating the MR scanner. Special thanks to Dr. rer. nat. Claus Tempelmann for his support regarding imaging questions.

Special thanks also to Dr. Jochem Rieger who taught me EEG and ERP recording.

Finally, I am grateful to our university library for providing all the articles and books needed for this thesis.

# List of figures

Fig.1.1 EEG recorded outside scanner. ..... 2
Fig.1.2 Scanner and structure MRI ..... 4
Fig.1.3 EPI and functional MRI ..... 5
Fig.1.4 Schematic diagram of artifacts superimposition over EEG. ..... 6
Fig.1.5 EEG-artifacts occurring in an MR environment. ..... 7

Fig.3.1 Schematic diagram of template subtraction ..... 12
Fig.3.2 Two artifact examples with different artifact sampling "phases" ..... 13
Fig.3.3 Schematic diagram of BSS-based BCG removal ..... 19

Fig.4.1 EPI sequence and gradient artifact. ..... 23
Fig.4.2 Watermelon in the scanner serving as a phantom. ..... 24
Fig.4.3 Example of a typical ERP[1] ..... 27

Fig.5.1 Long term fluctuation of artifact observed in the phantom (watermelon) recordings (position 1). ..... 28
Fig.5.2 Test of slice-specific averaged template conducted with the data recorded with the phantom (watermelon, position 1, electrode Cz) ..... 30
Fig.5.3 Artifact waveform as recorded in the phantom (watermelon) recordings in four different positions. ..... 31
Fig.5.4 Tracking data with different methods: ..... 32
Fig.5.5 The real case of applying eye-tracker during fMRI scanning. ..... 33
Fig.5.6 Vector representation of true EEG and artifact contaminated EEG (X): ..... 34
Fig.5.7 Estimation the number *N* used for averaging: ..... 35
Fig.5.8 Evaluation of different weighting profiles. ..... 37
Fig.5.9 Schematic diagram of MAS(old) and MAMAS(new) GAR removal methods ..... 39
Fig.5.10 Adjustment of the gradient artifact onsets with respect to the MRI triggers. ..... 40
Fig.5.11 Coordinate systems of the MRI device and of SPM. ..... 42
Fig.5.12 Examples of SPM-movement indicator and the selection of epochs ..... 42
Fig.5.13 Shape of the digitally simulated gradient artifact waveform. ..... 44
Fig.5.14 The relationship between st and the sampling interval dt. ..... 45
Fig.5.15 Alignment without resampling. ..... 46
Fig.5.16 Residual gradient artifacts to be removed by the special post processing algorithm. 48
Fig.5.17 Block diagram of special post processing to remove residual artifacts in case of brief movements not correctly identified by SPM. ..... 49
Fig.5.18 The schematic diagram of removing gradient artefacts. ..... 50
Fig.5.19 The frequency response of the butterworth bandstop filter applied for removing vibration artifacts ..... 51

Fig.6.1 Schematic diagram of the old BCG removal methods and the new BCG removal method (such as MNF). ..... 53
Fig.6.2 The last four MNF-independent components of four subjects. ..... 60
Fig.6.3 Schematic diagram of extracting the BCG identification signal (BIS) ..... 62
Fig.6.4 The schematic diagram of removing BCG artifacts ..... 66

Fig.7.1 Upsampling and resampling: ..... 68
Fig.7.2 MAMAS versus MAS: ..... 69

Fig.7.3 Comparison of gradient artifacts removal with MAS and MAMAS. ..... 70
Fig.7.4 Illustration of the criterion used to select ‘move’ and ‘no move’ segments: ..... 71
Fig.7.5 Classification of epochs according to type ‘move’ or ‘no move’ based on the temporal variation of the SPM related monitor data with 6 sec resolution. ..... 72
Fig.7.6 Estimation of the amount of residual gradient artifacts (MAS vs. MAMAS) at the gradient repetition rate and its harmonics for subject nc92 up to 120Hz. ..... 72
Fig.7.7 Bar diagram of cumulated spectral coefficients (RINPS-values, i.e. MAS-MAMAS/MAS ). ..... 74
Fig.7.8 Special postprocessing: ..... 75
Fig.7.9 Comparison of different processing steps (as indicated) as applied to one 6-sec-EEG-segment of subject nc92. ..... 79
Fig.7.10 The relative variance vs. number of included components. ..... 80
Fig.7.11 Correlations of the 10 components showing the largest correlation with the BIS. ..... 82
Fig.7.12 MNF- and ICA-processing of a ten-second EEG data set from subject be98. ..... 83
Fig.7.13 Correlation coefficients vs. number of independent components. ..... 84
Fig.7.14 10-second BCG contaminated EEG example (electrode O1) before processing, after application of MNF alone, subtraction alone, and combined MNF and subtraction. 85

# List of abbreviations

| | |
|---|---|
| EEG | Electroencephalogram |
| BCG | BallistoCardioGram |
| EOG | ElectroOculoGram |
| ECG | ElectroCardioGram |
| MEG | Magnetoencephalogram |
| MR | Magnetic Resonance |
| MRI | Magnetic Resonance Imaging |
| PET | Positron Emission Tomography |
| fMRI | functional Magnetic Resonance Imaging |
| BOLD | Blood Oxygenation Level Dependent |
| EPI | Echo Planar Imaging |
| IFT | Inversing Fourier Transformed |
| TR | repetition time |
| TE | echo time |
| FOV | Field of View |
| AAS | Averaged Artifact Subtraction |
| IAR | Image Artifact Reduction |
| ANC | Adaptive Noise Cancellation |
| RF | Radio Frequency |
| PCs | Principle Components |
| PCA | Principal Component Analysis |
| ICs | Independent Components |
| ICA | Independent Component Analysis |
| SSS | Stepping Stone Sampling |
| FASTR | fMRI artifact slice template removal |
| FIR | Finite Impulse Response |
| SNR | Signal to Noise Ratio |
| RLS | Recursive Least Squares |
| M-RLS | Multi-channel Recursive Least Squares |
| mGLM | moving General Linear Model |
| WT | Wavelet Transform |
| IWT | Inverse Wavelet Transform |

| | |
|---|---|
| WNNR | Wavelet-based Nonlinear Noise Reduction |
| JADE | Joint Approximate Diagonalization of Eigen-matrices |
| SPM | Statistical Parametric Mapping |
| BSS | Blind Source Separation |
| SOBI | Second Order Blind Inference |
| MNF | Maximum Noise Fraction |
| MSF | Maximum Signal Fraction |
| INPS | Improvement Normalized Power Spectrum |
| MAS | Moving Averaged Subtraction |
| MAMAS | Movement Adjusted Moving Average Subtraction |
| FID | Free Induction Decay |
| ERP | Event Related Potential |
| VEP | Visual Evoked Potential |
| LPF | Lowpass Filter |
| STD | Standard Deviation |
| LSE | Least Square Error |
| ISI | Inter-Slice Interval |
| DC | Direct Current |
| ADC | Analog-to-Digital Converter |
| LSB | Least Significant Bit |
| PCI | Peripheral Component Interconnect |
| GAR | Gradient Artifact |

# Abstract

Simultaneous recording of the electroencephalogram (EEG) and functional magnetic resonance imaging (fMRI) may reveal the brain's activity at high temporal and spatial resolution. However, the EEG recorded during fMRI scanning is corrupted by large repetitive artifacts, called gradient artifacts which are generated by the switched MR gradients. In addition, ballistocardiogram artifacts (BCG) are overlaid on the EEG resulting from heart beat related body movements and blood flow changes.

To remove the gradient artifacts, several methods have been proposed which subtract average artifact templates from the ongoing EEG. The most popular version is called 'moving average subtraction' (MAS). In the present thesis, an improvement was developed that accounts for head movements when averaging the template (this method named 'movement adjusted moving average subtraction' (MAMAS)). After having shown a strong relation between head movement and artifact waveforms the central point of this algorithm is to track the head displacements with an eye tracker hardware system or using the SPM (statistical parametric mapping) software package for cases where a dedicated eye tracker is not available. Based on the head position of the artifact to be removed, a more precise average template is achieved by averaging over only those adjacent artifacts observed at the same head position. To further reduce the residual noise the popular signal-*up*sampling is replaced by *re*sampling to synchronize the EEG samples strictly and adaptively with the fMRI timing. Finally, a new algorithm is introduced to suppress residual artifacts of brief strong movements which are not reflected by the SPM movement information due to the limited temporal resolution of the fMRI sequence. In total the new MAMAS algorithm reduces the residual artifact activity by typically 50% compared to MAS.

For removing BCG artifacts, a new algorithm named maximum noise fraction (MNF) is introduced and compared with other independent component analysis (ICA) methods. With the particular ordering feature of MNF (i.e. the decomposed components being ordered by their signal to noise ratios) most of the BCG artifacts are captured by the last or first components (depending on the direction of ordering), which is the base to simplify the complex identification of BCG related ICs. The new approach of combined MNF and a subsequent average subtraction technique automatically removes the BCG artifacts. It was evaluated to be efficient both in spontaneous EEG signals as well as in event related potentials (ERP).

*Keywords: EEG, fMRI, MAMAS, gradient artifacts, MNF, BCG artifacts*

# Zusammenfassung

Die simultane Registrierung des Elektroenzephalogramms (EEG) und der funktionellen Magnetresonanztomographie (fMRT) gestattet die Erfassung der Hirnaktivität mit hoher zeitlicher und räumlicher Auflösung. Allerdings überlagern sich als Folge der geschalteten Magnetfeldgradienten der fMRT dem EEG dabei repetitive hochamplitudige und steilflankige Störsignale (Gradientenartefakte (GAR)). Hinzu kommen ballistokardiographische Artefakte (BKG) infolge kleiner Körperbewegungen im statischen Magnetfeld des MR Tomographen.

Ein unter dem Namen *moving average subtraction* (MAS) bekannter Ansatz diente in dieser Arbeit als Ausgangspunkt für die Entwicklung eines verbesserten Verfahrens zur GAR-Unterdrückung unter dem Namen *movement adjusted moving average subtraction*(MAMAS). MAMAS beobachtet fortlaufend Kopf-Bewegungen, da sich die Form des GAR schon bei geringen Änderungen der Kopfposition massiv ändert. Eine modifizierte Augenpositionsüberwachungseinheit, alternativ – mit geringerer zeitlicher Auflösung - ein Modul des fMRT-Analyseprogramms SPM (statistical parametric mapping), dient zur Überwachung der Kopfposition, um die Extraktion von Artefakt-Templates aus dem EEG zu verbessern, indem die Mittelung nur Artefakte einschließt, die bei gleicher Kopfposition gemessen wurden. Zur weiteren Verbesserung der Artefaktunterdrückung wurde die bisher übliche massive Abtastratenerhöhung (*up*sampling) ersetzt durch eine Abtastung an optimierten Abtastzeitpunkten (*re*sampling), um die EEG-Abtastung mit dem MRT-Zeitablauf zu synchronisieren. Ein neu entwickelter Algorithmus reduziert verbleibende Artefakte, die gelegentlich bei sehr kurzen, starken und vom SPM-Monitor nicht korrekt erfassten Kopfbewegungen auftreten. Insgesamt verringert sich die verbleibende Artefaktaktivität gegenüber dem MAS-Algorithmus typisch um 50%.

Zur BKG Artefaktunterdrückung wird der ursprünglich zur Bildverarbeitung entwickelte Algorithmus *maximum noise fraction* (MNF) eingeführt und mit verschiedenen *independent component analysis*(ICA) Methoden verglichen. Dank der Eigenschaft des MNF Verfahrens, Komponenten nach ihrem Signal-Rausch-Verhältnis zu ordnen, konzentrieren sich die BKG-bezogenen Komponenten auf die ersten bzw. letzten (je nach Sortierrichtung) Komponenten, was die Entwicklung eines automatischen Verfahrens ermöglicht. In einem zweiten Schritt wird durch die Subtraktion gemittelter BKG-Templates (ähnlich MAS) die verbliebene BKG-Restaktivität weiter reduziert. Abschließend wird die Effizienz des Gesamtansatzes aus GAR- und BKG-Reduktion durch eine Spektralanalyse des EEG und zusätzlich durch ereigniskorrelierte Potentiale (ERP) überprüft.

# Contents

**Acknowledgments** ..... iii

**List of figures** ..... v

**List of abbreviations** ..... vii

**Abstract** ..... ix

**Zusammenfassung** ..... xi

**Contents** ..... xiii

**Chapter 1 Introduction** ..... 1
1.1 EEG ..... 1
1.2 MRI ..... 2
1.3 fMRI ..... 4
1.4 Simultaneous recording of EEG and fMRI ..... 5
1.4.1 Gradient artifacts and fMRI imaging ..... 8
1.4.2 Ballistocardiogram artifacts ..... 9
1.4.3 Vibration artifacts ..... 9

**Chapter 2 Aims of the present thesis** ..... 11

**Chapter 3 Review of Previous Methods to remove MRI-related EEG artifacts** ..... 12
3.1 Gradient artifacts ..... 12
3.1.1 Template Subtraction ..... 12
3.1.2 Other approaches ..... 16
3.1.3 Conclusion ..... 17
3.2 BCG artifacts ..... 18
3.2.1 Blind Source Separation (BSS) (PCA and ICA) ..... 18
3.2.2 Other approaches ..... 19
3.2.3 Conclusion ..... 21

**Chapter 4 Materials** ..... 23
4.1 fMRI scanning ..... 23
4.2 Phantom EEG-measurements ..... 24
4.3 Human EEG measurements ..... 25
4.4 Event related potentials (ERP) ..... 27

**Chapter 5 New movement adjusted algorithm to remove gradient artifacts** ..... 28
5.1 Variations of artifact shape as evaluated by phantom measurements ..... 28
5.1.1 Long term temporal instability ..... 29
5.1.2 Variability depending on MR-slice ..... 30
5.1.3 Variations due to electrode movements ..... 30
5.2 Deriving a head movements indicator ..... 31
5.2.1 SPM movement vector: low temporal resolution ..... 33
5.2.2 Video-eye-tracker: high temporal resolution ..... 33
5.3 New movement adjusted moving average subtraction (MAMAS) algorithm ..... 34
5.3.1 Basic method of weighted averaged subtraction: Is the residual EEG negligible? ..... 34
5.3.2 Comparison of different window functions ..... 36
5.3.3 Reduce the influence of head movement by introducing the moving average artifact ..... 37

5.3.4 Movement adapted moving averaged subtraction method ..... 38
5.3.4.1 Detection of gradient artifact onsets ..... 39
5.3.4.2 Position dependent artifact averaging. ..... 41
5.3.4.3 New resampling procedure to align sampling time of averaged artifact template ..... 43
5.3.4.4 Subtraction ..... 47
5.3.4.5 Postprocessing of residual artifacts occurring in case of transient brief movements ..... 48
5.4 The schematic diagram of removing gradient artifacts ..... 50
5.5 Removal of vibration artifact by bandstop filtering ..... 51

**Chapter 6 New algorithm to remove BCG artifacts** ..... 52
6.1 New algorithm based on the Maximum Noise Fraction (MNF) method ..... 52
6.1.1 Introduction of MNF ..... 52
6.1.2 Application of MNF to BCG removal ..... 59
6.1.3 Replacing the adaptive mixing matrix by a fixed matrix to reduce the computational load ..... 61
6.1.4 Separating BCG and EEG: Comparison of MNF to ICA approaches ..... 62
6.2 Additional Moving Average Subtraction algorithm to remove residual BCG activity ..... 63
6.3 INPS to evaluate removal performance ..... 65
6.4 The schematic diagram of removing BCG artifacts ..... 66

**Chapter 7 Results** ..... 67
7.1 Gradient artifacts, MAMAS-algorithm: Evaluation and Comparison with the MAS algorithm ..... 67
7.1.1 Gradient artifact resampling ..... 67
7.1.2 Head motion effect on the reduction of the gradient artifact ..... 68
7.1.3 The improved performance of using MAMAS ..... 70
7.1.4 Special post processing to reduce residual artifacts caused by brief movements ..... 74
7.1.5 Visual evaluation of the new method and comparison with previous methods ..... 76
7.2 BCG artifacts, combined MNF and subtraction algorithm: Evaluation and Comparison ..... 79
7.2.1 Selection of MNF-components to remove the BCG artifacts ..... 79
7.2.2 Comparison of MNF, fastICA and JADE: Power to discriminate BCG from EEG ..... 80
7.2.3 Reducing the computational load – Usage of a fixed mixing matrix A. ..... 83
7.2.4 Evaluation in the time and frequency domain ..... 84
7.2.4.1 Spectral evaluation at the ECG base frequency and its harmonics ..... 84
7.2.4.2 Evaluation in the time domain ..... 85
7.2.4.3 Total spectrum ..... 86
7.2.5 Evaluation with the ERPs ..... 87

**Chapter 8 Discussion** ..... 89
8.1 Gradient artifacts ..... 89
8.2 Vibration artifacts ..... 95
8.3 BCG artifacts ..... 95

**Chapter 9 Summary** ..... 98

**Bibliography** ..... 100

# Chapter 1 Introduction

## 1.1 EEG

Richard Caton (1875) discovered electroencephalography (EEG) by a mass of animal experiments. He found that "feeble currents of varying direction pass through the multiplier when the electrodes are placed on two points of the external surface, or one electrode on the grey matter, and one on the surface of the skull.". Although his finding was the milestone in the history of monitoring the electrical activity of the brain, the first case of human EEG was recorded by Hans Berger (1929) in Germany. His reports of human EEG, including studies of fluctuation of consciousness, first EEG recordings of sleep, the effect of hypoxia on the human brain, a variety of diffuse and localized brain disorders, and even an inkling of epileptic discharges, were the greatest contribution in the history of EEG (Ernst Niedermeyer et al., 1987).

EEG measures the scalp electrical potential which reflects the summed electrical activity of post-synaptic currents during the physiological and pathophysiological brain activities with the electrodes placed on the scalp. Consequently, this spontaneous EEG is constantly present in living humans. A typical EEG of a healthy adult subject is shown in Fig.1.1. According to the different rhythmic activity (frequency), EEG is divided into different wave patterns such as delta (up to 4 Hz), theta (4-8 Hz), alpha (8-12 Hz), beta (12-30 Hz) and gamma (30-100 Hz). In medicine the EEG serves as a basic parameter to evaluate the global brain function. Further medical applications are the diagnosis of epilepsy and sleep staging (see Zschocke (2002) for further details). Clinical EEG recordings usually include 21channels (in research up to 256) which are related to a corresponding number of electrodes which are equally spaced over the whole skull following the international 10-20-system for electrode placement (Jasper, 1958).

In contrast to the spontaneous EEG the brain generates the specific phasic electrical activity as a response to external or internal stimulation to the subject. External stimuli are such as the presentation of a certain pattern on a video screen, a certain acoustic click etc. whereas internal stimuli reflect mental processes like stimulus processing (for instance detection of a certain pattern), memory retrieval, word generation etc.. This specific brain response occurs with a reproducible stimulus-specific waveform and is called 'event related potential' (ERP). In general ERP amplitudes are much below the spontaneous EEG. Therefore, ERPs can only be extracted from the ongoing EEG using stimulus selective averaging over a large number

(some ten to some thousand depending on the type of ERP) of repeatedly presented stimuli. For more details see Luck (2005).

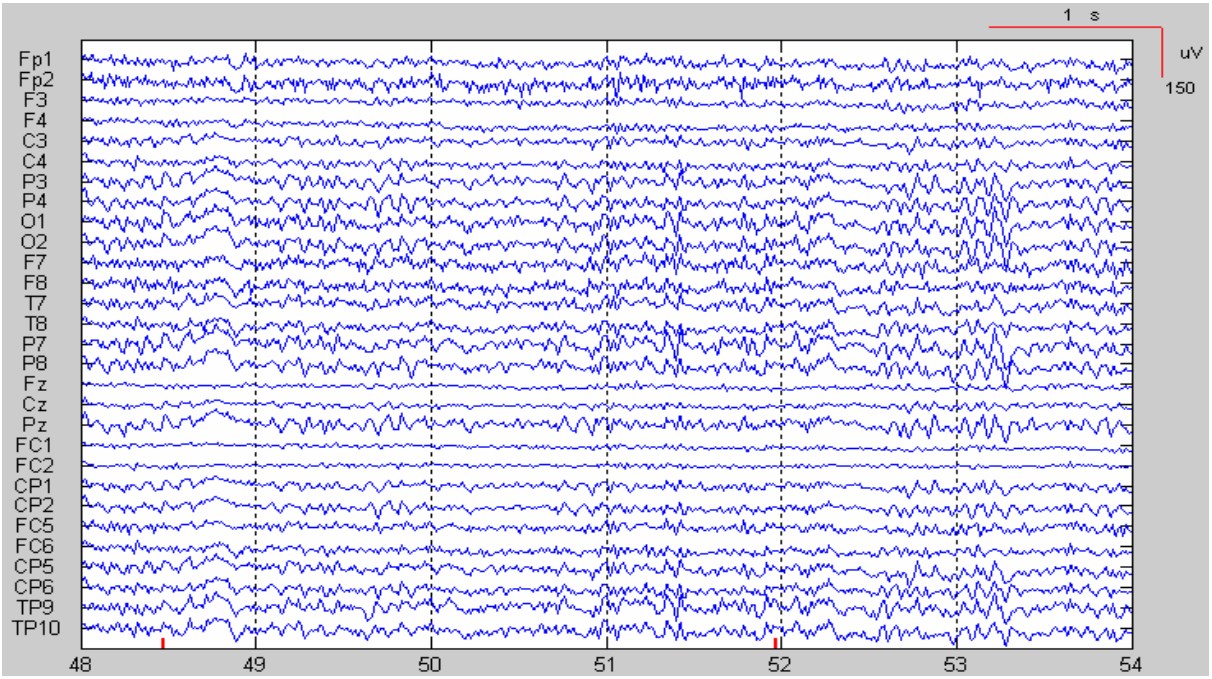


Fig.1.1 EEG recorded outside scanner.

EEG artifacts

In signal processing, the precise definition of an artifact is any perceived distortion or error picked by the recording device. EEG artifacts are non-cerebral signals, usually contaminating the true EEG and resulting in a difficult or sometimes impossible diagnosis. Basically, there are two types of artifacts: biological artifacts (generated by the physiological processes) and technical artifacts (generated by instruments). Examples of biological artifacts are eye movement artifacts, muscle artifacts, pulse artifacts, electrocardiograph (ECG) artifacts, artifacts due to sweating and many more (see Zschocke 2002). Among the technical artifacts there are steep slopes due to electrode movement, amplitude depression due to a shortening between adjacent electrodes caused by electrode contact gel, static electricity artifacts and 50 Hz line frequency superimposed on the EEG.

## 1.2 MRI

Magnetic Resonance Imaging (MRI) is a noninvasive imaging technique based on the interaction between an external magnetic field and a nucleus that possesses spin. In medicine MRI is used to produce 3-dimensional pictures of the brain or other parts of the body. The first magnetic resonance images were published in 1973 by Lauterbur et al. and the first study on a human was performed in 1977 by Damadian et al.. Fig.1.2 (left-above) shows the 3 Tesla scanner (Trio, Siemens Erlangen) of the Clinic for Neurology in Magdeburg used for some

experiments of the presented thesis. Fig.1.2 (right) was also acquired with this MR scanner and illustrates with a three plane view that highly resolved images with good internal contrast of the brain can be acquired. The spatial resolution in this case was 0.6 mm in all three directions.

In addition to various computers controlling the data acquisition and the image reconstruction each MR system has three major hardware components:

a) A strong magnet to create the required static magnetic field $B_0$. Permanent magnets, resistive electromagnets and superconducting magnets have been in use but most modern systems are equipped with a superconducting magnet. The magnetic field polarizes the magnetic moments of the water protons and the resulting net magnetization is the basis for the MR method.

b) A radiofrequency unit with rf transmitter, rf coil and receiver. The rf coil may be used as a transmit and receive coil, alternatively separate coils for transmission and reception can be employed. Short pulses of an rf field are applied via the transmit coil to disturb the magnetization of those proton spins whose resonance frequency - depending on $B_0$ - is contained in the frequency spectrum of the rf pulse. As a result the net magnetization created by the static magnetic field $B_0$ will be altered by the applied rf pulse. When the rf pulse is switched off the magnetization returns to the equilibrium and induces a small signal picked up by the receive coil. This signal is the main MR signal.

c) Three gradient coils to produce linear gradients of the magnetic field in x, y and z-direction. To separate information from different locations in the body a number of schemes combining field gradients and rf excitation have been devised. They all utilize the effect that the resonance frequency of the water protons changes with the magnetic field. Therefore, the resonance frequency becomes location dependent when a gradient is switched on. For most of these schemes numerous magnetic field gradients are switched on and off parallel to the rf transmission (slice selection gradients), in the time period between rf transmission and signal acquisition (phase encoding gradients) and during signal acquisition (frequency encoding gradients).

All three major components mentioned above make an MRI scanner a very harsh environment for EEG data acquisition. In particular the fast and frequently switched magnetic field gradients induce high voltages in the EEG electrodes and cables. The induced voltages

are magnitudes larger compared to the proper EEG signal and good correction algorithms are a prerequisite for the acquisition of an EEG parallel to the acquisition of MR images.

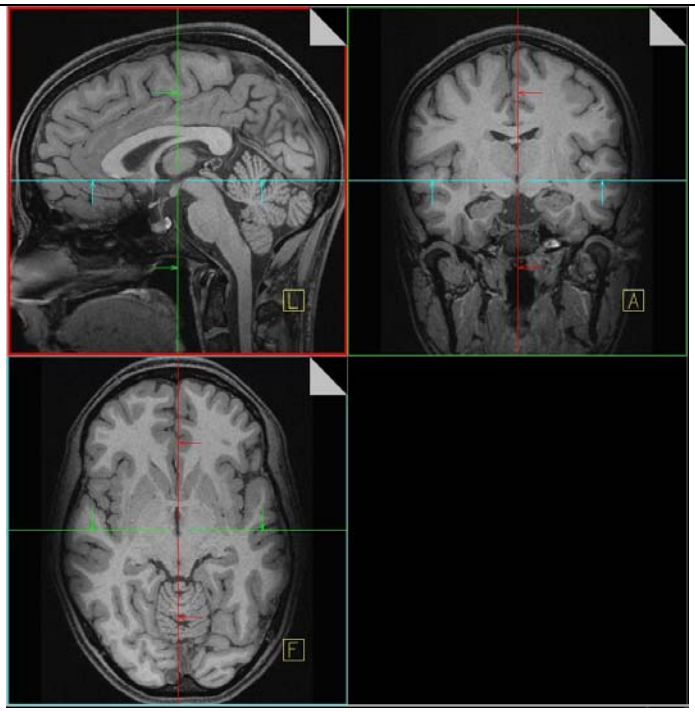


Fig.1.2 Scanner and structure MRI:
Above: Exterior view of the Siemens Trio system installed in the Clinic for Neurology in Magdeburg.
Right: Example for high resolution structural imaging of the brain.

### 1.3 fMRI

MRI can not only deliver high resolution images with excellent soft tissue contrast, it can also be utilized to study the function of many organs; it is for example possible to monitor the heart in all phases of the heartbeat. Another quite new method called functional Magnetic Resonance Imaging (fMRI) has become an important method to detect and analyse activities of the human brain.

The underlying principle was already discovered in 1890 when Roy and Sherrington indicated that the hemoglobin oxygenation is closely linked to neural activity. However at that time it was practically impossible to observe the expected changes directly inside the brain. Later, Pauling and Coryell (1936) elaborated this idea and showed that deoxyhemoglobin is a paramagnetic particle. On contrary, oxyhemoglobin is diamagnetic and this difference in magnetic properties causes relaxation times of the MR magnetization to depend on the oxygen content of the venous blood in the surrounding tissue. The so called blood oxygenation level dependent (BOLD) fMRI first applied by Seiji Ogawa (1990) and Kenneth Kwong (1992) exploits the fact that the hemodynamic response overcompensates for the increased oxygen demands of an active neuronal ensemble and therefore leads to an increase in oxygen content of venous blood in the vicinity of active brain areas. The change in oxygen content modulates the strength of the MR signal. Thus, differences in MR signal between active and passive periods are allowed to identify brain regions involved in the activity. For

most fMRI studies it is essential to get the MR data in the shortest time possible. For this reason, an ultrafast imaging sequence called Echo Planar Imaging is used. As can be seen in the schematic sequence diagram in Fig.1.3 (above, from Huettel et al.) an EPI sequence applies particularly fast switching magnetic field gradients and therefore it gives rise to very strong gradient induced artifacts in the EEG signal if EEG is acquired parallel to the fMRI data.

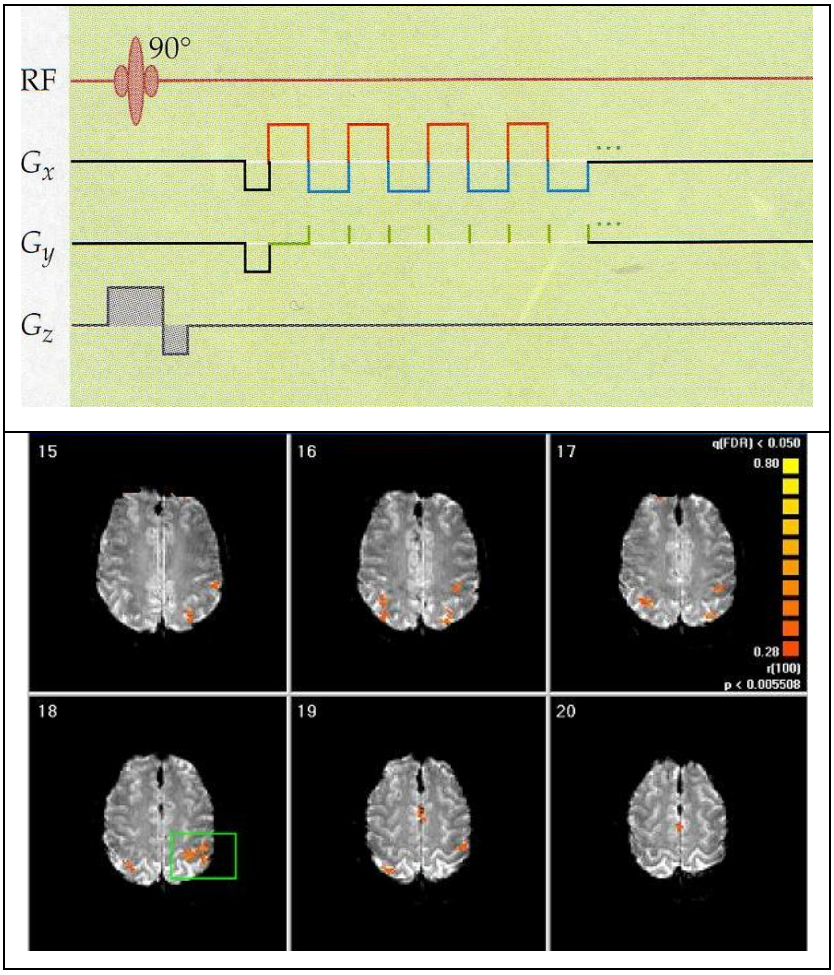


Fig.1.3 EPI and functional MRI:
Above: Schematic sequence diagram of an EPI sequence (taken from Huettel et al., 2003) typically applied in fMRI and
Bottom: Exemplary low resolution EPI images with overlaid statistical maps indicating brain regions activated by finger movements of the volunteer, the green rectangle depicts the primary motor cortex.

## 1.4 Simultaneous recording of EEG and fMRI

Both of EEG and fMRI are used to measure non-invasively brain activity with their own different features. EEG directly measures the brain activity within a millisecond timescale so that it can capture neural function at a rather good temporal resolution but with a poor spatial resolution of a few centimeters for physical reasons (Nunez, 1981). fMRI measures the brain activity indirectly by the haemoglobin oxygenation changing with excellent spatial few

millimeters but a poor temporal resolution of a few seconds. Combining these two methods provides a high temporal and spatial resolution at the same time.

In practice the combination of both modalities means the simultaneous recording of EEG and fMRI but also brings the extra artifacts compared with the EEG recording alone. The whole sketch of the superimposed procedure is shown in Fig.1.4 where all kinds of artifacts related to the magnetic field are added to the physiological EEG indicated as eq.1.1.

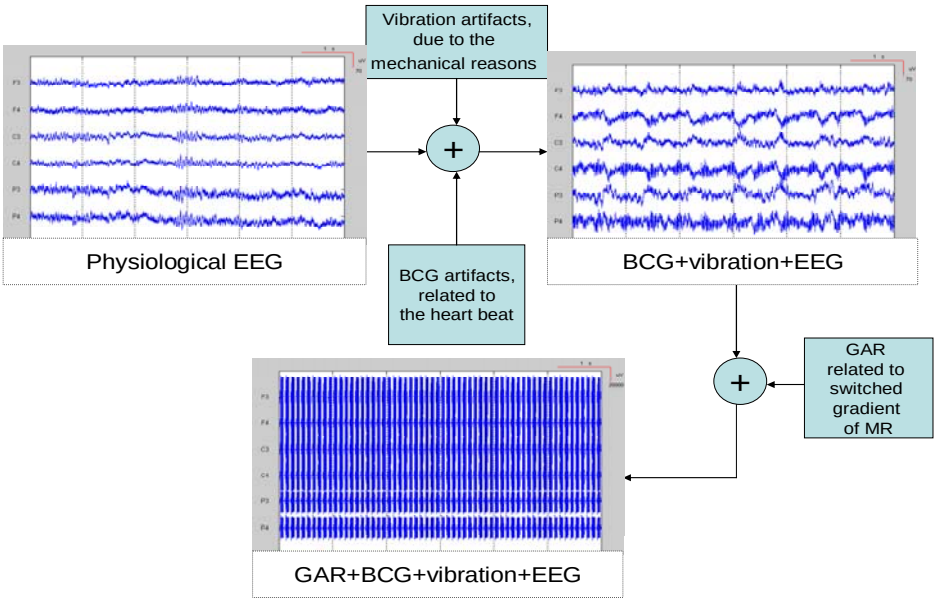


Fig.1.4 Schematic diagram of artifacts superimposition over EEG.

$$EEG_{raw} = EEG_{physio.} + Artifact_{GAR} + Artifact_{BCG} + Artifact_{vibration} \quad (1.1)$$

About 15 years ago several groups (Ives et al.,1993; Hill et al.,1995; Huang-Hellinger FR et al., 1995; Warach et al., 1996; Lemieux et al.,1997) have proved that this combination is technically feasible and that it is safe for the subjects. But they also reported from extremely strong artifacts with steep signal slopes and huge amplitude (far beyond physiological EEG amplitudes) occurring from the beginning of the MR imaging process as a consequence of the sequentially switched magnetic gradients leading to a strong voltage being induced in the closed loop resulting from the EEG electrodes being galvanically coupled to the EEG amplifier input (by cables) and to the scalp surface. An example of this 'gradient artifact'(GAR) is given in Fig.1.5A. The waveform of this artifact is to a large extent but not perfectly stable over its sequence of occurrences (for reasons of variability see later in this thesis).

Hill et al. (1995) were the first mentioning a second, yet less strong MR specific artifact which can be observed as soon as the subject is placed in the MR magnet. This artifact is

characterized by a repeatedly occurring waveform which is strongly linked to heart beat and which is a consequence of tiny head- and electrode movements caused by the heart beat. They are called 'ballistocardiogram artifacts' (BCG). They are characterized by a largely yet clearly not perfectly reproducible waveform. An example is shown in Fig.1.5B.

A

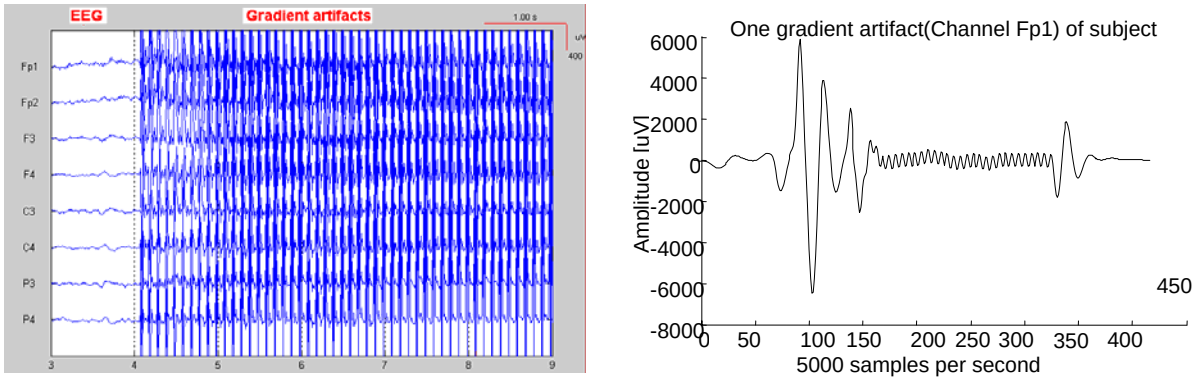


B C

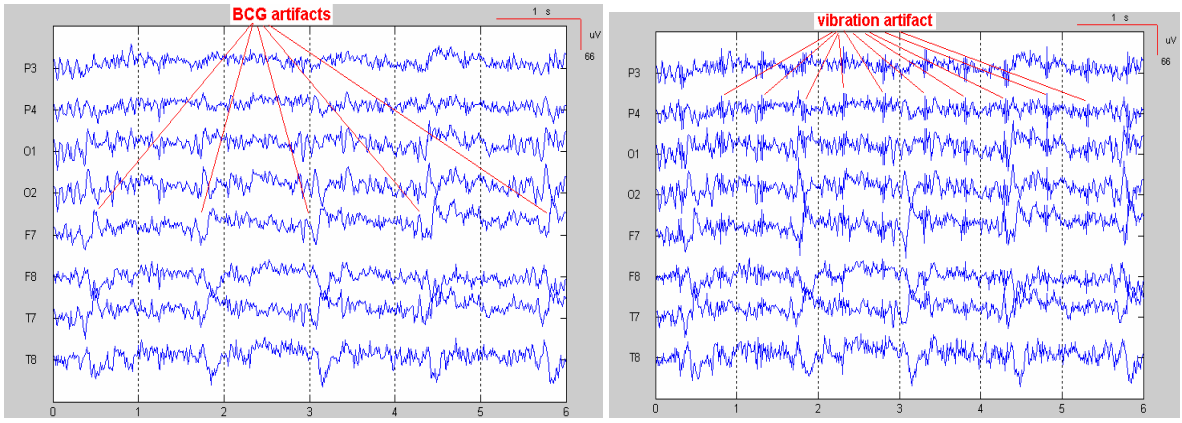


Fig.1.5 EEG-artifacts occurring in an MR environment. Here only a subset of all recorded channels are shown. The electrode labels according to the 10-20-system for electrode placement are listed at the vertical axis.

A) Gradient artifacts.
Left: Overview. Right: Zoom of one artifact template.
B) BCG artifacts.
C) Vibration artifacts

A third type of artifact occurring in simultaneous EEG-MRI recording is caused by the continuously running vacuum pump of the MR scanner. It leads to mechanical vibration which transform to quasi-periodic bursts of oscillations in the frequency range of about 40..50 Hz which we will later refer to as 'vibration artifact'. Fig.1.5C shows a typical example.

Applying various types of artifact removal techniques (for details see subsequent chapters of this thesis) simultaneous recording of EEG and fMRI has been applied in many fields such as the analysis of EEG alpha waves activity (Goldman et al., 2002; Laufs et al., 2003; Moosmann et al., 2003; Niazy et al.,2004), ERP analysis (Bonmassar et al.,1999; Kruggel et al.,2000; Liebenthal et al., 2003; Sommer et al., 2003; Foucher et al., 2003; Ellingson et al., 2004), and epileptic activity (Warach et al., 1996; Krakow et al., 1999; Schomer et al., 2000;

Hoffmann et al.,2000; Seeck et al., 2001; Krakow et al., 2001; Salek-Haddadi et al., 2003; Be´nar et al., 2003; Mirsattari et al., 2004).

### 1.4.1 Gradient artifacts and fMRI imaging

Echo planar imaging (EPI) has become a popular technique in MR imaging research since it was proposed as a fast magnetic resonance imaging technique by Peter Mansfield (1977). EPI is a technique using sequentially switched gradients to read out multiple echoes after just one rf-excitation thereby substantially reducing the time to collect an image. With respect to functional brain imaging EPI is the premise for a fast BOLD imaging allowed to collect a full volume of functional MR images (typically 20 – 30 slices covering the whole brain) within typically 1 – 2 sec. As described in Section 1.2 a large number of BOLD image volumes is acquired per experiment (which usually measures the BOLD signal during processing of external or internal stimuli as described in Section 1.1/ERP) leading to a sequence of switched gradients with a repetition frequency according to the number of slices/second. The exciting application of EPI is in the dynamic study of the brain activity with BOLD fMRI discovered the spatial fluctuation.

Depending on the purpose of study, an fMRI experiment usually lasts from several minutes to more than hours. Following Faraday's law of induction each switched gradient (that is, each slice) leads to a gradient artifact in the EEG. The artifact observed in the EEG thus summarizes the voltages induced by the various concurrently switched gradients as shown in Fig.4.1. The resulting template occurs with the frequency as defined by the MR slice time since the gradients are switched in almost the same manner for each acquired slice.

Several different approaches have been presented to reduce the gradient artifacts. A rather simple method applies a kind of non linear filtering by setting the artifact related components of the spectrum (Sijbers et al., 1999; Hoffmann et al., 2000) or directly the waveform (in the time domain) to zero (Goldman et al., 2000). An alternative method exploits the fact that the shape of the artifact is largely (yet not perfectly) stable within each EEG-channel but different between different channels (Hoffmann et al., 2000; Anami et al., 2003; Garreffa et al., 2003). Given this observation this method subtracts an averaged artifact template from each individual artifact. This so called 'averaged artifact subtraction' (AAS) (Allen et al., 2000) first uses an interpolation technique to virtually increase the sample rate. Next it averages a large number of subsequent artifacts as the template which is finally used as the true waveform to be subtracted.

Several variants of AAS have been proposed (see Section 3.1 for an overview). Among these is a temporally windowed variant named 'moving averaged subtraction' (MAS) (Becker et al., 2005) focussing the averaging process on artifact templates located close to the artifact to be removed. This was the starting point of that part of the current thesis aiming at an improved gradient artifact reduction.

### 1.4.2 Ballistocardiogram artifacts

The ballistocardiogram artifact was already mentioned in the first publication on simultaneous EEG-MRI recording by Ives et al. (1993). Its amplitudes are in the range of or slightly larger than typical EEG amplitudes. It can be easily detected visually by its periodic occurrence according to the heart beat. Ives (1993) has suggested that this artifact results from the acceleration and abrupt directional change in blood flow in the aortic arch during each heart beat. Several years later the sources of BCG artifacts have been thought coming from that "the EEG electrode tiny regular movement on the scalp due to expansion and contraction of scalp arteries between systolic and diastolic phase, fluctuation of the hall voltage due to the pulsatile changes of the blood in the arteries and the small cardiac related movements of head" (Srivastava et al., 2005).

Various methods are found in the literature to remove this kind of artifacts (see Section 3.2 for an overview). Besides subtraction methods (Allen et al., 1998; Müri et al., 1998; Goldman et al., 2000; Kruggel et al., 2000; Ellingson et al., 2004), several approaches developed for blind source separation (BSS) have been applied for this purpose, among them are principal component analysis (PCA) (Negishi et al., 2004; Niazy et al., 2005) and independent component analysis (ICA) (Be´nar et al., 2003; Srivastava et al., 2005; Briselli et al., 2006; Nakamura et al., 2006; Debener et al., 2007; Mantini et al., 2007). The present thesis presents another BSS-method called 'Maximum Noise Fraction' (MNF) to achieve a more efficient BCG reduction.

### 1.4.3 Vibration artifacts

According to own measurements on three different MR scanners this kind of artifact does not occur on different scanners with different amplitudes. It was clearly present on the 3T MR device (for details see Section 4.1) mainly used for this thesis. Vibration artifacts contaminate the EEG as a consequence of the vibrations originating at the scanner's vacuum pump (Briselli et al., 2006). For regular MR usage this pump is continuously running no matter if the scanner is active or idle. On the 3T MR scanner the amplitude reaches about 200 μV and

is thus larger than the normal EEG (10-100 μV). The frequency of this artifact is slightly fluctuating and mostly extends over a range of 40 Hz to 50 Hz. It can only be suppressed by either band stop filtering (thereby also loosing a fraction of the underlying EEG) or by switching the pump off. However, running the scanner with a suspended vacuum pump can only be accepted for a very limited period and is therefore no regular artifact suppression technique.

# Chapter 2 Aims of the present thesis

The aims of the present thesis were:

(i) Analysing the reasons for the residual artifact activity persisting after application of the existing subtraction methods for gradient artifact reduction, with special emphasis on the quantification of the effect contributed by head movements.

(ii) Guided by the results of step (i) to develop a new method to improve the reduction of gradient artifacts with emphasis on high frequencies (beyond 30 Hz), trying to get the residual artifact down to a level that allows to analyze activity in the γ-frequency band.

(iii) Developing an improved BSS-based BCG removal algorithm that better separates

(iv) Devoloping a fully automatic procedure for BCG removal with more efficient separation between EEG and BCG activity than existing approaches.

(v) Optimizing the algorithms with respect to computational efficiency.

# Chapter 3 Review of Previous Methods to remove MRI-related EEG artifacts

## 3.1 Gradient artifacts

The removal of the gradient artifact is challenging given a noise-to-signal ratio of typically 100. The principal goal is to remove as much artifactual activity as possible and at the same time to keep the true underlying EEG. Besides some other approaches (discussed in Section 3.1.2) the actually most popular subtraction approach (see Section 3.1.1) – which was also applied in the present thesis - exploits the fact that the gradient artifact's waveform is largely stable over time and can thus be removed by subtracting an appropriate waveform (to be derived from the artifactuous signal) from each artifact in the recorded EEG. Various realizations of this approach are commercially available as add-on to commercial MR-compatible EEG recorders (for instance Brain Products, Munich; Neuroscan/Compumedics, Australia).

Before revisiting existing methods, the terms "epoch" and "template" are defined which are repeatedly used throughout the subsequent section. An "epoch" is an EEG segment (true physiological EEG plus artifact) recorded during and starting at the beginning of the MR-acquisition of one slice. Consequently, the duration of each epoch is TR/N sec with TR specifying the MRI repetition time (in sec) and N the number of slices per MRI volume. The artifact "template" is the average over a sequence of subsequent EEG gradient artifacts.

### 3.1.1 Template Subtraction

The basic assumption of this approach is that the gradient artifact is invariable over time and therefore the subtraction method has been proposed by several groups, all applying basically the following steps: i) extract the template of the gradient artifact, ii) subtract this template from the raw data, and iii) postprocess to remove the residual gradient artifacts. However, the presence of residual artifact activity indicates that the basic assumption is not perfectly met.

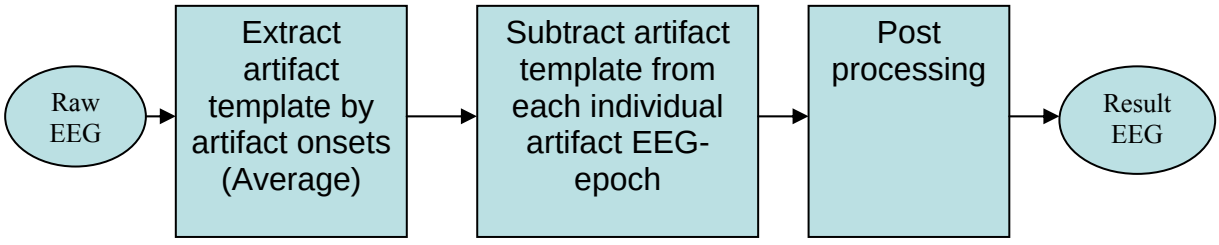


Fig.3.1 Schematic diagram of template subtraction

$$\begin{cases} EEG_{clear}(t) = EEG_{raw}(t) - GAR(t) \\ GAR(t) \approx \sum_{i=-\infty}^{\infty} TGAR_i(t - I_{GAR}^i) \end{cases} \tag{3.1}$$

where $TGAR_i(t)$ is the estimated GAR template of the i$^{th}$ epoch at time t and $I_{GAR}^i$ is the shifted phase error of the i$^{th}$ epoch.

This basic procedure of template subtraction is drawn in Fig.3.1 and the general formula is described in eq.3.1. All methods with subtraction are based on the same hypothesis, that the true gradient artifact of one epoch can be estimated by averaging over a number of epochs. The differences between them only are in the methods of the estimation of the artifact template and the postprocessing of removing residual gradient artifacts with the same aim of removing more residual gradient artifacts.

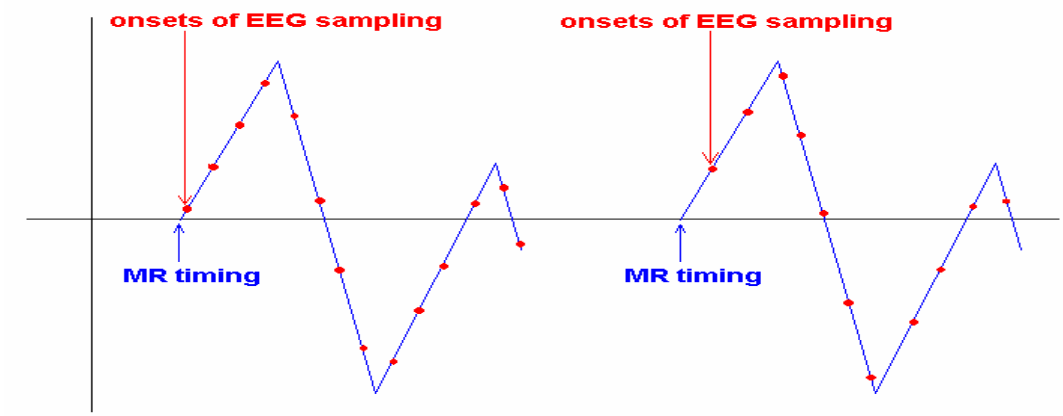


Fig.3.2 Two artifact examples with different artifact sampling "phases".

In the subtraction method, one important factor of influencing the quality of EEG is the gradient artifacts' timing error resulting from the asynchronism of EEG sampling and MR-timing (Fig.3.2). So, although two sampled discrete gradient artifact epochs represent the same continuous gradient artifact, the timing of the sampling onset respect to the artifact onset varies giving rise to severe errors if these two epochs are averaged for template extraction (this timing difference is subsequently called "phase difference"). In order to decrease this phase error and to further improve the subtraction result, interpolation has to be used to upsample the signal in order to increase the accuracy of subtraction by aligning the two gradient artifacts. After interpolation and aligning, downsampling is used to restore the original sampling rate, which is not only reasonable with respect to subsequent postprocessing algorithms but also with respect to computer memory required for the algorithm. In the following, the typical subtraction method is outlined in more detail. Besides the artifacts stable waveforms all of these algorithms assume (i) that the underlying true EEG is not correlated with the superimposed artifact and (ii) that the EEG has zero mean. The second

assumption does not restrict the general application of these methods since either the amplifier has a non-zero lower cut off frequency (thereby suppressing a potential DC offset) or the non-zero mean can be determined and subtracted before any processing).

The typical subtraction method comprises the following steps:
1. Upsample and align each gradient artifact by interpolation.
2. Estimate the artifact template by averaging over a set of *M* artifact epochs with *M* as well as the type of averaging varying over the different approaches proposed so far.
3. Subtract this template from each gradient artifact.
4. Downsample the result.
5. Postprocess to remove residual gradient artifacts.

Allen (2000) was the first to present the averaged artifact subtraction (AAS) method. He extracted the artifact template by averaging over all artifacts observed in the current recording. Resiudal artifact activity remaining after AAS was reduced by an adaptive noise cancellation (ANC) technique which was guided by a MR slice timing trigger signal. Upsampling to 100 KHz frequency was accomplished by a 25-coefficientsinc interpolation (up to 50KHz). A unique artifact template was extracted by averaging over the first 25 artifact epochs and subsequently subtracted from all artifact epochs of the recording. This method still leaves a residual artifact of about 10 μV (Allen, 2000) and potentially removes some fraction of the underlying true EEG since the effect of the ANC with respect to the EEG cannot be controlled. Furthermore, the sinc algorithm applied for interpolation is time consuming.

Another variant of the subtraction method was proposed by Be´nar et al. (2003) who concentrated on the asynchronismof EEG sampling and MR timing. To get around this problem they used several different artifact templates which were generated by averaging over several groups of artifact epochs. Each group included only artifact epochs showing the same lag (as determined by cross correlation) with respect to a reference epoch (usually the first one). The reference epoch and each epoch were interpolated and upsampled by a factor of 10 to refine the lags. Then, each averaged template was only averaged over all epochs in the corresponding group. Finally, the subtraction was performed using the template best matching the artifact epochs in terms of its lag.

The real-time artifact filter (Garreffa et al., 2003) brought the artifact removal technique into another new development direction (real-time processing) with the assumption of the averaged artifact template for each individual artifact being long term stable. This approach in effect represents a non linear online filter algorithm. First the waveform of the averaged artifact template is defined by the initial 48 seconds data. Next this template is used for the peak detection algorithm to locate the onsets of artifacts by correlation. Then the procedure of subtraction is performed as a real-time process. Additional filters are applied to reduce the

residual noise. This algorithm requires a powerful computer to meet the computational demands of the real time processing.

An approach called 'stepping stone sampling' (SSS) (Anami et al., 2003) achieves a higher signal-to-artifact ratio by (i) strictly synchronizing the EEG sampling with the MR timing and (ii) by modifying a standard fMRI measurement sequence so that EEG sampling might be performed at every 1000 μs (i.e. digitization rate 1000 Hz) exclusively in the period in which the gradient artifact resided around the baseline level. Since the gradient artifact isn't perfectly zero at the time of EEG sampling some gradient related activity can still persist but with an amplitude much below (by a factor < .1) amplitudes observed with standard fMRI settings. The remaining residual artifacts are subsequently removed with the subtraction technique. In this realization the template was extracted by averaging over all artifact epochs of the recording.

Becker et al. (1005) introduced the 'weighted moving averaged subtraction'(MAS) method which accounts for temporally varying artifact waveforms by applying a weighted moving average scheme to extract an individual artifact template for each artifact to be removed. Before this processing step the signals are upsampled to 50 KHz by cubic spline interpolation, aligned by cross correlation and finally downsampled to the original 5 KHz sampling rate. The weighting function has an exponential profile and extends over 120 epochs. After the subtraction step, a bandpass filter of 0.53-70 Hz is applied as to remove the residual noises. However, according to own test of this method, residual artifacts are still a problem in case of head motion.

'FMRI artifact slice template removal' (FASTR) (Niazy et al., 2005) combines a local moving artifact template subtraction with subsequent applications of PCA and ANC to remove the residual artifacts. Each epoch is upsampled to 20 KHz with since interpolation and realigned with all other epochs. Beyond the mere artifact subtraction this algorithm relies on a PCA to capture residual artifact activity caused by temporal artifacts variations. The ANC was applied according toe the method described by Allen (2000) to remove any remaining residual components (not captured in PCA). The problem with this approach is that there is no strict rule to determine the appropriate number of PCA components to be suppressed (that is to find a compromise between removing the artifact and keeping the true underlying EEG).

Recently, a variant of the average-subtraction method was proposed (Goncalves et al., 2007a; Goncalves et al., 2007b) to correct the temporal misalignment between EEG and fMRI data by estimating three MR sequence timing parameters in terms of the EEG recorder's time

base (before any subtraction processing). The estimated parameters are: the MR sequence repetition time $TR_{EEG}$, the time between the beginning of the MR-volume acquisition and the acquisition of the first slice *DT*, and the acquisition time of one slice (i.e. the slice time)*ST*. Next, the shifts needed for an optimal temporal alignment are derived from these three parameters. Then, the alignment is performed by a resampling procedure applying a FFT based interpolation scheme. Second, after these sub-sample shifts, separate templates are derived for each slice within the MR volumes and an additional template is determined averaging over these slice specific templates of volumes. Finally, the slice template and the volume template are combined and subtracted from each epoch.

### 3.1.2 Other approaches

Besides subtraction, there are two different methods working without any subtraction. One of them is called ‘frequency removing method’ (Hoffmann et al., 2000) which eliminates all artifact related frequency components outside the clinically relevant frequency window of the EEG (0.1–40 Hz) by high- or low-pass filters. Components below 40 Hz are removed by employing a series of band-stop filters. This method necessarily causes a loss of information of the true underlying EEG below 40 Hz frequency. A similar method has been proposed by (Goldman et al., 2000) for the time domain which sets all artifactuous epochs of the ongoimg EEG to zero. Although it is not hard to locate the gradient artifacts, there are two obvious disadvantages: i) the scanning frequency must be low (such as 4 slices per second) in order to save a sufficient fraction of the EEG as not being suppressed, and ii) the processed EEG data is fractioned in to usable and non usable parts.

A more sophisticated filtering approach was developed by Sijbers et al. (1999) aiming at keeping as much EEG as possible. This technique, called ‘adaptive restoration scheme’, applies a non-linear filter as follows: First the spectrum of the artifact template is estimated by averaging over a number (15 for slow MR sequences to 31 for faster ones) of spectra of gradient artifacts detected by MR triggers. A scaled version of this average spectrum is subsequently subtracted from each of the artifact epochs whereby the scaling parameter is set to minimize the difference between the two spectra. The resulting difference spectrum is finally transformed back to the time domain thereby yielding the EEG signal. At the same time, the average artifact spectrum is updated to track potential changes of the artifact template. The problem with this method is that the amount to which the true EEG is influenced by this processing cannot be controlled.

Negishi et al. (2004) – after realignament of the artifacts - applied a PCA to the EEG to identify principal components (PC) mainly carrying artifact activity. An artifact template of each epoch is then computed as a linear combination of these PCs (details regarding the calculation of the weighting factors are found in Negishi et al., 2004). Finally these combined PCs are subtracted from the original epoch. The resulting signal is smoothed with an 80Hz lowpass filter.

Yet another method, (Wan et al., 2006b) estimated each gradient artifact epoch by a band-limited Taylor expression assuming that each gradient artifact can be defined as a linear combination of the average artifact template and its derivatives with the linear coefficients varying over the epochs. These varying coefficients are fitted by a least square error (LSE) algorithm minimizing the sum of squares of the differences between the epoch and the estimated epoch. After convergence of the LSE and subtraction of the estimated epoch an 8-order Butterworth lowpass filter (LPF), with a cut-off frequency of 70 Hz, removes the residual noise. According to Wan et al. (2006b) this approach is comparable to an adaptive finite impulse response (FIR) filter. The analyses of Wan et al. (2006b) also demonstrated the temporal instability of the gradient artifact template. It is hard to compare the removal effect of the techniques to other approaches since Wan et al. did not apply any interpolation and upsampling technique.

Finally, Mantini et al. (2007) applied AAS as the first processing stage but subsequently applied an ICA to capture and suppress specific independent components carrying residual artifact activity.

### 3.1.3 Conclusion

Summarizing the approaches published so far and taking into account the practice of many imaging labs (which mostly use commercially available artifact suppression programs), template subtraction is by far the most popular technique to remove gradient artifacts. All of them upsample the signal as a premise for an appropriate alignment of the artifact epochs. The main difference between the various algorithms is the way they determine the template to be subtracted. In all cases some residual activity remains after subtraction. Some of them reduce it by application of a PCA or ICA technique after the subtraction, but all of them finally smooth the data using a low pass filter. So far the reason for some residual artifact activity persisting after processing has not been sufficiently identified.

## 3.2 BCG artifacts

### 3.2.1 Blind Source Separation (BSS) (PCA and ICA)

BCG artefacts are less reproducible than gradient artifacts, so that the subtraction method won't work as efficiently. Thus the research is focussed on the othogonality of the true EEG and the BCG artifacts. From a statistical perspective 'orthogonality' between two signals means that they are not correlated, i.e. each varying separately. Principal component analysis (PCA) is one of the standard methods to separate such orthogonal components. The basic idea is to identify and suppress those principal components (PC) which mostly capture artifact activity so that the amount of EEG lost after suppression can be neglected. Negishi et al. (2004) and Niazy et al. (2005) proposed this concept to remove BCG artifacts (as the second step after gradient artifact removal, see above). In principle they subtracted a linear combination of some PCs from the signal, including all PCs (Negishi et al., 2004) or a limited number (Niazy et al., 2005) explaining the largest amount of the total variance. Independent component analysis (ICA) is a different BSS-approach which tries to identify statistically independent (rather than orthogonal) components within a composite signal. With respect to BCG removal the problem with any ICA procedure is that components resulting from the PCA or ICA analysis are randomly ordered regarding the amount of artifact activity captured by each component. This hampers an automatic procedure to identify components which should be suppressed for artifact removal. Thus, the identification of BCG ICs reflects an important key aspect, especially with respect to automated removal algorithms. At the moment there are two kinds of methods: interactive processing (i.e. visually selecting the relevant ICs) (Be´nar et al., 2003) and fully automatic processing (Srivastava et al., 2005). For the semi-automatic processing, the BCG ICs have to be visually identified by an observer (human, not computer) which consequently introduces a man caused factor increasing the likelihood of either distorting the underlying EEG (if too many ICs are removed) or leaving too much residual artifacts (if a too low number or a wrong choice of ICs is removed ICs). For the automatic processing, a rule is needed guiding the selection of BCG related ICs automatically. Usually, the electrocardiogram (ECG) is recorded simultaneously with the EEG as an additional reference channel. Basically, Srivastava et al. (2005) accomplish the BCG removal task in five steps: i) Decomposing the original EEG into different ICs (i.e. application of the ICA), ii) Computing the correlation coefficient between the ECG and each IC, iii) Choosing those ICs with high correlation coefficient as BCG-related ICs and setting them to zeros, and iv) reconstructing the underlying EEG by recombining the remaining non-zero ICs.

Briselly et al. (2006) refined the ICA approach by running it multiple times having in mind the idea of reducing the BCG residuals more and more with an increasing number of iterations.

When these introduced BSS-based BCG removal methods (ICA or PCA) are applied, the basic processing steps are described in Fig.3.3. The only discrepancy of different methods is the procedure of the identification of BCG ICs which becomes the main problem of removing artifacts.

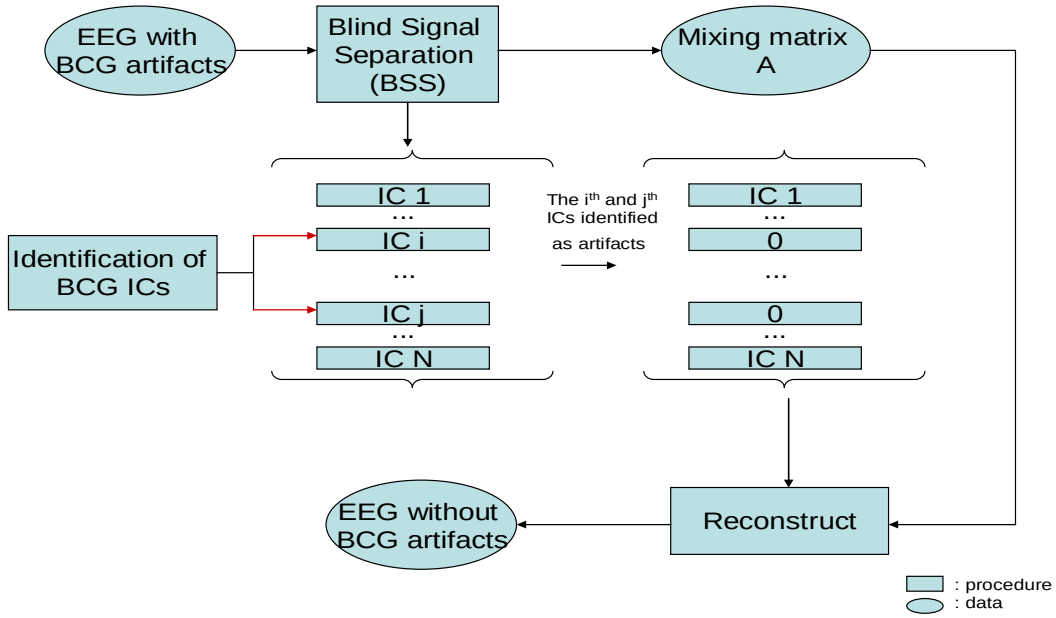


Fig.3.3 Schematic diagram of BSS-based BCG removal.

### 3.2.2 Other approaches

Subtraction – similar to the approach applied for gradient artifact removal – was the first method ever to be applied for BCG removal (see Allen et al., 1998). Due to all kinds of reasons, such as motion, respiration and heartbeat, each individual BCG artifact differs from all others so that there is more residual BCG activity after subtraction compared to gradient artifact removal. Moreover, in contrast to gradient artifacts the BCG onsets can not be identified by a clear feature like, for instance a steep slope. Therefore, one important task in this context is to locate the temporal BCG position in order to derive a proper BCG template for an efficient subtraction based BCG artifacts removal. Mainly the following three steps need to be done: identifying ECG peaks, averaging the BCG artifacts time-locked to the ECG peaks, and subtracting the averaged template time locked to the ECG peaks. Though this type of subtraction was described by several groups (Allen et al., 1998; Müri et al. 1998; Goldman et al., 2000; Kruggel et al., 2000; Ellingson et al., 2004), the problem of all these approaches

is the considerable residual BCG activity remaining due to the BCG artifact's temporal instability (according to own empirical tests).

A different algorithm was developed by (Bonmassar et al., 1999) who designed a linear spatial filter to recover the BCG artifacts contaminated EEG directly, however, exclusively focussing on the processing and extraction of visual evoked potentials (VEP). In principle this method tries to maximize the signal to noise ratio by the well known generalized maximum eigenvalues of the signal covariance matrix and the noise covariance matrix. The noise covariance matrix is estimated from all VEP epochs recorded during fMRI by subtracting the averaged VEP as recorded outside the scanner, whereas the signal covariance matrix is estimated by using epochs recorded outside the scanner without any subtraction. Although this method does not need to record an extra ECG, it is time consuming since it requires extra EEG data (including visual stimulation) recorded outside the scanner as the base to compute the two signal-to-noise ratio values.

The adapter filter technique by Sijbers et al. (2000) is based on a average-subtraction method extended by the following features: An improved detection of QRS waves, the estimation of the BCG artifact template by means of wavelets, and a filter which is continuously adapted to the ongoing BCG epochs. To detect QRS onsets, a band-pass filter was first applied to remove irrelevant information. Second, local maxima within an interval of 0.5 seconds were retained and subjected to a selection criterion applying constraints on the distance between subsequent maximum values. The BCG artifact template was estimated by median-filtering a number of the wavelet filtered artifacts. Given this primary template, the final adaptive filtering procedure proceeds as follows: the template is updated with each new artifact guided by criterion of minimizing the difference between the template and the actual artifact. Another adaptive filter version was applied by Bonmassar et al. (2002), who used a piezo based motion sensor to pick up head movements and evaluate it in terms of an adaptive noise cancellation method to suppress any kind of motion related artifacts including the BCG. This procedure was applied to remove BCG artifacts in the context of an interleaved EEG/fMRI recording protocol with alternating periods of active EPI scanning and non-scanning. The relationship between the noise (artifacts) and the motion sensor signal is modeled linearly using a time-varying finite impulse response (FIR) kernel which is adaptively updated with kalman filter algorithm.

Kim (2004) suggested to combine the average template subtraction with a noise reduction approach using a wavelet decomposition (i.e. wavelet transform, selective suppression of some wavelet scales and finally inverse transform) and finally with an adaptive recursive

least-square (RLS) eliminating remaining residual artifactual activity. For a successful application this method needs two ECG channels guiding the template extraction process. Wan et al. (2006a) used a similar wavelet decomposition technique but combined it with a nonlinear noise reduction originally developed by Grassberger et al. (1993) as a general denoising concept derived from chaos theory. Residual artifact activity remaining after this procedure is removed by subtracting a BCG template derived by spatially averaging (guided by the ECG) over all EEG channels. According to Wan et al. (2006a) this 'Wavelet-based Nonlinear Noise Reduction' (WNNR) is computationally very demanding making it less suitable for routine applications. In addition – similar to most of the above described methods – potential distortions of the ongoing spontaneous EEG cannot be controlled.

The template subtraction approach was substantially extended by Vincent et al. (2007) with respect to the observation that the BCG waveform substantially fluctuates over time, and is usually longer than the heart beat interval leading to overlap effects. To include points the authors defined a three-dimensional BCG template (i.e. a multichannel template) and estimated by a 'moving general linear model' (mGLM) which estimates the coefficients of the Fourier transform of the template. This estimated 3D-template is finally time locked to the ECG-subtracted from the signal. Despite its advantages in handling overlapping BCG artifacts this method is primarily suited to research EEG recordings (Vincent et al., 2007) since it requires substantial user interactions which is not acceptable under clinical routine conditions. The 'multi-channel Recursive Least Squares (M-RLS) algorithm proposed by Masterton et al. (2007) includes four extra channels representing the head motion. These non-physiological signals are used for an adaptive BCG template estimation (similar to the method of Bonmassar, 1999) which is subsequently subtracted to remove the BCG artifact as well as arbitrary other movement artifacts. With respect to clinical EEG recordings this method is hampered by the need of extra wires to be connected to the head and extra electronics to record the motion signals

### 3.2.3 Conclusion

Due to the temporal variability of the BCG artifact waveform the artifact subtraction approach (like AAS) as developed for gradient artifact removal cannot be applied here. Instead, several groups have extended AAS using algorithms allowing for an adaptive estimation and modification of the artifact template. However, the majority of published papers replaced the template subtraction by a spatiotemporal approach applying blind source separation (BSS) techniques like PCA and ICA. Though being successfully applied under a

wide range of research and routine conditions the problem with these techniques is that- due to the missing orthogonality between the artifact and the EEG signals - it cannot be controlled how much of true EEG is lost after suppression of components mainly (but not exclusively) carrying for artifact activity. Furthermore, most of the proposed algorithms are not suited for an automatic procedure since they require a user interaction.

# Chapter 4 Materials

## 4.1 fMRI scanning

Functional echo planar imaging (EPI) was performed on a 3T magnetic resonance (MR) scanner (Siemens Trio, Germany) with an 8 channel head coil applying the following sequence parameters: echo time (TE) 40 ms, repetition time (TR) 2000 ms, flip angle 80 degree, field of view (FOV) 20 x 20 cm, matrix size 64 x 64, slice thickness 5,0 mm and number of slices 24 or 20. Per each slice one gradient artifact occurs in the EEG. This means that the artifact repetition rate was 12 Hz (24 slices) or 10 Hz (20 slices).

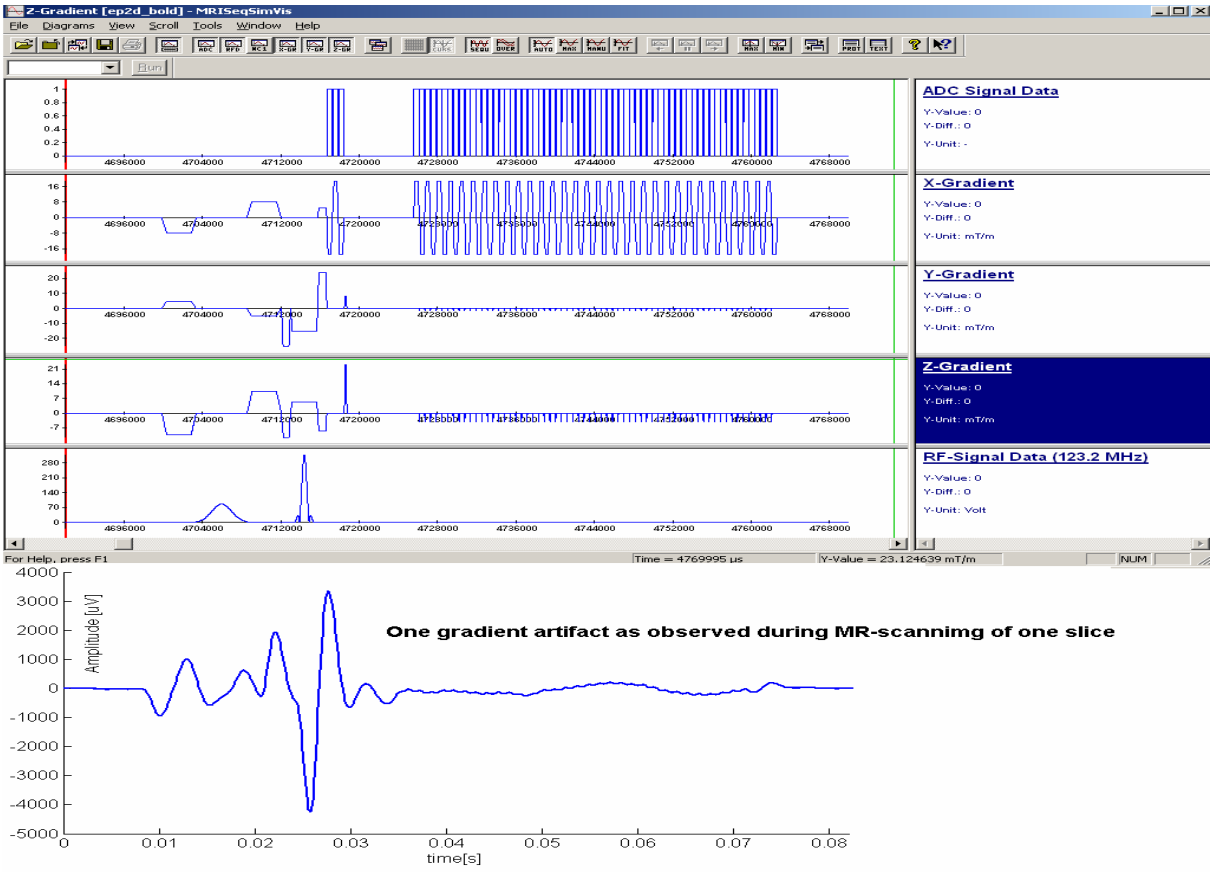


Fig.4.1 EPI sequence and gradient artifact.

Upper : EPI sequence during scanning one fMRT slice (3T Siemens Trio).

Lower : Gradient artifact observed during the time course of scanning one slice

The timing of the EPI sequence needed to acquire one slice is graphically illustrated in Fig.4.1 showing the X-Gradient (readout), Y-Gradient (phase encoding) and Z-Gradient (slice selection). This sequence uses a so called “blipped” phase-encoding technique which applies a small-amplitude gradient of phase encoding pulse prior to each sampling period. The phase-encoding gradient is incrementally applied prior to detection of each echo. No phase-encoding gradient is applied during signal detection so that the phase encoding for each echo is constant

(Fig.4.1 Y-Gradient and X-Gradient). The signal emitted by the tissue upon excitation by the Rf pulse is sampled by an analog-to-digital converter (ADC) of the MRI receiver according to the time diagram shown in Fig.4.1 ('ADC Signal Data'). When 'ADC Signal Data' is high ('1'), the frequencies of tissue are read out and sent to the k-space matrix to create the image. One recorded individual gradient artifact (Fig.4.1, down) properly reflects the changes of signal amplitudes during this sequence.

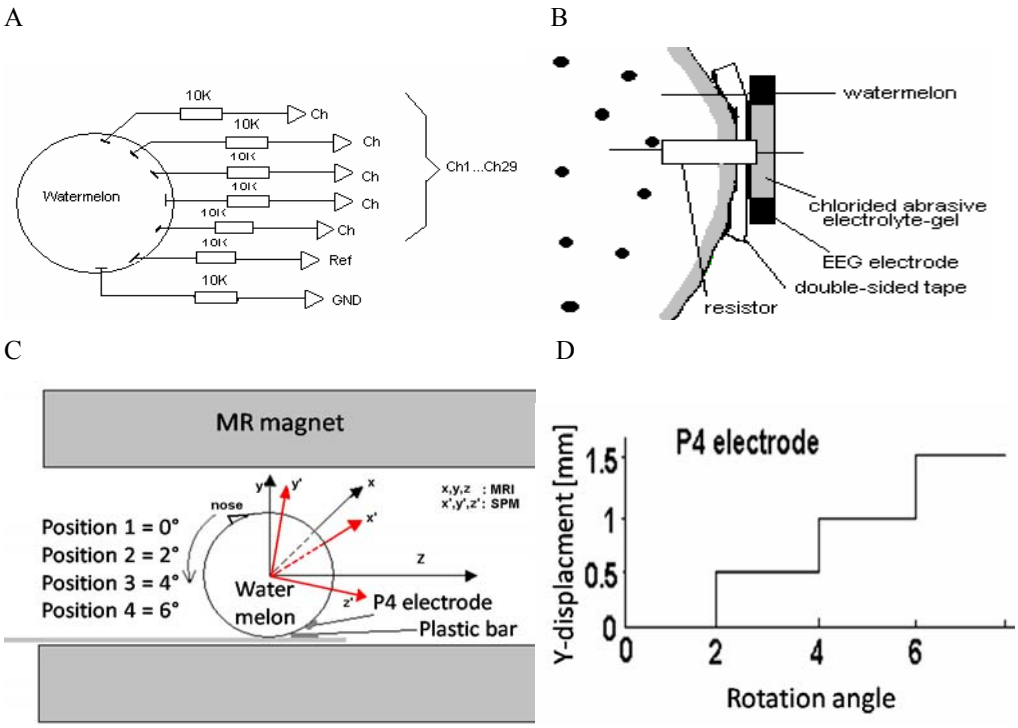


Fig.4.2 Watermelon in the scanner serving as a phantom; 4 positions, 29 electrodes, electrode P4 highlighted.
A) Schematic diagram of the complete setting
B) Physical connections between watermelon, 10 kΩ-resistor and EEG electrode.
C) Four different positions at which signal were recorded. The two slightly differing coordinate systems refer to the MRI and to SPM respectively.
D) Four y displacements corresponding for the four watermelon positions corresponding illustrated in A).

## 4.2 Phantom EEG-measurements

In order to analyse the pure gradient artifact and its temporal and spatial fluctuations (i.e. without underlying EEG), we recorded signals from a phantom made of a watermelon with diameter 140mm. The circuit diagram, physical connections, physical position of the watermelon inside the scanner and the four different rotation angles applied during measurements are shown in Fig.4.2. Given the 10 KΩ resistor connecting the electrode to the watermelon tissue the electrode impendence of the EEG recording setting was about 10 KΩ (as confirmed by an electrode impedance measurement). Signals were acquired from 29 Ag/AgCl electrodes placed on the watermelon according to the international 10-20-system for

electrode placement (Jasper, 1958) and were identical to the real human EEG recordings, see next section. The whole phantom EEG recording consisted of four runs, each of 10 min duration (according to 300 MR volumes) while the MR scanner acquired images. Between each run, the watermelon was rotated by about 2° around the x axis (see Fig.4.2) while keeping the same position. To prevent any motion during the measurement the melon was fixed by support jaw. Hence the watermelon only simulated a head motion in one direction thus simulating a subject moving its head during scanning. As shown in Fig.4.2D the displacement of the P4 electrode per rotation step was about 0.5 mm in the vertical (i.e. y) direction resulting from a 2.4 mm displacement in tangential direction which is comparable to a realistic strong head movement.

The idea to run the watermelon experiment was to record the pure gradient artifact without any additional BCG artifact and without any EEG. This provided the opportunity to uncover both to analyze the relationship between the electrode position and the gradient artifact's waveform and the temporal stability of the artifact. The 10 KΩ antimagnetic resistance (DALE CMF55 10K .1%T9 0410) was connected between the water melon and EEG electrodes in order to simulate a real measurement situation. Those electrodes were fastened with double-sided tapes.

### 4.3 Human EEG measurements

Six volunteers (five male and one female, average age 25, range 20-27 years) participated in the study. Four subjects(three male and one female) were requested to keep their head motionless as good as possible during the recording when seeing a series of pictures (see next subsection). The other two subjects (male) were asked to slightly move their heads according to the different types of picture. In two of the subjects the head movements were recorded online with high temporal resolution (20 ms) applying a video-based device developed by the Magdeburg MR-group (Kanowski et al., 2007), for details see chapter 5.2.2. These recordings served to check the quality of the offline head movement information derived from the MR-image sequence by the statistical parametric mapping (SPM) analysis program with a resolution of 1 sec, for details see chapter 5.2.1.

The EEG was recorded using a BrainAmp MR-Plus MR-compatible EEG-amplifier (Brain-Products, Germany). In each subject the EEG was obtained under the three different conditions: (i) Inside the scanner concurrent to BOLD-imaging according to section 4.1. These recordings contain both gradient and BCG artifacts. (ii) Inside the scanner but without BOLD-scanning. These EEG-recordings can be expected to show only BCG artifacts. (iii) Outside the scanner room thereby providing EEG recordings without any scanner specific

artifacts. These recordings served as a reference for the artifact correction developed in this work.

Generally, each EEG data set consisted of a continuous recording of 10 minutes duration applying the following acquisition parameters: Analog bandpass filtering with cut off frequencies of 0.0016 Hz and 250 Hz respectively, sampling rate per channel 5 kHz, 16 Bit digital resolution with the least significant bit (LSB) representing 500 nV resulting in a dynamic range of ± 16 mV. The amplifier and digitizer box was located close to the subjects' head (distance about 1 m). After digitization the EEG data were transferred out of the shielded magnetic resonance (MR) cabin by a fiber optic cable to a digital signal collecting card (Peripheral Component Interconnect (PCI) bus) of a personal computer (PC) located outside the shielded room. As empirically analysed, the amplifier noise level with grounded input was 1uV (standard deviation (STD)) at the bandwidth specified before. Inside the scanner room, the EEG amplifier box was fixed with band to prevent additional artifacts due to amplifier movements. The power of the amplifier/digitizer box was supplied by a rechargeable Li-battery. Thirty-four electrodes (Ag/AgCl) were placed on the scalp: Twenty-nine electrodes (Fp1, Fp2, F3, F4, C3, C4, P3, P4, O1, O2, F7, F8, T7, T8, P7, P8, Fz, Cz, Pz, FC1, FC2, CP1, CP2, FC5, FC6, CP5, CP6, TP9, TP10 according to the international 10-20-system (Jasper 1958) plus some extensions according to the 10-10-system (Chatrian et al., 1985) used to record EEG data for four of the six subjects. All these electrodes were applied using a textile cap holding the electrodes ('electrode cap'). A further electrode was placed near the right eye to record the electrooculogram (EOG). Two additional electrodes were placed at the subjects back close to the superior and inferior end of the heart to pick up two electrocardiogram (ECG) signals (Ecg1 and Ecg2) later serving as reference channels to support the correction of heartbeat related artifacts such as the cardioballistic artifact. The reference and ground electrodes were placed at the center between Fz electrode and Cz electrode and close to the frontal Fz, Fp1 and Fp2 electrodes respectively. For technical reasons (subject's comfort) a modified electrode setting (F3, F4, C3, C4, P3, P4, PO3, PO4, FC5, FC6, CP5, CP6, F7, F8, T7, T8, P7, P8, TP9, TP10, PO9, PO10, Fpz, Fz, Cz, Pz, POz, Oz, Iz) was used for two subjects. Here, the reference electrode was located between Cz and Pz and the ground electrode was located between Fz and Cz. In all recordings the calibration routine of the EEG recording system confirmed an electrode-skin impedance of < 5K in all recording channels for all subjects. All electrode cables were anchored using small sandbags to prevent movement. Great care was taken to spatially arrange the cable such that the amplifier did not saturate due to excessive artifacts during scanning.

### 4.4 Event related potentials (ERP)

Event related potentials are a standard neuroscientific technique to analyze higher neural functions. In physiological terms, ERPs reflect the brain's specific electrical response to stimulus processing or to other mental processes. Typically their amplitudes are much below the ongoing EEG. Therefore, stimulus locks averaging over a sequence of epochs is needed to extract the underlying ERP from the EEG. One normal ERP is shown in Fig.4.3[1]. Due to their low amplitudes ERP are especially susceptible to artifacts and can thus serve as a sensitive indicator for the quality of artifact removal. This was the motivation to include this modality in our measurements. A set of photos of natural scenes containing a clearly identifiable living (deer, chicken etc.) or non-living (cars, bridges etc.) object was selected from a commercial database (Corel Stock Photo Library). In the scanner the stimuli were projected (JVC DLA-G150CL projector) onto a back-projection screen placed 27 cm in front of the subject's eyes in the magnet bore and were visible by the subject via a mirror fixed to the head coil. Each image was presented for 500 ms, the interval between successive stimuli (inter stimulus interval (ISI)) was jittered between 1sec and 2 sec (mean 1.5 sec). The viewing angle was 26.1° deg (vertical) and 17.4° deg (horizontal). The subjects' task was to discriminate living from non-living scenes and to maintain the eyes fixated on a central fixation cross that was displayed between successive images. After each stimulus subjects gave their response by pressing one out of two possible buttons with the fingers of the same hand. Every 20 presentations a short break was included in which subjects could blink. We recorded 480 trials (i.e. 480 stimuli) for each of the three EEG measurement conditions (two in the scanner, one outside).

Four (three male, average age 25, range 20-27 years) of the six 'EEG-subjects' were included in the ERP measurements. The other two subjects were excluded due to the head motion. The ERP recordings were part of the EEG recording mentioned beforehand.

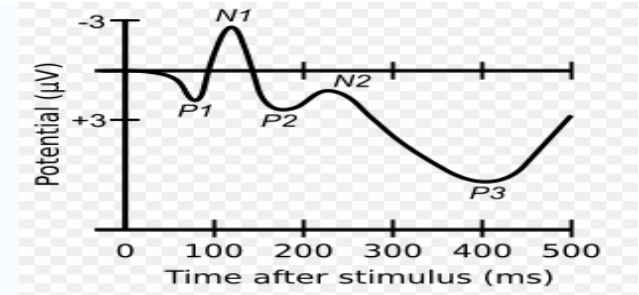


Fig.4.3 Example of a typical ERP[1]: Average specific electrical brain response upon repeated visual stimulation. Various ERP components (P1, N1, P2,…) can be identified being characterized by their latency (with respect to stimulus onset), polarity and amplitude.

[1] http://en.wikipedia.org/wiki/Event-related_potential

# Chapter 5 New movement adjusted algorithm to remove gradient artifacts

## 5.1 Variations of artifact shape as evaluated by phantom measurements

The basic assumption of all subtraction methods proposed so far is that the artifact template is stable over a sufficiently long period. Before modifying the usual subtraction method, the first step of this work was to analyze the variability of the gradient artifact template due to temporal fluctuations and phantom movements (simulating head movements). This issue was assessed by comparing the artifacts observed in the phantom measurements at different times and at different angles respectively (see section 4). The methods and results of these analyses are presented in this section.

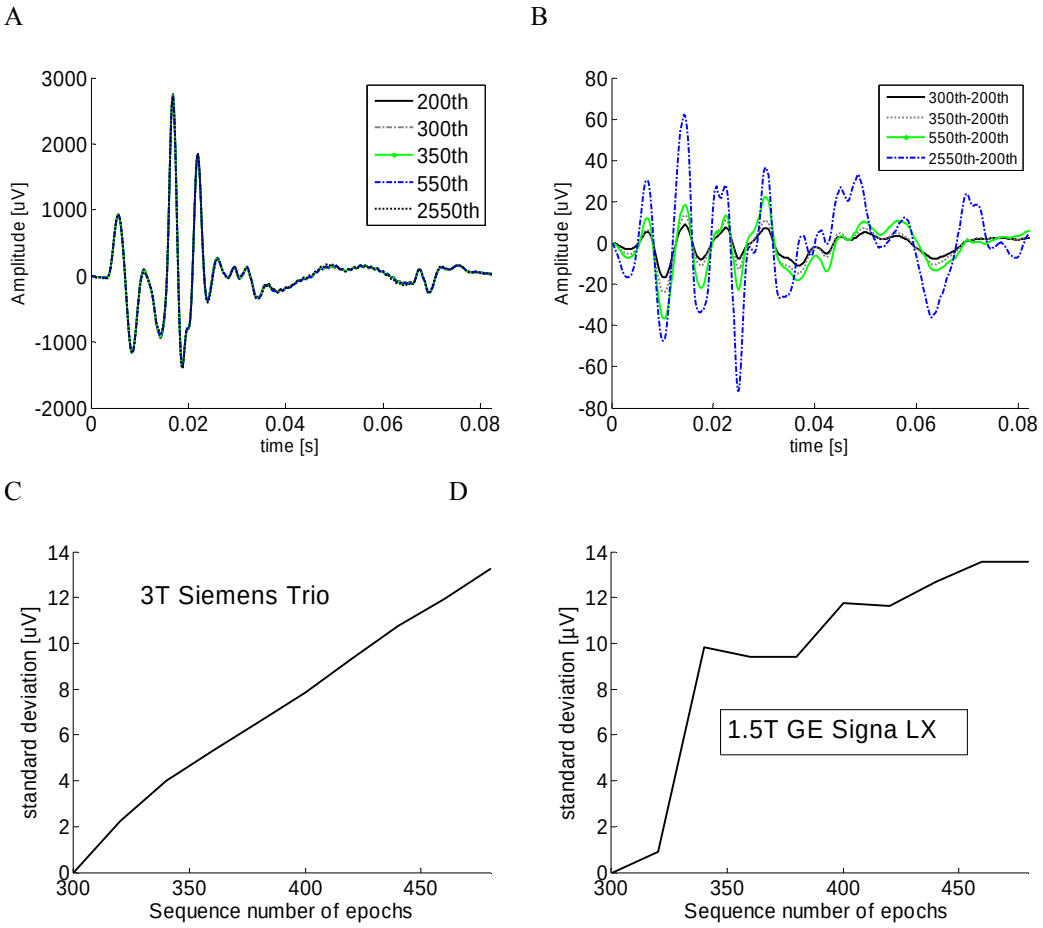


Fig.5.1 Long term fluctuation of artifact observed in the phantom (watermelon) recordings (position 1).
A) The averaged template of 200$^{th}$, 300$^{th}$, 350$^{th}$,550$^{th}$ and 2550$^{th}$ gradient artifact at the P4 electrode.
B) The results of each template subtracting the reference template (which was the 200$^{th}$ template).
C) Standard deviation of the difference between artifact templates estimated at different times spaced by 20 epochs starting at gradient artifact epoch 300 (i.e. the 15th volume) of the first run, each extracted from 50 subsequent artifact epochs.
D) Same as C but different scanner.

Before any processing the artifact signals were filtered by an order 34 FIR highpass filter with 10 Hz cutoff frequency which preserved the components at the gradient repetition frequency (12 Hz for TR 2000 ms and 24 slices per volume) and its harmonic but suppressed low frequency signal fluctuations occurring as a consequence of either changing electrochemical conditions in the electrolyte gel (needed to guarantee a 100 impendence between electrode and surface ) or unstable environment electrostatic fields.

### 5.1.1 Long term temporal instability

Fig.5.1 presents several different artifact templates, all computed as an average over 200 consecutive artifacts but starting at different epoch numbers (i.e. times) (all acquired at electrode P4 (see Fig.4.2) during the first phantom measurement, i.e. before any rotation. The averaged template resulting after the first 200 epochs was taken as the reference. As can be seen in Fig.5.1A, the gradient waveforms obtained at the different time are largely identical. However the differences (see Fig.5.1B) between those templates observed at later times and the reference template show amplitudes which are well in the range of typical physiological EEG waveforms and can thus not be neglected. According to Fig.5.1A the wider two templates are temporally separated the larger is the difference. For example the difference between the two templates averaged at the $2550^{th}$ and the $200^{th}$epoch is much larger than the difference between the averages at the $300^{th}$ and the $200^{th}$ epoch. Among the potential reasons for this temporal instability of the artifact are slight changes in electrode position, subtle change of the magnetic gradient due to warming or thermoeffect at the electrodes.

The standard deviations of differences between the average artifact template(this time averaged over only 50 epochs) obtained for the sequence starting at artifact epoch 300 after the onset of the MR scan and those observed at later epochs are depicted in Fig.5.1C. The data represent the mean over all standard deviation values calculated separately for each channel of the watermelon. Obviously, fluctuations of the artifact's shape occur even over short intervals and tend to increase with longer temporal shifts. Given the 1 μV noise level of the amplifiers (see before), fluctuations can only be neglected for temporal shifts of less than 40 epochs (i.e. 40 slices). That means, that given that 50 artifact periods were included in the current average the number of periods used to extract the artifact template should be kept below 90 artifact periods. Correspondingly, if a weighted average is applied the kernel function should be shaped to focus on this limited number of periods.

One could argue that the temporal fluctuations are a specific issue of just this scanner. However, similar measurements conducted in a second MR scanner (GE signa LX) with a different static magnetic field strength (1.5 T) and supplied by a different company show a

very much comparable variability of the gradient artifact waveform (see Fig.5.1D) thus suggesting that this observation reflects a more general effect.

### 5.1.2 Variability depending on MR-slice

Besides long term variation, the gradient artifacts may also differ in shape depending on the slice number within each volume. To evaluate this potential source of variability, a slice-based averaged method was applied to create slice-specific templates by averaging only over those epochs obtained at the same slice number within the different volumes (i.e., the 1st slice-number template is averaged over all 1st slices in each volume). Fig.5.2 shows the fluctuations of the standard deviations of the subtracted resulting differences between all but the first slice-based templates and the first slice-based template (each slice template averaged over all volumes). These results clearly show that the between slices differences of the gradient artifact are negligible given the amplifier noise level of about 1 µV STD. Obviously, the long term variability by far exceeds the slice-dependent variation.

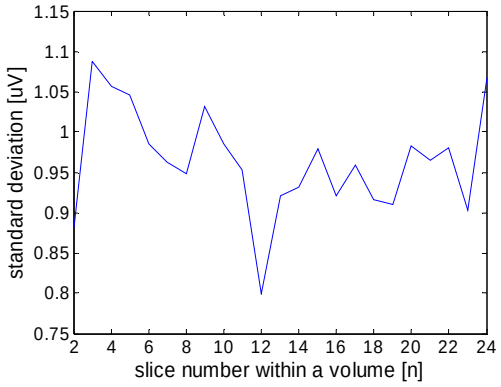


Fig.5.2 Test of slice-specific averaged template conducted with the data recorded with the phantom (watermelon, position 1, electrode Cz): The std of difference between all but the first and the first slice in one volume. The alignments between all epochs used to generate the slice-specific templates were assembled applying the resampling technique (see section 5.3.4.3).

### 5.1.3 Variations due to electrode movements

Next, unavoidable head movements were analysed as potential sources of artifact template variations. For this purpose we recorded phantom EEG signal at four different phantom orientations (See Fig.4.2) in order to measure the influence of the electrode positions on the template. During this experiment, the phantom was rotated by a fixed angle increment between consecutive recordings. During each recording its position was fixed by a hard plastic block as shown in Fig.4.2. The rotated watermelon simulates the head motion of the subject along y-direction. Regarding electrode P4 (See Fig.4.2) which was evaluated here, the displacement per rotation step was about 0.5 mm in the vertical (i.e. y) direction resulting from a 2.4 mm displacement in tangential direction which is comparable to a realistic strong

head movement. A representative template for each position was derived by averaging over 200 consecutive gradient artifacts waveforms. The resulting templates are shown in Fig.5.3 for the four different phantom positions. Although the phantom was rotated by a slight degree, the electrodes may be rotated with a different degree (more or less). Therefore, the different channel shows the different changes for the four positions in Fig.5.3A and 5.3B. Obviously, at these slight rotations the artifact templates significantly change their shape giving rise to the idea of including head movement information in the algorithm to extract the subtracted template.

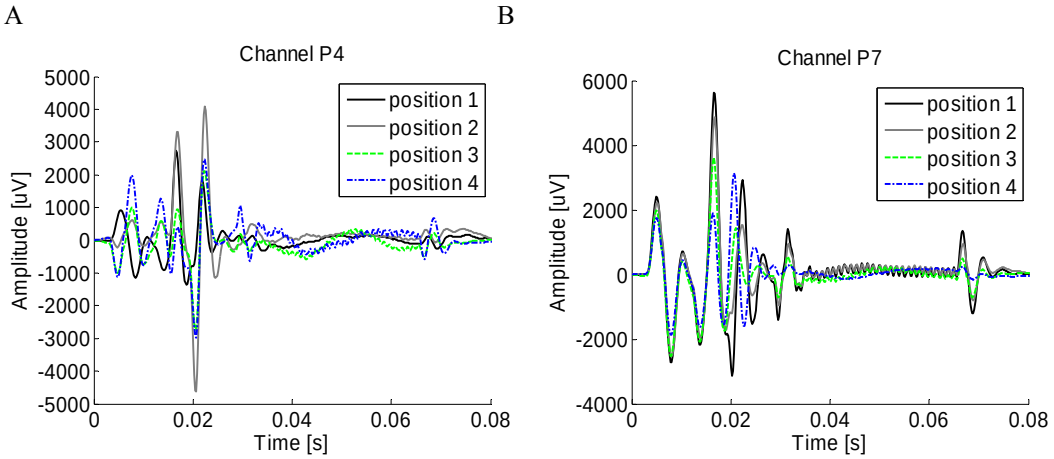


Fig.5.3 Artifact waveform as recorded in the phantom (watermelon) recordings in four different positions. Each separated by a rotation of 2 degrees, keeping the absolute position within the MR bore.
A) The pattern at the P4 electrode (see Fig. 4.2)
B) The pattern at the P7 electrode

## 5.2 Deriving a head movements indicator

It is impossible for subjects to stay motionless during the whole scanning period. Having in mind the motion-dependence of the artifact shape, it is necessary to design an additional system to track the head motion as a premise for a motion guided artifact removal concept. This system will help us locate the relative position of electrodes accurately and subsequently classify and average the gradient artifacts according to electrodes position in order to achieve the least error of the residual gradient artifacts. An eye tracker system (Kanowski et al., 2007) can be modified to serve as such a tool (see section 5.2.2 (below) for details) but it needs some extra hardware parts which usually not available in MR laboratories. Another method, using the alignment function of the freely available statistical parametric mapping (SPM) software package can replace the procedure of the hardware movement tracking.

SPM was developed by the Functional Imaging Lab (FIL) London for (i) image preprocessing and (ii) statistical analysis in the context of functional imaging (either fMRI or positron emission tomography (PET)). In the case of fMRI analysis the sequence of BOLD

images must be realigned (with respect of the first image which serves as a reference) before any further analysis to correct for movements during image acquisition. This alignment is performed by shifting each image in all three dimensions and by rotating it around all three axes (in total 6 degrees of freedom). The shift and rotation values for each image are stored in a log file and can be used as a motion indicator for any further purposes.

However, it is worth to note that this method only provides a coarse temporal resolution plus a time delay because the motion can only be analyzed after each half volume assuming an interlaced acquisition where first all even images and the all odd images (or vice versa) are acquired. The resulting resolution thus is TR/2. See the next section for details.

A

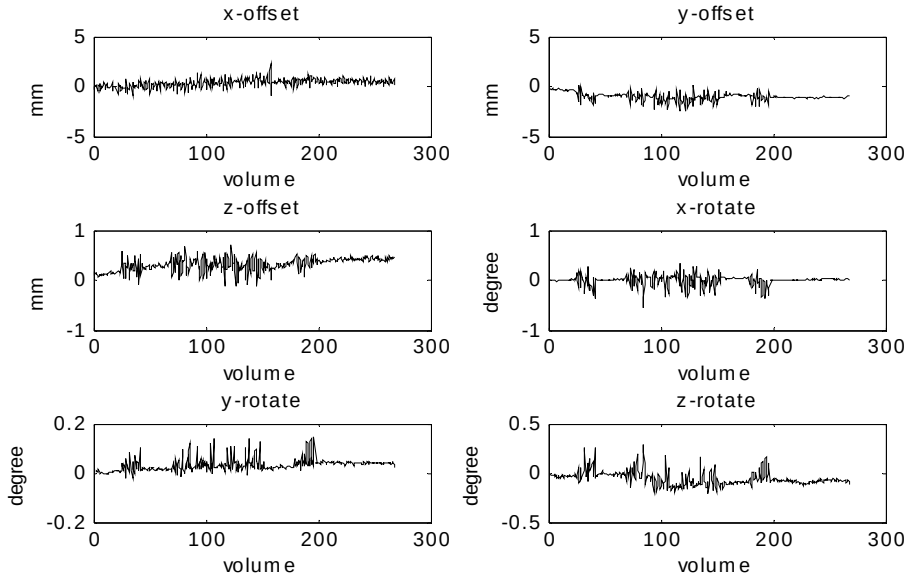


B

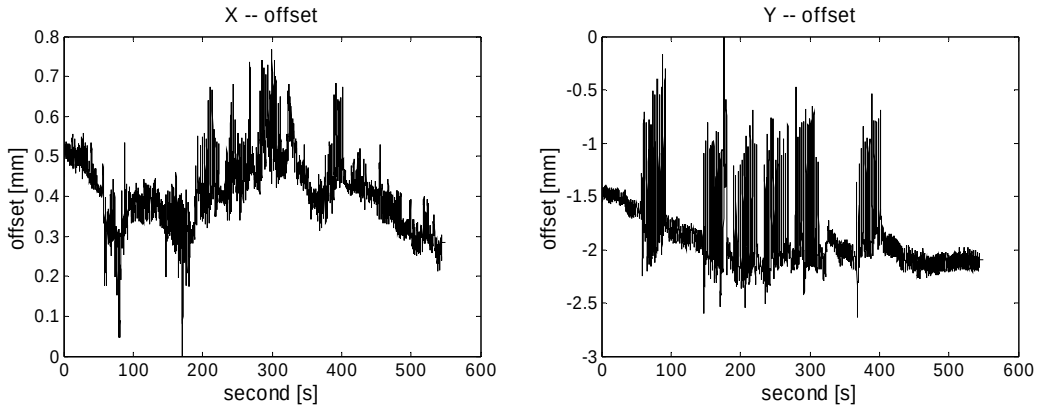


Fig.5.4 Tracking data with different methods:
A) Tracking data on all six degrees of freedom with SPM alignment.
B) Tracking data (x- and y-direction) with the eye-tracker (Fig.5.5).

### 5.2.1 SPM movement vector: low temporal resolution

The realignment routine (spm_realign.m) of the SPM software (see Friston KJ, et al., 1995) was used as the core of our alignment as follows and a typical example of head movement trace extracted by this algorithm shown in Fig.5.4A.

fMRI volume realignment procedure (Algorithm 5.1)
1. Specify the reference volume. Usually, it is the first volume.
2. Load the data of the reference volume.
3. Loop for all subsequent volumes
   3.1. Load the next volume.
   3.2. Compute the current set of realignment parameters (spm_realign.m).
   EndLoop until all other volumes has been done.

Half volume alignment procedure (Algorithm 5.2)
1. Split each volume into two new volumes. Each new volume is half of the full volume and consists of odd or even slices of one volume.
2. Use Algorithm 4.1 for these new volumes.

This technique minimizes the sum of squares between two images following nonlinear spatial deformations and transformations of the voxel (intensity) values. The spatial and intensity transformations are obtained simultaneously, and explicitly, using a least squares solution and a series of devices. The approach is completely noninteractive (automatic), nonlinear, and noniterative. It can be applied in any number of dimensions.

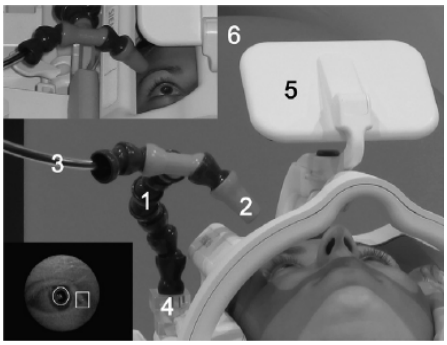


Fig.5.5 The real case of applying eye-tracker during fMRI scanning.
Photo of the video eye-tracker (temporal resolution 40 ms).
Numbers indicate the: (1) flexible positioner, (2) lens, (3) fibre optical cable, (4) dovetail connection to the headcoil, (5) mirror, and (6) rear projection screen.

### 5.2.2 Video-eye-tracker: high temporal resolution

A higher temporal resolution of the movement tracking can be achieved by a device that directly measures the head movement by means of a slightly modified video-based device which was originally developed by Kanowski et al. (2007) to track eye movements during fMRI measurements. A camera is placed at the head coil close to the subject eyes, see Fig.5.5A. It is used to monitor the head motion by tracing one a mark fixed on the forehead. When the head moves, this video system (including an image processing software constantly

identifying and thus tracing the mark) can record the magnitude of head motion and easily indicate the different positions of the subject's head with x and y axis (see Fig. 5.4B) offset.

## 5.3 New movement adjusted moving average subtraction (MAMAS) algorithm

### 5.3.1 Basic method of weighted averaged subtraction: Is the residual EEG negligible?

The basic assumption of the subtraction method is that the gradient artifacts are superimposed on the true EEG and that the artifact shape is stable and can be extracted by an appropriate averaging method. As illustrated in Fig.5.6, the signal (data vector) $X_i$ observed in channel $i$ (i.e. at electrode $i$) and consists of a number of $l$ samples is a superposition of the true EEG- and the gradient artifact- as follows:

$$X_i = \{x_j^i \mid j = 1,2,...,l\} = A_i + EEG_i = \{a_j^i \mid j = 1,2,...,l\} + \{eeg^i{}_j, j = 1,2,..l\} \qquad (5.1)$$

where $EEG_i$ represents the artifact-free EEG and $A_i$ the artifact waveform.

Given this assumption, the true artifact template can be extracted from the ongoing measured signal by averaging over a sufficient number of artifact epochs thereby suppressing the underlying EEG because it is not correlated with the artifact.

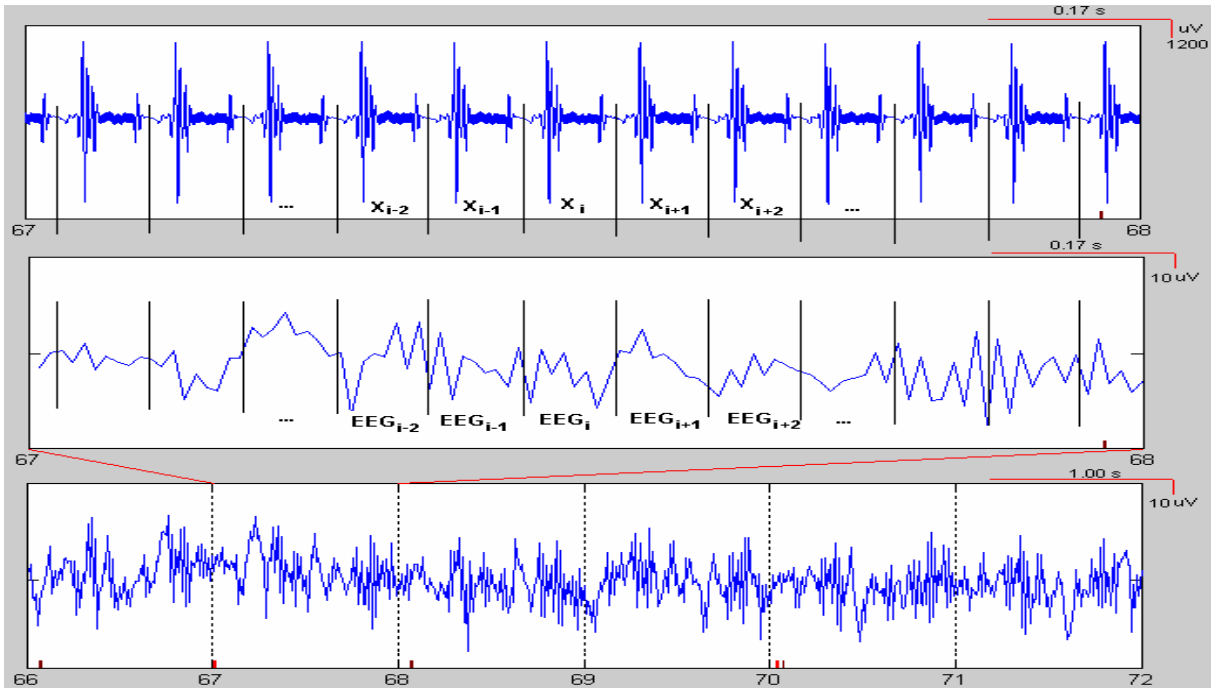


Fig.5.6 Vector representation of true EEG and artifact contaminated EEG (X):
Top: EEG contaminated with gradient artifacts contaminated; a complete artifact epoch labelled as $X_i$ with $i$ representing the epoch's running index.
Middle: Same signal after removal of artifacts with $EEG_i$ representing these true EEG epochs.
Bottom: Same EEG at a different time scale as used in clinical practice.

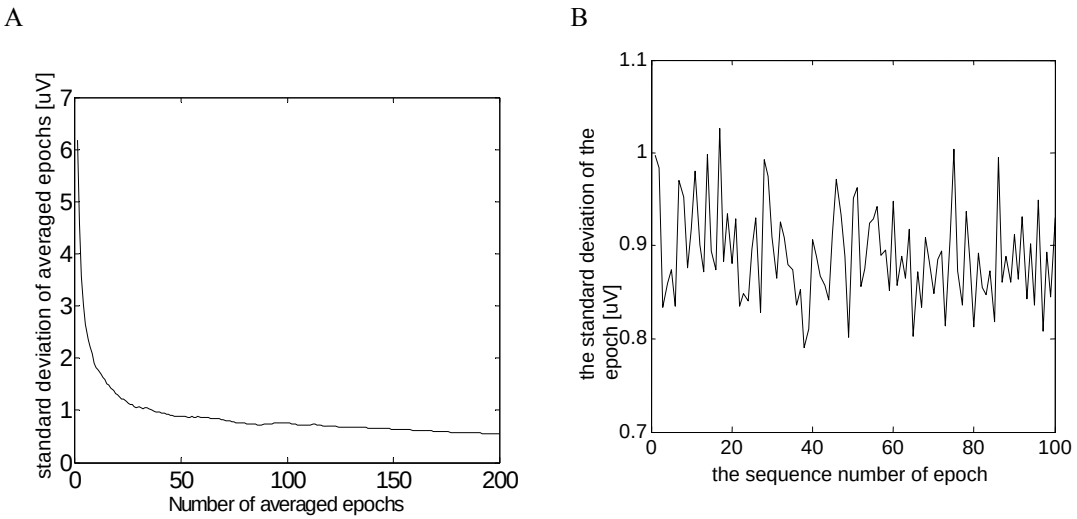


Fig.5.7 Estimation the number *N* used for averaging:
A) Decrease of the standard deviations of human EEG (recorded outside scanner) with increasing number of averaged epochs, averaged over six subjects and 29 channels; each epoch of duration 80 ms.
B) Typical values of the technical noise standard deviation of 80 ms-epochs which was observed in a channel of the EEG amplifier with all input shortened.

The assumption of the EEG to be suppressed by the averaging procedure implicitly assumes that the mean over a sequence of EEG epochs tends to zero with an increasing number *N* of included epochs for all channels. However, in reality, since *N* is limited, a zero-mean EEG can only be achieved within a certain residual range. The question then is to determine a minimum *N* that leads to a residual EEG with a standard deviation that stays below the intrinsic noise of the measurement equipment.

In order to evaluate the general validity of this hypothesis in practice and to determine the minimum number of epoch needed to get the residual EEG down below the technical noise floor we derived the residual EEG as observed in the EEG recorded outside the scanner (i.e. without gradient artifacts) after averaging over a limited number of epochs as follows: assuming the weighted epoch averaging algorithm that was applied in this work (see Fig.5.8A; weighting profile taken from Beck et al., 2005) with weighting factors *w(i)* the standard deviation of the average conducted over all channels, all recordings and all epochs result as follows.

$$\frac{1}{S \cdot C} \sum_{s=1}^{S} \sum_{c=1}^{C} std \left( \frac{1}{\sum_{n=1}^{N} W(n)} \sum_{n=1}^{N} W(n) * X_{scn} \right) \tag{5.2}$$

where *C* is number of channels included, *S* is number of subjects included. Here $X_{SCN}$ represents the $N^{th}$ epoch of channel *C* and subject *S*. According to Becker et. al. (2005) we here applied the weighted exponential function, $W(n) = w^{|n-i|}$ as a weighting function, where *w* is 0.9, *n* is the position of one epoch within the moving window and *i* is the center of moving window.

As demonstrated in Fig.5.7A the standard deviation of the averaged EEG-epochs asymptotically decreased with increasing *N*. Each epoch's duration was 80 msec and the first epoch started 2 min after recording onset. With respect to the weighted subtraction method the main result is as follows:

For $N > 50$ the standard deviation of the residual EEG activity (acc. to eq. 5.2) stays below 1 µV which well compares to the average amplifier noise level observed with shortened inputs, see Fig.5.7B. Taking together this finding and the result from section 5.1.1 regarding the temporal instability of the artifact waveform the weighted moving average procedure (using the Becker-window profile) is justified if the weighting function focusses on not more than 90 epochs. With this in mind a set of 4 weighting functions (see Fig.5.8A) were evaluated, all extending in total over 120 epochs and focussing (width at half maximum) on not more than 90 epochs. In addition, the rectangular window with the same width of 120 epochs was included for comparison.

### 5.3.2 Comparison of different window functions

To study the effects of different weighting functions on the efficiency of the artifact removal, the moving averaged subtraction method was applied five times on the same randomly selected sequence of 120 epochs. Each time using another one out of the following five different profiles (see Fig.5.8A): Rectangular, square root, linear, square, exponential (i.e. Becker-type). The reduction of spectral components at the gradient repetition frequency and its harmonics served as a quality criterion (Fig.5.8C and D). A more efficient removal will result in a stronger decrease of these spectral peaks. Visual comparison of the EEG after artifact removal with different weighting functions was used as an additional subjective criterion.

A B

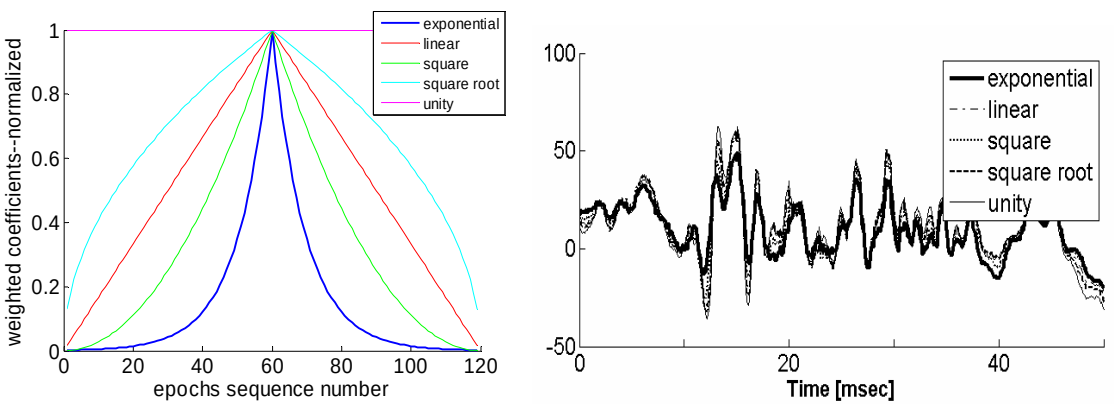

C D

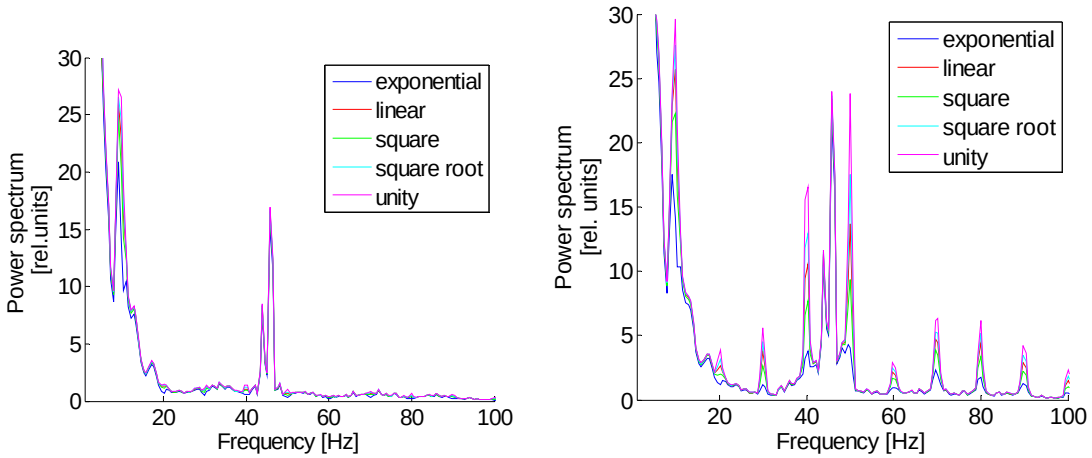


Fig.5.8 Evaluation of different weighting profiles.
A) Evaluated weighting profiles.
B) Short term EEG-epoch after removal of gradient artifact using the MAS algorithm with the various weighting profiles.
C) Power spectrum averaged over 10 consecutive short term spectra (each estimated from 6-sec-EEG segments) and averaged over all 29 EEG channels; typical example during mild movement.
D) Same as C, but obtained from 10 other EEG segments recorded from the same subject during strong movement.

### 5.3.3 Reduce the influence of head movement by introducing the moving average artifact

Assume the additive superposition model of the EEG and the artifacts as formalized in eq.5.1 (section 5.3.1) rewritten in eq.5.3.

$$X_i = EEG_i + A_i \ , \ i=1, 2, ..., N. \tag{5.3}$$

The algorithm to extract a weighted average template according to the procedure introduced by Becker et al., 2005 may be written as

$$\sum_{i=1}^{N} w_i X_i = \sum_{i=1}^{N} w_i EEG_i + \sum_{i=1}^{N} w_i A_i \tag{5.4}$$

With $i$ denoting the artifact epoch and $w_i$ representing the weight assigned to the individual epoch.

The weighted average over this sequence of $N$ subsequent epochs is

$$\frac{1}{\sum_{i=1}^{N} w_i} \sum_{i=1}^{N} w_i X_i = \frac{1}{\sum_{i=1}^{N} w_i} \sum_{i=1}^{N} w_i EEG_i + \frac{1}{\sum_{i=1}^{N} w_i} \sum_{i=1}^{N} w_i A_i \tag{5.5}$$

As shown beforehand (Fig.5.6A) the first term, i.e. the residual EEG, is negligible for sufficiently large N so that eq.5.5 reduces to

$$\frac{1}{\sum_{i=1}^{N} w_i} \sum_{i=1}^{N} w_i X_i \cong \frac{1}{\sum_{i=1}^{N} w_i} \sum_{i=1}^{N} w_i A_i \tag{5.6}$$

If the artifact waveform is stable over time, i.e. if $A_i \approx A_j = A$ for arbitrary *i* and *j*, then

$$\frac{1}{\sum_{i=1}^{N} w_i} \sum_{i=1}^{N} w_i X_i \cong \frac{1}{\sum_{i=1}^{N} w_i} \sum_{i=1}^{N} w_i A \tag{5.7}$$

Therefore, $$A_i = A_j = A = \frac{1}{\sum_{i=1}^{N} w_i} \sum_{i=1}^{N} w_i X_i \tag{5.8}$$

By substituting eq.5.8 into eq.5.3, we obtain the $j^{th}$ EEG epoch:

$$EEG_j = X_j - \frac{1}{\sum_{i=1}^{N} w_i} \sum_{i=1}^{N} w_i X_i \,, \tag{5.9}$$

that is, the EEG can be fully retrieved. Unfortunately, in practice the artifacts are not perfectly equal each time for various reasons, among them are: (i) missing synchronization of the EEG-sampling and the MRI clock (Cohen, et al., 2001), (ii) slight electrodes movements, and (iii) systematic changes over time as shown in section 5.1.1.

Bearing in mind the strong movement related changes of the artifact's waveform reported in section 5.1.3, one possible reason of differences occurring between gradient artifacts observed in real EEG recordings could be the change of electrode positions caused by head movements. These movements occur in the presence of a magnetic field lead to an additional change in magnetic flux thus leading to an induced voltage which changes the artifact waveform.

### 5.3.4 Movement adapted moving averaged subtraction method

Fig.5.9 outlines the basic idea of extracting the individual template of each epoch for the old method (MAS) and our new method (MAMAS). Our MAMAS method is a modified version of MAS method (Becker et al., 2005) which derives one average template for each individual gradient artifacts by means of a weighted moving average window and subtracts it from each individual artifact (later in this manuscript labelled as the 'reference artifact'). In contrast, our method accepts only those artifacts for the averaging procedure which were obtained at a similar head position and orientation. As a consequence residual differences after subtraction are minimized because differences between the reference artifact and each of the artifact epochs include in the average are minimized. The momentary head position is extracted from the SPM-realignment procedure so that no extra hardware is needed to identify the head position. This new approach is complemented by a new method that eliminates the influence of the phase jitter between EEG and MR system (Schmid et al., 2006) (after the data have been sampled, i.e. without changing the sampling device) by means of a time shift correction (resampling). Finally, an additional procedure has been developed to reduce

residual artifacts remaining in case of brief fast movements (not adequately detected by the SPM with its temporal resolution of 1 sec) after the MAMAS procedure. The outline of this method is described in algorithm 5.3.

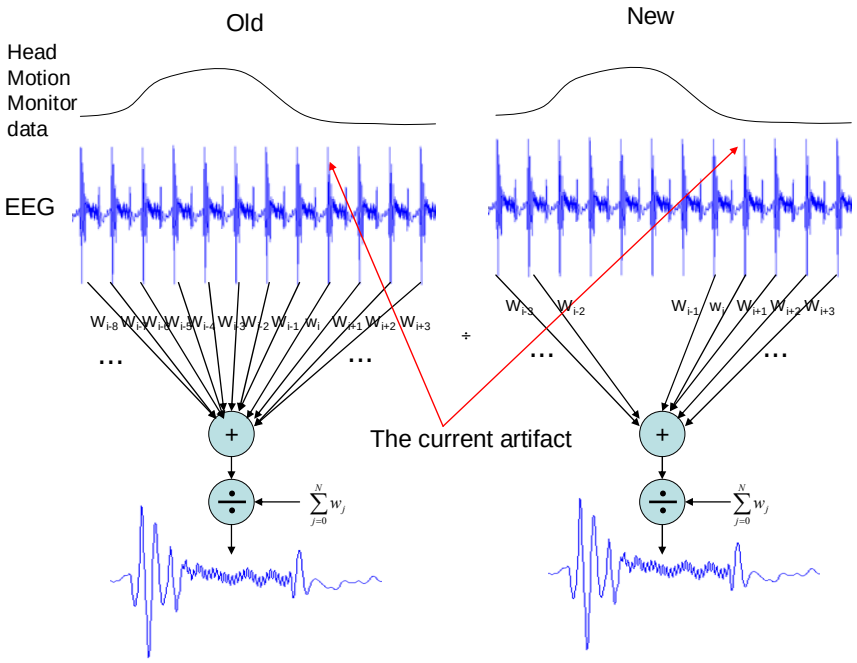


Fig.5.9 Schematic diagram of MAS(old) and MAMAS(new) GAR removal methods

MAMAS (Algorithm 5.3)

1. Detect onsets of gradient artifacts.
2. Class gradient artifacts into different levels guided by SPM-head motion monitoring data.
3. Create for each individual gradient an individual average artifact template by averaging over epochs obtained at the same head position levels. The resampling technique is applied to each epoch.
4. Subtract the individual template from the corresponding gradient artifact.
5. Detect residual gradient artifacts occurring in case of brief motion.
6. Apply the special algorithm to reduce this residual artifact.

### 5.3.4.1 Detection of gradient artifact onsets

The number of samples ($l$ ) per artifact epoch can be directly determined from the MR-repetition time ($TR$), the number of slices per volume ($nsl$) and the EEG sampling frequency ($fs$) according to the following rule:

$$l = \frac{TR}{nsl} \cdot fs \tag{5.10}$$

With this number one could in principle predict the onsets of all artifact epochs once the start of the first epoch has been determined. However, in practice this leads to inaccuracies since the TR value is only known with limited precision leading to a shift of several samples between theoretical and effective onsets of the artifact epochs (see also Goncalves et al. (2007a) for further discussion of this issue). In addition, as already described in section 3.1, the missing synchronization between the EEG sampling clock and the MR-timer causes an

additional alignment error ('phase jitter'). As a consequence the onsets of the artifact epochs need to be determined before any further processing.

The purpose of the first part of this algorithm (described in the current section) is the alignment of the artifacts keeping an accuracy of on sampling whereas the adjustment of asynchronous clock errors will be addressed in the over next section 5.3.3 introducing a new resampling technique.

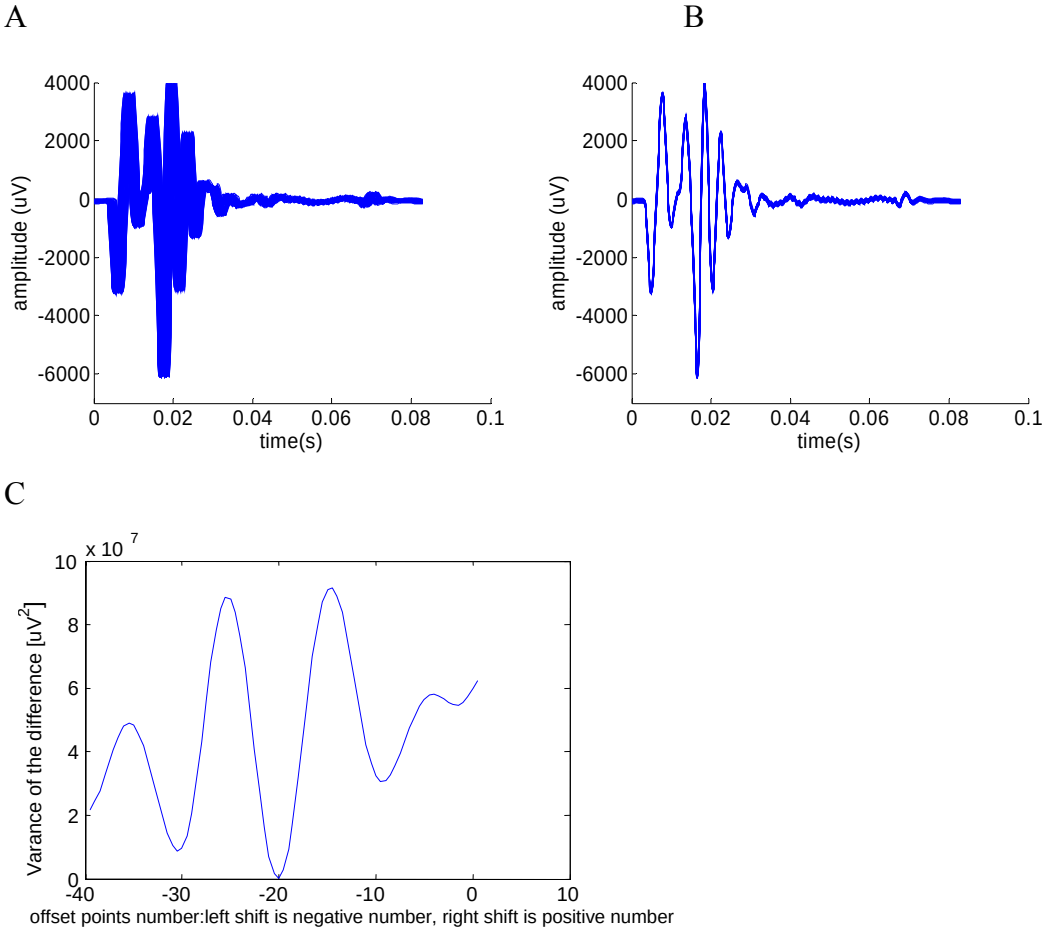


Fig.5.10 Adjustment of the gradient artifact onsets with respect to the MRI triggers: (subject km42).
A) Overlay of 50 gradient artifacts according to the MRI triggers.
B) Adjustment these onsets with algorithm 5.4.
C) Variance observed at different shift intervals.

In the following two alternative methods will be described to determine and adjust the artifact epochs. The first method uses a trigger signal provided by the MRI to indicate the acquisition of the next slice. If this MRI trigger is available (which is the case in the scanner used here), the gradient artifact onset can be retrieved directly using the markers recorded simultaneously with the EEG. However, an additional realignment algorithm is needed to cope with the fact that in practice a tiny jitter occurs between the effective onset of the artifact and the trigger (see Fig.5.10A). For this purpose the onsets are adjusted by calculating the variance of the difference between the reference artifact, usually the first one, and all other

artifact at different lags. The best fitting lag (that is the additional shift for a precise alignment) is determined as the value achieving the minimum difference variance, see the description of algorithm 5.4 below. For an example of the variances observed at different lags see Fig.5.10C, the result of the realignment procedure is demonstrated in Fig.5.10B.

Locate artifact onsets (Algorithm 5.4)
Assume two artifacts. One is as the reference artifact (usually the first one) and the other is as the working artifact to be realigned ('working artifact'). The latter will be shifted to the left or to the right by one sample continuously. The maximum offset is specified by pre-setting the OFFSET variable to 40 (8ms).

1. Compute a series of variances
   For i= -OFFSET:OFFSET
      The working artifact shift i samples.
      The difference = the reference one – the working one;
      Variance (OFFSET+i) = cov( difference);
   Endfor
2. Return the best onset being relative to the minimum of variances.

The second method does not rely on the availability of a slice time trigger, but exploits the fact that the artifact amplitudes exceed the regular EEG amplitudes by far (typically by more than a factor of 50). This allows a rough determination of the artifact onset by a simple threshold criterion which was set to 1000 μV. The precise alignment is then performed by means of the optimization procedure described before. In the following this second method was applied since the goal was to develop the artifact removal method as simple as possible regarding hardware requirements.

### 5.3.4.2 Position dependent artifact averaging.

Without loss of generality, the z axis of MR scanner (see Fig.5.11) is parallel to the direction of the static magnetic field and thus roughly coincides with the direction extending from the subject's foot to the head. The x- and the y-axis are parallel to the left-right and the vertical direction respectively. Due to the geometry of the head coil (including fixating measures like foam pads etc.) the head movement is widely restricted to rotate around the x axis. Thus a movement-sensitive algorithm should either focus on the rotation angle around the x-axis or on the y-displacement caused by this rotation. In this work the y-displacement (later also called 'y-offset') was used because the fast video based eye tracker (which was used for one detailed analysis, see below) is unable to directly trace rotations. The y-values provided by the SPM alignment routine can be directly taken as the y-displacements since the two coordinate systems only marginally differ from each other (see Fig.5.11).

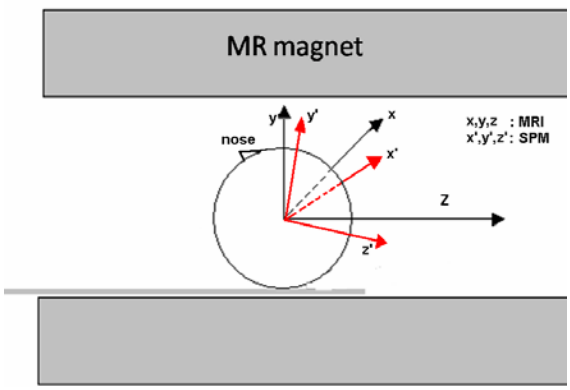


Fig.5.11 Coordinate systems of the MRI device and of SPM.

A B

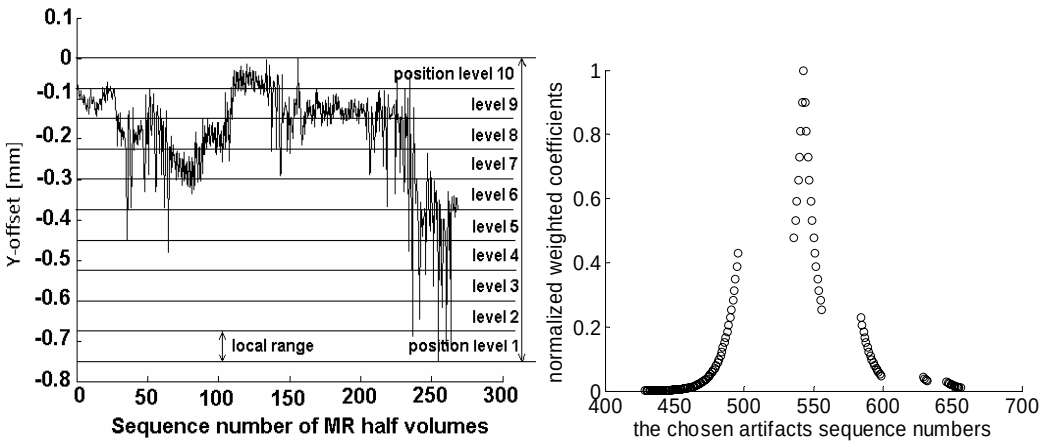


Fig.5.12 Examples of SPM-movement indicator and the selection of epochs
A) SPM-movement data, y-direction (subject nc92). This is an example of a strongly moving subject. In case mild movements the displacement range stays below 0.1mm.
B) Selection and weighting of gradient artifact epochs included in the average. The selection depends on the y- positions with the exponential weighting coefficients applied to the included epochs.

The aligning function of fMRI analysis in SPM provides the head motion information in terms of six degrees of freedom (three offsets along three directions, three rotations). An example of the y-offset trace observed during a full fMRI run is given in Fig.5.12A. With respect to the movement adjusted algorithm, the difference between the maximum and the minimum of the y-offset-trace ("total range" of movement) is divided into several small ranges by equal division. Each small range is named "local range" and represents one position level. Given that even displacement of only 0.5mm lead to substantial change in the artifact template (see Fig.5.3), we required the local range to be not larger than 0.1 mm. Therefore, the number of local range was adapted to the global range to meet this constraint. Typically, 10 local ranges were needed to cover the global range, for a representative example see Fig.5.12A. Since SPM derives the movement data from the individual fMRI volume-images, each point represents one volume (2 sec, corresponding to 24 or 20 slices and thus to 24 or 20 gradient artifacts) or half volume (12/10 gradient artifacts) if fMRI uses interleaved scanning

splitting the volume into two half volumes (corresponding to all even and odd numbered slices) before aligning. This low sampling rate is adapted (i.e. upsampled) to the gradient repetition rate by cubic spline interpolation. Next all gradient artifacts are classified into one of the appropriate local range according to their y-offset. When the number of artifacts in one level is below 200, the actual level is combined with the next larger or lower one to build a new local range. This action transforms the uniform division into a non uniform distribution of the local range width. This case often occurs at the fringe of the global range because the number of epochs observed at the maximum and minimum local ranges is usually by far not sufficient for the averaging procedure. Finally, the moving average window includes only those artifacts which pertain to the same local range as the artifact to be removed.

When classification into levels is finished, the averaging procedure to generate a template must obey the following three conditions. (i) The number of artifacts should be at least 50 in order to keep the residual EEG below noise. (ii) The included artifacts should be temporally located close to the current individual artifact to be removed by subtraction. The maximum accepted distance is 200 epochs. (iii) If at least 50 epochs pertaining to the same local range as the reference artifact is available within the 400 epoch-interval, then those at least 50 epochs (up to 120) are averaged applying the Becker weighting profile. However, if there are less than 50 within local range of the reference artifact, epochs pertaining to adjacent local ranges are accepted as well still applying the weighting function as shown in Fig.5.12B.

Schematic description of the selection algorithm (Algorithm 5.5)

1. Place the moving window (width is *wd*) such that the center of this window is the current – to be removed - artifact and the current levels($l_1$ level and $l_2$ level, $l_1 = l_2$) are the level of the current artifact.
2. Find artifacts which are in current levels (local ranges) in that window.
3. If *a* artifacts have been found, go to 7.
4. If the width of the current window is four times of the original one, go to 6. Otherwise go to 5.
5. If less than *a* artifacts have been found in the current window, then the width of the window is extended to *4*wd*, go to 2.
6. If the width of the window has been extended to four times of the original width and the number of artifacts is less than *a*, then set $l_1 = l_1 - 1$ and $l_2 = l_2 + 1$, reset the width of window to *a,* go to 2.
7. end

### 5.3.4.3 New resampling procedure to align sampling time of averaged artifact template

Given the large amplitude and its steep gradients of the artifacts under consideration, a missing synchronization between the EEG sampling clock and the timing of the gradient switching can lead to substantial residual artifacts after subtraction, unless each artifact included in the average is resampled to match precisely the phase of the sampling points of the artifact to be removed (‘reference artifact’). Resampling here means the calculation of data samples at a predefined shifted grid of virtual sampling times. It has been proposed that

this problem can be solved by massive oversampling of the signal (Becker et al., 2005) and subsequent alignment guided by cross correlation. Others (Allen et al., 2000) have resampled the EEG synchronously with the slice timing trigger by means of interpolation techniques. Recently, an electronic solution for the synchronization of the MR scanner and the EEG digitizer clock has been introduced by a commercial company (*Brain Products*, Munich) thereby providing a simple way to capture the true waveform at precisely the same relative sampling times as the reference artifact. Goncalvez et al. (2007a, 2007b) addressed this issue in the context of their approach of iteratively optimizing the MR-sequence parameters (time/volume, time/slice, onset delay before first slice) measured in 'EEG-time'. Since in the actual MR environment a trigger is available at the beginning of each volume, there was no need to run this computationally costly procedure. Instead, a software approach was developed that avoided *up*sampling but appropriately *re*sampling each artifact that is included in the average to precisely match the timing of the samples that represent the reference artifact. This technique broadly resembles the electronic solution and the approach of Allen et al. mentioned above, but is additionally capable of tracking potentially spurious jitter that might occur during the MR slice acquisition. The new algorithm is also computationally more efficient than that employed by Becker et al., (2005), and Goncalvez et al., (2007a, 2007b).

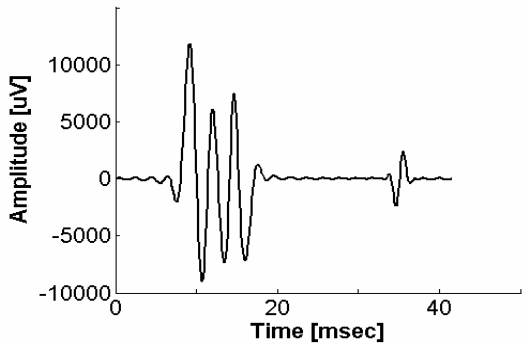


Fig.5.13 Shape of the digitally simulated gradient artifact waveform.

The resampling algorithm derives for each artifact an individual temporal adjustment of the signal sampling by the application of a cubic spline interpolation scheme, i.e. it determines sampling times and corresponding amplitude values best matching the sampled reference artifact which is to be removed. For reasons of computational efficiency, the precision of this procedure should be kept at the lowest acceptable limit, and the search algorithm that determines the best adjustment should be optimized.

To develop and test an appropriate algorithm a closed form model (see Fig.5.13) was constructed to simulate the gradient artifact according to eq.5.11,

$$SART = 1200\sum_{k=1}^{20} A(k)\left[\sum_{n=0}^{2} b(n)\sin(2\pi k f_b(t-0.01-0.005n)) + 0.2\sin(4\pi k f_b(t-0.06))\right] \quad (5.11)$$

with $f_b=ns/TR$ as the gradient repetition rate, $t$ representing the time, $b$ as a vector of coefficients used to adjust the artifact shape (predefined as {-1,-0.8,-0.6}). The weighting factors $A(k)$ were derived from the center period of the sinc-function (defined as $sin(x)/x$) and are specified as {0.11, 0.23, 0.37, 0.50, 0.64, 0.76, 0.86, 0.94, 0.98, 1, 0.98, 0.94, 0.86, 0.76, 0.64, 0.50, 0.37, 0.23, 0.11}. The amplitude was set according to the largest peak amplitudes observed in real gradient artifacts. The waveform represented by this function was digitized by taking the amplitude values at temporal grid positions determined by a 5 KHz sampling rate. Thirty variants of this digitized reference template representing 30 asynchronously sampled artifact epochs were generated by introducing random phase shifts that were equally distributed over the original sampling interval (being normalized to 1 in this representation).Next, each of these artifacts was resampled by applying cubic interpolation to calculate new samples at a grid of sampling points spaced by the original normalized sampling interval $dt=1$ (corresponding to 0.2 msec) but shifted by an interval $st$ (Fig.5.14). For each artifact template $st$ was individually optimized with the goal of minimizing the standard deviation between the samples of the actual and the reference template, but constrained by a limited precision (step size) $\delta t < dt$ (see algorithm 5.6 below). This procedure was repeated as the resolution $\delta t$ was improved stepwise from $\delta t=0.1$ *(i.e. 0.1 * dt)* to $\delta t=0.0001$ (see algorithm 5.8 below). The cutoff point to determine the minimum resolution $\delta t_{opt}$ needed for an adequate resampling was set to that value of $\delta t$ where both the standard deviation and the maximum difference stay below the EEG amplifier noise level, so that the pulsed structure of the artifact was taken into account.

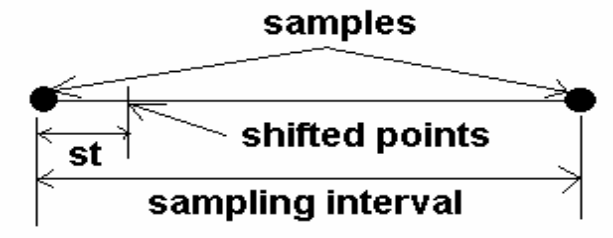


Fig.5.14 The relationship between st and the sampling interval dt.

The resampling algorithm was computationally optimized with respect to the artifact removal algorithm by starting with a coarse resolution, optimizing $st$ for this setting and subsequently repeating this step with decreasing values of $\delta t$ down to $\delta t_{opt}$.

The criterion to find the optimal $\delta t$ is to calculate the minimum variance of the difference which is identical to calculate the maximum cross correlation to determine the shift interval (the shifted distance between the accurate onsets of two epochs). If the shift interval is more

than one unit, the result is improved after alignment between artifacts with a precision of multiples of the sampling interval. But a precise alignment with a sub-sampling interval precision can improve the result even more as sketched in Fig.5.15 showing a case of two artifacts being misaligned by less than one sampling interval. In this case a further shift by *dt1* would certainly lead to a better result than a shift by a full sampling interval. However, even if inside one epoch, there are alignment errors between different peaks. It could happen that some peaks achieve smaller errors but others show larger errors. To balance this effect over all peaks of the gradient artifact, the minimum variance of the difference between the artifact epochs is calculated before and after shifting to find the optimum shift interval for the resampling method.

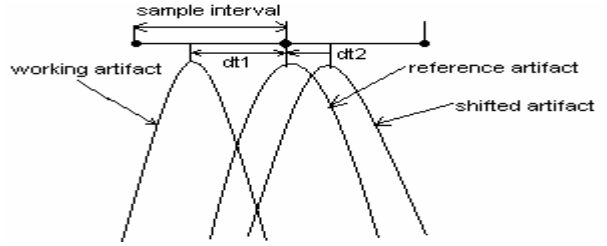


Fig.5.15 Alignment without resampling. The dots indicate the sampling times. A sub-sampling interval *dt1* would be needed for an optimum alignment. If shifted by a full sampling interval the working artifact would be m is aligned by an interval *dt2*.

Schematic description of the resampling procedure (Algorithm 5.6)
Assume two artifacts, one is as the reference artifact and the other is called the working artifact to be shifted with different shift intervals.

1. After shifting the working artifact by a tiny interval (0.1μs) the correlation coefficient between the shifted working artifact and the reference is computed.
2. Repeat step 1 until the minimum variance of the difference between the reference artifact and the working artifact with varying-shift-interval has been achieved. The corresponding shift interval is kept as the result.
3. All channels data are resampled with that shift interval with spline interpolation.

Due to the inaccurate onsets of gradient artifact exacted according to MRI trigger, shown in Fig.5.10A, the shifted interval usually is larger than several units (unit = sampling interval). Thus, the pre-alignment could rapidly shift the target into the coarse aim (less than one unit). However, for another way to determine the gradient artifact onsets by means of the threshold plus correlation, this pre-alignment will be not necessary.

Pre-alignment (Algorithm 5.7)

Assume two artifacts to be aligned. One is the reference artifact and the other is the working artifact which needs to be shifted to match the reference. The shift interval *st* between the two artifacts may be larger than one unit. The maximum shift interval is initially set as ten times of the averaged shift interval(usually it is less than 10) to restrict the exhaustless shifting and is labeled as *offset*. In principle, the *offset* can be any number, but here it is limited to 100, that the maximum shift interval is 10 times of 10 units.

1. Decide the shift direction of the working artifact
   1.1. Shift it to the left by 1 unit
   1.2. Shift it to the right by 1 unit.

1.3. Calculate the variances of differences between the working artifact at the three positions (left, right, unchanged) and the reference.
1.4. If two variances of the three are the same the working artifact needs no shift. Return directly. If the left shifted variance is less than the unshifted variance, the shift direction is left. Otherwise right.

2. Estimate the step size. Step means the length of shifting per iteration counting by unit. In this phase, there are two defined steps, ten and one. For example, if the current step size is 10, the shift process will shift ten units per iteration.
3. Find the optimal shift interval (integer number of units) which deviates from the optimum no more than one unit.
   Do until all steps have been used. (if two steps, i = 1 to 2)
   3.1. Shift the working artifact with step(i);
   3.2 Find the optimal shift interval by calculating the minimum variance of difference between the reference one and the shifted working one.
   3.3 If found and the last step (inside step(2) repetition), break otherwise goto 3.1.
   End Do
4. Adjust the optimal shift interval by shifting it by ± 1 unit to test if the current position is the minimum variance position.
5. The working artifact is shifted by the determinate optimum shift interval.

Fast high precision alignment (Algorithm 5.8)

The final step required after pre-alignment is the precise alignment in the sub-unit range (i.e. shifting it within one sampling interval). As before, there are the reference and the working artifact which need to be aligned.

1. Decide the shift direction.(right or left)
   1.1. The working artifact is shifted to the left with 0.001.
   1.2. The working artifact is shifted to the right with 0.001.
   1.3. The variances are calculated for the difference between the working artifact at the three positions (left, right, unchanged) and the reference.
   1.4 If two variances of the three are the same the working artifact needs no shift. Return directly. If the left shifted variance is less than the unshifted variance, the shift direction is left. Otherwise right.
2. Set three step values: 1/10, 1/100, and 1/1000 of the sampling interval (1 unit). step = [0.1 0.01 0.001]
3. Set up the initial shift interval (st = 0,i=1).
4. Do while st < 1
   4.1. st = st + step(i)
   4.2. The working artifact is shifted by st.
   4.3. Compute the variance of the difference between the shifted working artifact and the reference artifact.
   4.4. When the minimum variance is achieved and the actual step size is > 1/1000, the step size is replaced with the smaller one in the step array and the optimization continues at 4.1.
   End do
5. Ensure that the optimized shift interval achieves the minimum variance of difference by backing one of the least step (0.001).
   Do until finding the minimum variance
   5.1. st = st – 0.001;
   5.2. The working artifact is shifted by st.
   5.3. Compute the variance of the difference between the shifted working artifact and the reference artifact.
   5.4. When the minimum of variance is achieved, exit.
   End do

Comparing algorithm 5.6 to algorithm 5.8, the number of iterations for a single alignment is clearly reduced from usually 1000 iteration (algorithm 5.6) to typically 30 (algorithm 5.8) for the same resolution 0.0002 ms.

#### 5.3.4.4 Subtraction

Finally, the averaged template is subtracted from the reference artifact to be removed. The movement adapted averaging is individually conducted for each artifact to be removed.

### 5.3.4.5 Postprocessing of residual artifacts occurring in case of transient brief movements

As previously noted by Allen et al. (2000), atypical artifacts were occasionally (typically in 2% of the artifact epochs, depending on the subject) observed that occurred during brief subject movements, which leads to strong residual artifacts (See Fig.5.16) after subtraction. The reason for this is presumably due to the fact that the actual artifact changes its waveform during a few consecutive MR slice periods. Because the temporal resolution of the SPM-information is limited, these movements cannot be reliably detected. Consequently, the estimated reference artifact does not match the actual template, leading to a large residual artifact after subtraction. In the example shown in Fig.5.16, the relatively fast video based movement detector clearly shows a transient brief movement which is associated with an almost stable SPM movement index.

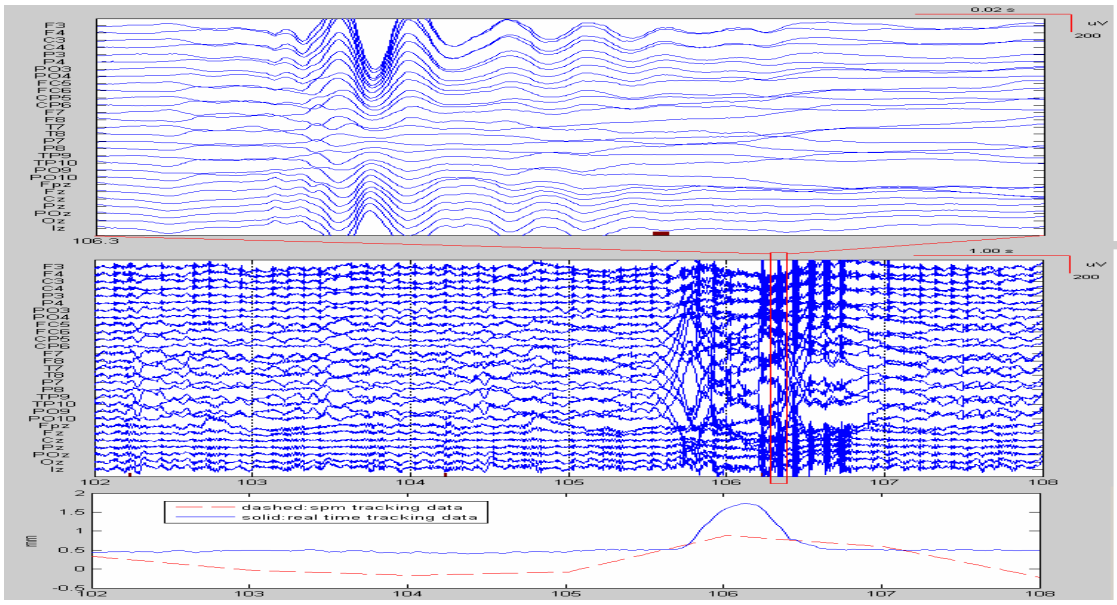


Fig.5.16 Residual gradient artifacts to be removed by the special post processing algorithm (6-sec-segment of subject tr81-EEG).
Upper: The larger part of the artifact waveform shown in an extended time scale.
Middle: Same segment with normal EEG time scale.
Bottom: SPM movement data (red) and video based high resolution tracking data (blue).

Artifacts of this type can be easily detected by an amplitude threshold criterion applied to the ongoing EEG signal. Here we set the threshold to twice the maximum peak-to-peak amplitude observed in a short period before start of MR scanning. However, these residual artifacts usually persist for only a few slices, making it impossible to extract an artifact template by averaging over neighbouring slices. To overcome this problem we exploited the fact that empirically the actual artifact template is largely similar (although differing in absolute amplitude and polarity) across all channels (see Fig.5.16), with the strongest

opposing polarity artifacts occurring at electrode locations F3 and Iz respectively. We employed the following algorithm to reduce the artifact:

First, we correlated the activity pattern occurring at each electrode during the acquisition of each slice with two opposing polarity reference templates, one taken from the F3 and the other from the Iz electrode. These correlations were used to assign each electrode to a positive or negative polarity group. Patterns with a correlation coefficient below 0.6 were not classified. Next, the templates were separately averaged within each polarity group. The final template used for correction was derived by subtracting the sub averages of the two polarity groups. In total this means that the averaging over time was replaced by an averaging over channels. This waveform was subtracted from each channel's (including the ones with a correlation below 0.6) individual artifact waveform by applying a channel adaptive weighting factor α ranging from -2.5 to +2.5 optimized (with a step size of 0.1) under the constraint of minimum variance after subtraction. Finally, a third order low pass filter (40 Hz cut off, Butterworth) was applied to remove spurious residual peaks that the algorithm did not sufficiently eliminate. The schematic diagram is listed in Fig.5.17.

This method well reduced the residual artifact to allow for a visual inspection of the ongoing EEG. However, with respect to quantitative analyses a conservative approach of discarding these epochs may be more appropriate because the amount of (invisible) residual artifact as well as residual grand average EEG overlaid on each EEG-signal by the subtraction cannot be controlled.

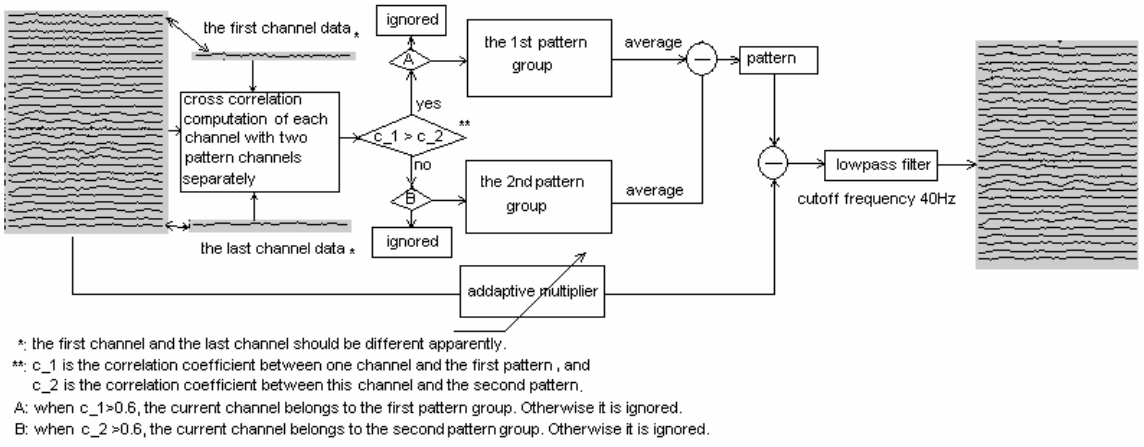


Fig.5.17 Block diagram of special post processing to remove residual artifacts in case of brief movements not correctly identified by SPM.

## 5.4 The schematic diagram of removing gradient artifacts

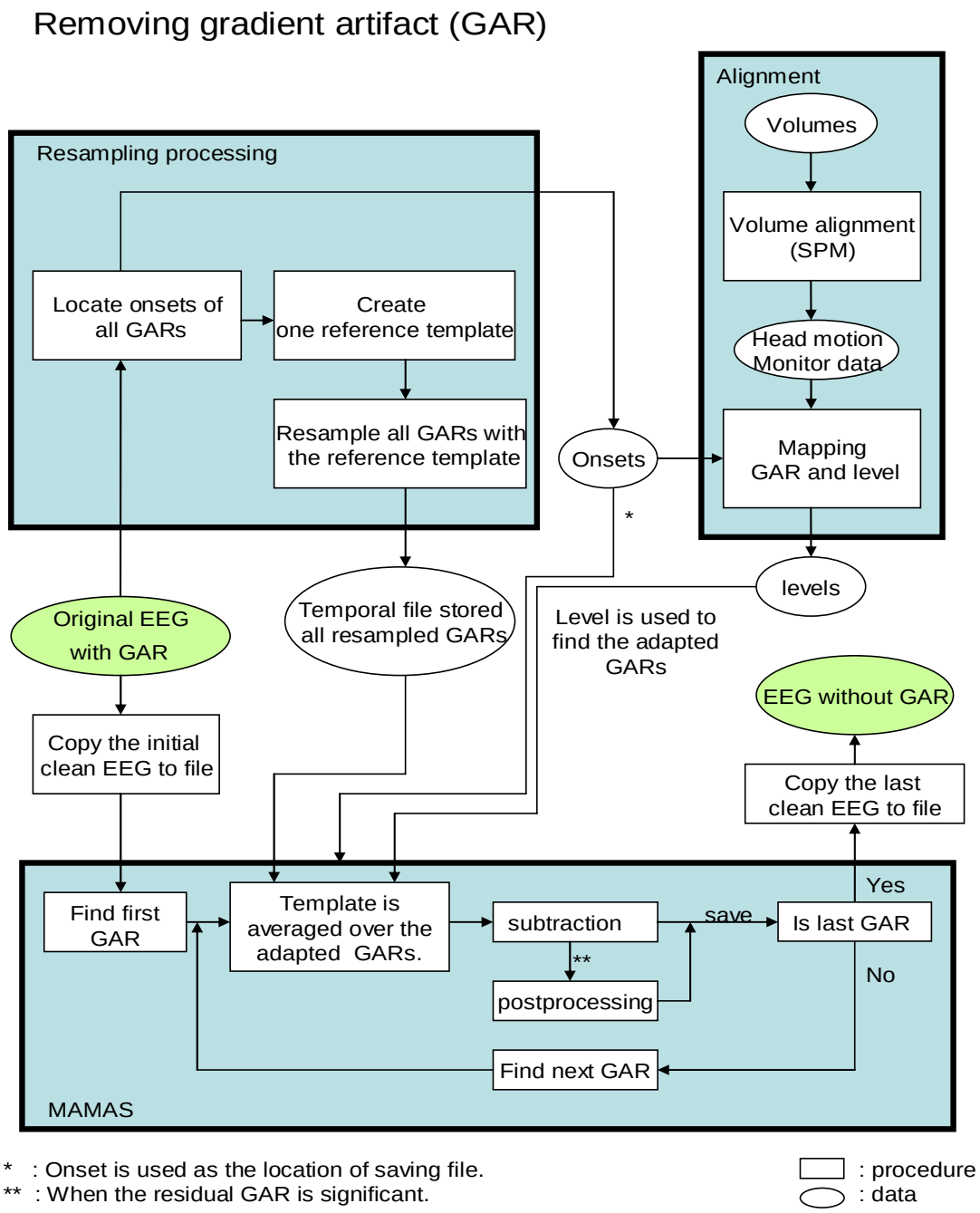


Fig.5.18 The schematic diagram of removing gradient artefacts.

As described in Fig.5.18, the whole procedure of removing GAR consists of three parts. Firstly, the head motion monitor data is extracted from the series of images. Secondly, all epochs (GARs) are located, resampled with one reference template and subsequently saved to a temporary file. According to the monitor data and the onsets of all epochs, the level of each epoch is mapped by the temporal location. Thirdly, by using those levels and the temporary file, MAMAS is applied to each epoch. The final result (GAR removed) is saved to a new file.

## 5.5 Removal of vibration artifact by bandstop filtering

After eliminating all gradient artifacts, the vibration artifacts with a frequency varying between roughly 40 and 50 Hz are clearly visible in the resulting signals. They can be removed by an appropriate bandstop filter. Here a simple third order Butterworth-type bandstop filter (>40 Hz and <50 Hz) was applied (see Fig.5.19) for the characteristic.

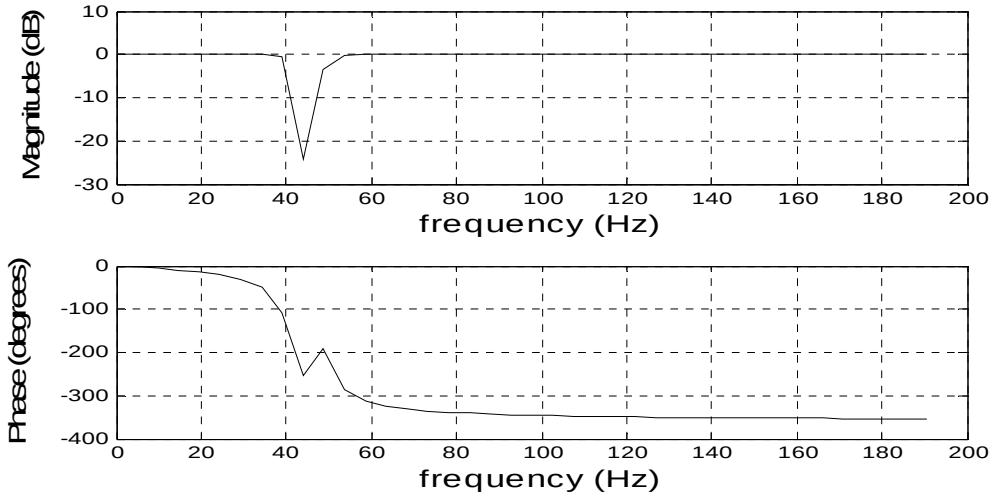


Fig.5.19 The frequency response of the butterworth bandstop filter applied for removing vibration artifacts. Cutoff frequency 40 Hz and 50 Hz.

# Chapter 6 New algorithm to remove BCG artifacts

## 6.1 New algorithm based on the Maximum Noise Fraction (MNF) method

### 6.1.1 Introduction of MNF

As described in detail in section 3.2, blind source separation (BSS) methods have been applied by several groups for BCG removal (Briselli et al., 2006; Nakamura et al., 2006; Mantini et al., 2007). The most popular BSS method in this field has been independent component analysis (ICA).

The basic algorithm to apply this technique for the purpose of EEG-artifact removal is described by the following generator model:

Assume an n-channel *data matrix* $X = [x_1, x_2, ..., x_n]$ to be a linear mixture of the *source matrix* $S = [s_1, s_2, ..., s_n]$ according to

$$X = SA \tag{6.1}$$

with the *n x n mixing matrix A* defining the signal generation. Each component $x_i^T = \{x_{ij} \mid j = 1,...k\}$ represents one real valued signal channel at k sampling times and $s_i^T = \{s_{ij} \mid j = 1,...k\}$ represents one real valued source *component*. To remove a certain artifact a number of *r* components need to be identified that primarily represent artifact activity. These components are then identified by a selection matrix *T* which is initialized as an *n x n* identity matrix. For all indices *i* corresponding to an artifact component of *S* the element *T(i,i)* is set to *0*, that represents the $i^{th}$ component is set to zero. Using this selection the artifact reduced signal matrix $\hat{x}$ is reconstructed from the source matrix which is deduced as follows:

$$X = SA \Leftrightarrow S = XA^{-1} \tag{6.2}$$

$$\hat{S} = ST = S \cdot \begin{bmatrix} 1 & \cdots & 0 & 0 & \cdots & 0 \\ \vdots & \ddots & \vdots & \vdots & \cdots & \vdots \\ 0 & \cdots & 1 & 0 & \cdots & 0 \\ 0 & \cdots & 0 & 0 & \cdots & 0 \\ \vdots & \cdots & \vdots & \vdots & \ddots & \vdots \\ 0 & \cdots & 0 & 0 & \cdots & 0 \end{bmatrix} \tag{6.3}$$

After setting zeros of several source components, the artifact reduced signal matrix $\hat{X}$ can be estimated from the other source components.

$$\hat{X} = \hat{S}A \tag{6.4}$$

According to eqs.6.2 and 6.3, the eq.6.4 can rewritten as

$$\hat{X} = STA = XA^{-1}TA \tag{6.5}$$

With respect to this concept the difference between the various BSS approaches is the way the mixing matrix *A* and the component matrix *S* are derived. Besides the different separation way to achieve the mixing matrix *A*, the simplest way of choosing BCG IC is another important factor to use the new BCG removal method as described in Fig.6.1. Because the new BCG removal method – MNF- decomposes the signals according to their SNR, the identification of BCG ICs in the new BCG removal method becomes easy, directly specifying the last several ICs (Fig.6.1B). However, the old method needs an extra procedure for identifying some random distributed BCG ICs (Fig.6.1A).

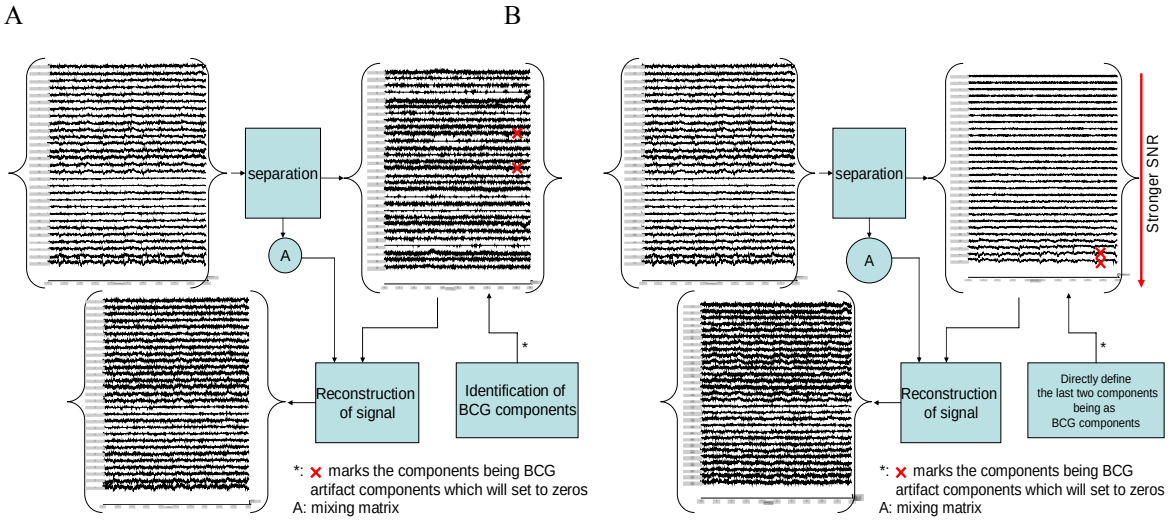


Fig.6.1 Schematic diagram of the old BCG removal methods and the new BCG removal method (such as MNF).

Before introducing the maximum noise fraction (MNF) method – yet another variant of BSS approaches – we will briefly introduce the various ICA methods and their applications to derive the motivation of trying MNF in this work.

ICA is an extension of principle component analysis (PCA). PCA is also called Karhunen-Loève transform or the Hotelling transform defined as an orthogonal linear transformation and is based on the second order moment. In contrast, ICA uses higher order moments of random vectors and assumes the components to be mutually statistically independent instead of just being uncorrelated. The ICA was initially proposed and named by Jeanny Herault and Christian Jutten (1986). They described an algorithm based on a fully interconnected neural network model and a Hebb learning rule which controls the weights of the interconnections, derived from the Hebb concept for ``Synaptic plasticity" in Physiology, to blindly separate the mixture of independent signals (Herault, et al., 1986). In 1989, Jean-Francois Cardoso proposed one new solution based on high order moments. In that solution, a simple algebraic method was developed to extract the independent components from multidimensional data

(Cardoso, 1989). Sources were identified by the estimation of the diagonalization (orthonormality) of the weighted covariance of sensors. A variant of this method providing more robust estimates was introduced by Souloumiac et al. (1991) and Souloumiac et al. (1996). Comon (1994) developed an algorithm that minimizes the mutual information between cumulants of components. A good introduction is presented by De Lathauwer et al. (2000).

Up to now, based on different principles, several algorithms have been developed. The most popular one is fastICA (Hyvaerinen, 1999) which is based on minimization or maximization of an objective function, such as the likelihood, negentropy or mutual information. When the function about mutual information is applied in fastICA, it is similar to another often used algorithm - the infomax method (Bell et al., 1995; Lee et al., 1999) which maximizes the mutual information. For the orthogonal tensor decomposition, the cumulant based methods are developed by Comon(1994) and Cardoso(1999)with the different way to find the mixing matrix, joint approximate diagonalization of eigenmatrices(JADE) (Cardoso) and pairwise rotation (Comon). One version of this algorithm (proposed by Blaschke Tobias, 2004) performs a diagonalization of the cumulant tensors taking into account third- and fourth-order cumulants simultaneously. The typical representative of this approach is JADE (Cardoso, 1999) algorithm. Several ICA programs written in MATLAB can be downloaded from internet[2] directly.

Since some artifacts, such as eye movement and blink EEG artifacts (Joyce et al., 2004), artifacts in magnetoencephalogram (MEG) (Barbati et al., 2004) and ocular artifacts in EEG (Flexer et al., 2005), have been removed successfully with ICA, this type of BSS methods became also the main tool of separation of BCG artifacts (Srivastava et al., 2005). FastICA has been used in removing BCG artifacts in most cases. One idea (Briselli et al., 2006) , to eliminate the influence of stochastic behavious (see above), was to carry out FastICA several times with different initial conditions on the same EEG data. Then, using clustering techniques EEG-components are achieved with a more statistical reliability. In another ICA based approach (Nakamura et al., 2006) combined ICA with a subsequently applied high-pass filter to solved the problem of residual BCG activity caused by non periodic BCG waveforms. Recently ocular artifacts were removed together with BCG by ICA (Mantini et al., 2007).

[2] Comon's algorithm: http://www.i3s.unice.fr/~comon/codesICA.txt
JADE: ftp://tsi.enst.fr/pub/jfc/Algo/Jade/jadeR.m
FastICA: http://www.cis.hut.fi/projects/ica/fastica/loadcode.shtml

However, it is an inherent problem of all ICA (and also PCA) based approaches that the more efficiently they remove the BCG the more some fraction of the underlying true EEG is suppressed (Huiskamp et al., 2005) since the BCG and the EEG are not perfectly statistically independent. Therefore, although ICA has been used widely in this field, in all realizations some residual BCG artifacts still existed in the reconstructed data due to the uncompelete orthogonal decomposition. As a second problem these applications are hardly suitable for an automatic removal procedure because the independent components mainly carrying BCG information need to be identified and marked interactively (Be´nar et al., 2003) or by a correlation analysis including an additionally recorded electrocardiogram (ECG) (Srivastava et al., 2005).

Therefore the goal and motivation of the work presented here was

(i) to develop a BSS method which better separates between the BCG and the EEG than former ICA approaches (see above) and

(ii) to embed this procedure in a fully automatic removal concept.

As will be shown in the following, the maximum noise fraction (MNF) method, also named maximum signal fraction (MSF) method (Hundley et al., 2001) largely meets this requirements. Similar to PCA MNF is based on second order moment to separate signal, however the two approaches are different in the way they create the mixing matrix out of these moments. PCA derives the eigenvectors and eigenvalues of the covariance matrix of observed signals, with each eigenvector (‘component’) corresponding to one eignevalue. In contrast, MNF as a first step assumes the signal matrix X being an additive superposition of some signal components (matrix $P$) to some noise components (matrix $Q$)

$$X = P + Q$$

Assume orthogonality between $P$ and $Q$. Each matrix is with $n$ channel and $m$ samples.

Given this model MNF creates the mixing matrix by searching the *generalized* eigenvectors and eigenvalues of the covariance matrix of the signal parts and the covariance matrix of the noise parts. This means, MNF explicitly addresses the problem of a signal contaminated by noise. MNF was originally developed to denoise multispectral satellite images (Green et al., 1988) and subsequently extended to the denoising of time-series (Anderle et al., 2001). MNF finds a set of orthogonal basis vectors (later also labelled as ‘components’ or ‘ICs’) whose directions represent the different generalized eigenvectors of the signal part and the noise. As will be illustrated later, larger generalized eigenvalue means a stronger signal to noise ratio

(SNR). Usually, the noise is unknown and can only be approximated by the derivative of the observed data. As will be shown in eqs.6.6 to 6.10 the mixing matrix can be determined by the orthogonal eigenvectors of the signal's derivative and the whitened signal derived from the observed data.

In summary, MNF constructs a subspace of basis vectors maximizing the noise fraction of separated components. As a side effect the basis vectors have a natural ordering according to their noise fraction (= SNR). Having in mind the goal of introducing an automatic artifact removal method this feature is in advantage of the randomly distributed ICs within the ICA subspace, since the first or last few components (depending on the direction of ordering) always carry the artifact information as long as the BCG artifact on average is the largest type of artifact. In case of the – very rare – situation that if another artifact type is larger than the BCG artifact, the EEG cannot be used anyhow due to its bad quality. Beyond this special feature MNF is superior to the various popular ICA variants with regard to the segregation of artifact activity from the EEG (see later in the results section).

The mathematical principle of MNF (Hundley et al., 2001) is deduced from the beginning of the assumed EEG mixing model, the general production formulation. Another alternative formulation, sum can replace the production (eq.6.1).

As introduced before (eqs.6.1 and 6.5) assume the two models to describe the generation of the signal matrix $X$ by mixing the components of the source matrix $S$ according to $X = SA$ and alternatively to defining $X$ as consisting of the true signal $P$ plus additive orthogonal (not necessarily white) noise $Q$ as according to

$$X = P + Q$$

Combining the two equations, $P$ and $Q$ may be written as

$$P = [p_1, p_2, \cdots, p_n] \text{ and } p_j = \sum_{i=1}^{m} s_i a_{ij}, j=1,\ldots,n$$

$$Q = [q_1, q_2, \cdots, q_n] \text{ and } q_j = \sum_{i=m+1}^{n} s_i a_{ij}, j=1,\ldots n$$

with $a_{ij}$ representing the elements of $A$ in the *ith* row and the *jth* column and $m$ is the supposed number to construct $P$.

Here, $Q^T P = 0$ and $P^T Q = 0$ because of the assumption of orthogonality of $P$ and $Q$.

So,
$$X^T X = (P+Q)^T (P+Q) = P^T P + Q^T P + P^T Q + Q^T Q = P^T P + Q^T Q \tag{6.6}$$

We define the signal to noise ratio as

$$SNR = \max_{\psi \neq 0} \frac{\|P\psi\|}{\|Q\psi\|} = \max_{\psi \neq 0} \frac{\psi^T P^T P \psi}{\psi^T Q^T Q \psi} \tag{6.7}$$

With eq.6.6and eq.7.7, a new representation of SNR is derived.

$$SNR = \max_{\psi \neq 0} \frac{\psi^T (X^T X - Q^T Q)\psi}{\psi^T Q^T Q \psi} = \max_{\psi \neq 0} \frac{\psi^T X^T X \psi - \psi^T Q^T Q \psi}{\psi^T Q^T Q \psi}$$

$$\Rightarrow SNR = \max_{\psi \neq 0} \left( \frac{\psi^T X^T X \psi}{\psi^T Q^T Q \psi} - 1 \right)$$

$$\Rightarrow SNR = \max_{\psi \neq 0} \frac{\psi^T X^T X \psi}{\psi^T Q^T Q \psi} - 1 \tag{6.8}$$

Move 1 to the left of eq.6.8,

$$SNR + 1 = \max_{\psi \neq 0} \frac{\psi^T X^T X \psi}{\psi^T Q^T Q \psi}$$

Defining $SNR_1$ as $SNR + 1$ leads to the following eq.6.9 which is the equivalent form of eq.6.7.

$$SNR_1 = \max_{\psi \neq 0} \frac{\psi^T X^T X \psi}{\psi^T Q^T Q \psi} \tag{6.9}$$

The set of solutions to this problem are defined recursively by requiring all solution vectors to be orthogonal in the sense that the inner product of the transformed data vectors by arbitrary pairs of solution vectors is zero. i.e. $\psi_i X^T X \psi_j = 0$ *for all i≠j.*

The solution to this problem leads to the generalized eigenvalue problem (see Kirby, 2001)

$$X^T X \psi = \lambda Q^T Q \psi \tag{6.10}$$

where $\psi$ represents the eigenvector (or basis vector) and $1/\lambda$ is the noise fraction captured by the basis vector. Hence, a set of orthogonal maximum noise fraction basis vectors possess a natural ordering based on the noise fraction $1/\lambda$.

Now, we need to estimate the covariance of $Q$, i.e. $Q^T Q$ from $X$.

Define $X_s$ as the set of observations $X$ shifted forward by one time step. Then,

$$dX^T dX = (X - X_s)^T (X - X_s) = (P + Q - P_s - Q_s)^T (P + Q - P_s - Q_s) \approx (P - P_s)^T (P - P_s) + (Q - Q_s)^T (Q - Q_s)$$

Assuming that the noise is temporally uncorrelated,, the following relations hold:

$Q_s^T Q = Q_s Q^T = 0$ and $Q^T Q \approx Q_s^T Q_s$, $dX^T dX \approx 2Q^T Q + (P - P_s)^T (P - P_s)$

If the signal is smooth, then $P–P_s$ will be close to zero. The smoothness condition is well met having in mind that the largest part of the BCG spectrum is mostly restricted to frequencies below 20 Hz (see Fig.7.15) and thus clearly below the sampling frequency. Therefore, a good estimation of $Q^T Q$ is $\frac{1}{2} dX^T dX$.

Observed $SNR_1$ and $SNR_2$, eq.6.11 has the same concept as eq.6.9.

$$SNR_2 = 2 * SNR_1 = \max_{\psi \neq 0} \frac{\psi^T X^T X \psi}{\psi^T dX^T dX \psi} \tag{6.11}$$

Cichocki and Amari (2003) have shown that this eigen decomposition solves the mixing problem given that the signal and the noise are orthogonal and that the one-lag autocorrelations of the signal and the noise have different structures (that is, even in case of non white noise).

Next, the mixing matrix *A* can be calculated as follows:

The singular value decomposition (SVD) of *dX* can be defined as

$$dX = U_1 \Sigma_1 V_1^T \tag{6.12}$$

Where $V_1$ and $U_1$ are the unitary matrices.

Therefore $V_1^T V_1 = I$ and $U_1^T U_1 = I$ which will be used in eq.6.13.

For the whiten data has the same correlation property as the original data, by applying the whitening transformation, $V_1 \Sigma_1^{-1}$ , to *X* and *dX*, the problem (eq.6.11) can be transformed into

$$\max_{\psi \neq 0} \frac{\psi^T \Sigma_1^{-1} V_1^T X^T X V_1 \Sigma_1^{-1} \psi}{\psi^T \Sigma_1^{-1} V_1^T dX^T dX V_1 \Sigma_1^{-1} \psi} = \max_{\psi \neq 0} \frac{\psi^T \widetilde{X}^T \widetilde{X} \psi}{\psi^T \psi} \tag{6.13}$$

With

$$dX V_1 \Sigma_1^{-1} = U_1 \Sigma_1 V_1^T V \Sigma_1^{-1} \xrightarrow{V_1^T V_1 = I} dX V_1 \Sigma_1^{-1} = U_1 \Sigma_1 \Sigma_1^{-1} \xrightarrow{\Sigma_1 \Sigma_1^{-1} = I} dX V_1 \Sigma_1^{-1} = U_1$$

And

$$\Sigma_1^{-1} V_1^T dX^T = \Sigma_1^{-1} V_1^T V_1 \Sigma_1^T U_1^T \xrightarrow{V_1^T V_1 = I} \Sigma_1^{-1} V_1^T dX^T = \Sigma_1^{-1} \Sigma_1^T U_1^T$$
$$\xrightarrow{\Sigma_1^T = \Sigma_1} \Sigma_1^{-1} V_1^T dX^T = \Sigma_1^{-1} \Sigma_1 U_1^T \xrightarrow{\Sigma_1^{-1} \Sigma_1 = I} \Sigma_1^{-1} V_1^T dX^T = U_1^T$$

So,

$\Sigma_1^{-1} V_1^T dX^T dX V_1 \Sigma_1^{-1} = U_1^T U_1 = I$ and $\widetilde{X} = X V_1 \Sigma_1^{-1}$

Thus, the generalized eigenvector problem transforms into the problem of SVD of $\widetilde{X}$.

Back to eq.6.1, the mixing matrix *A* also can be represented by $A = U_A \Sigma_A V_A^T$.

Then

$$dX^T dX = A^T dS^T dS A = A^T A = V_A \Sigma_A^T U_A^T U_A \Sigma_A V_A^T$$
$$\xrightarrow{U_A^T U_A = I, \Sigma^T = \Sigma} dX^T dX = V_A \Sigma_A^2 V_A^T \tag{6.14}$$

with the assumption of $dS^T dS = I$ (*Source components* are the orthogonal components). $V_A$ and $\Sigma_A$ can be computed by the eigenvector and eigenvalue decomposition of $dX^T dX$.

Applying the whitening transformation, $V_A \Sigma_A^{-1}$ to *X* yields

$$\hat{X}=XV_A\Sigma_A^{-1}=SAV_A\Sigma_A^{-1}=SU_A\Sigma_AV_A^TV_A\Sigma_A^{-1}=SU_A. \tag{6.15}$$

Using the assumption that $S^TS=\Lambda$ (where $\Lambda$ is the diagonal matrix carrying the squared eigenvalues of *S*). $U_A$ is now found by

$$\hat{X}^T\hat{X}=U_A^TS^TSU_A=U_A^T\Lambda U_A. \tag{6.16}$$

$U_A$ is the eigenvector matrix of $\hat{X}$.

According to eq.6.12

$$dX^TdX=V_1\Sigma_1^TU_1^TU_1\Sigma_1V_1^T=V_1\Sigma_1^2V_1^T$$

and eq.6.14

$$dX^TdX=V_A\Sigma_A^2V_A^T$$

Then

$$V_1\Sigma_1^2V_1^T=V_A\Sigma_A^2V_A^T \tag{6.17}$$

Although eq.6.17 has a lot of solutions, we can give one solution of $\Sigma_A=\Sigma_1$ and $V_A=V_1$.

Therefore, *A* is known ($V_A=V_1$ and $\Sigma_A=\Sigma_1$, and according to eq.6.16 $U_A$ is calculated).

With this approach, the independent components (S) have the nature character of SNR order, that is the ranking of components according to their SNR. If BCG is the largest artifact, then it will always be represented by the first or last (depending on the ordering direction) component which is important for automatic removal. The detail algorithm of MNF is listed in algorithm 6.1.

MNF approach (Algorithm 6.1)

1. Calculate the derivative *dX* of data X, i.e. the difference between the original data vector and the vector resulting from the one-sample shift.
2. Compute the eigenvectors of the covariance of *dX*, leading to the matrices $V_1$ (eigenvectors) and $\Sigma_1$ (eigenvalues)
3. Create whitening matrix $\Sigma_1^{-1}V_1^T$.
4. Whiten data *X* according to $\widetilde{X}=\Sigma_1^{-1}V_1^TX$.
5. Compute the eigenvectors of the covariance of the whitened data $\widetilde{X}$ resulting in the matrices $U_A$ (the eigenvectors) and $\Lambda$ (the eigenvalues)
6. Create the separation matrix as $A=U_A^T\Sigma_1^{-1}V_1^T$.
7. Derive the source matrix as $S=XA^{-1}$.

### 6.1.2 Application of MNF to BCG removal

Before removing BCG artifacts, gradient artifacts have to be removed by the MAMAS method and vibration artifacts should also be suppressed as described before.

Once the source matrix has been derived (step 7 of algorithm 6.1), the last or first (depending of the direction of ordering along the SNR) *r* components need to be suppressed

(applying selection matrix T, see section 6.1.1) to reconstruct the artifact reduced signal from the remaining components (applying eq.6.2). Due to the SNR-related ordering of the components the selection matrix T is easily defined by simply specifying the number of ICs that need to be suppressed (later it will be described how this number was optimized). Once this number *r* is known a fixed predefined *T* can be used for reconstruction with the last or first *r* elements *{T(i,i), i=1,...r}* all set to *0*. For a formal description of the reconstruction procedure see algorithm 6.2.

Application of MNF to BCG removal (Algorithm 6.2)

1. Randomly get one segment data (usually 10 seconds). MNF is applied to achieve the mixture matrix and predefine the number of chose BCG ICs (usually 2 ICs) to create the selection matrix T.
2. For each segment data, from the beginning, the mixture matrix A and the selection matrix T are directly applied to reconstruct the EEG (according to eq.6.14) until all EEG have been processed.
3. The additional subtraction method (see section 6.2) is applied to remove the residual BCG artifacts.

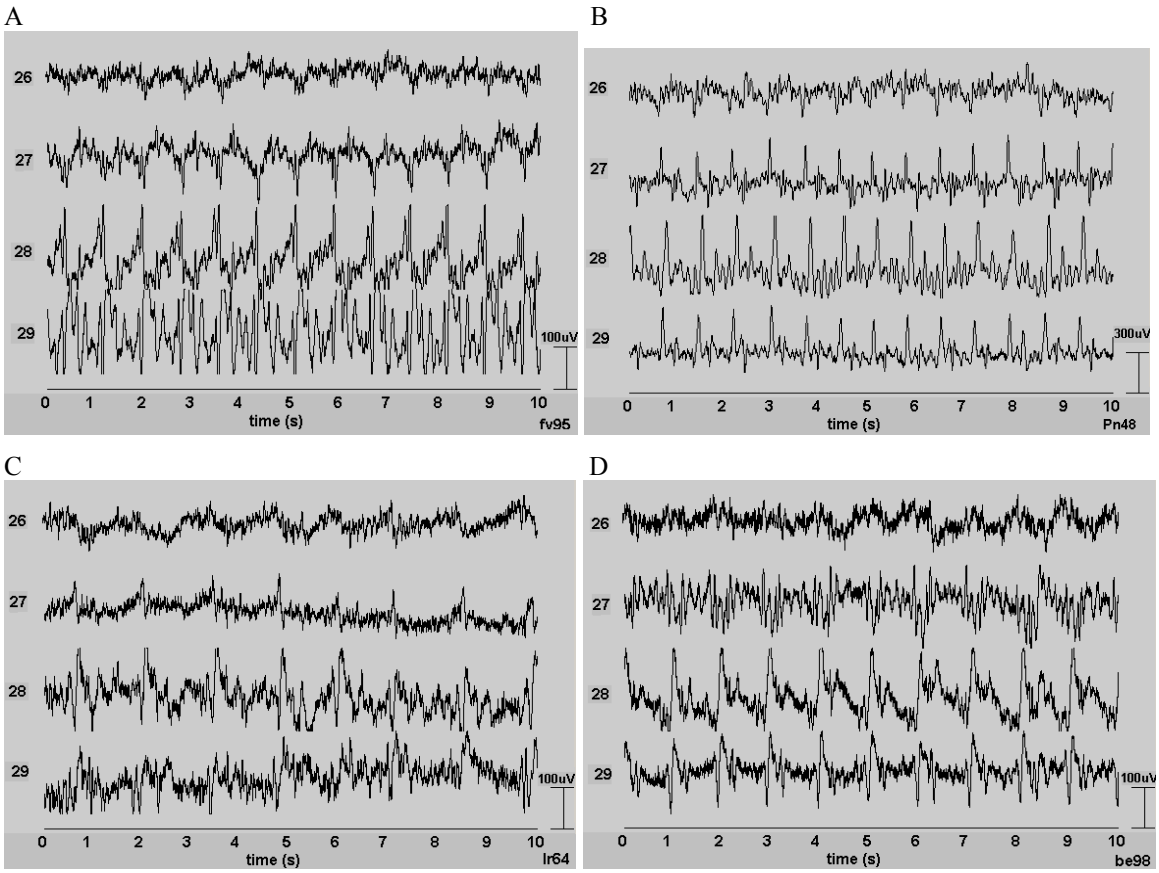


Fig.6.2 The last four MNF-independent components of four subjects.

Since the BCG artifacts focus on the last vectors of the full set of components resulting from the MNF, Fig.6.2 shows the last four ICs of 29 ICs decomposed from one ten-second 29 channels EEG to clearly demonstrating that the presence of the BCG artifact increases towards the last components in the row. Although an arbitrary number of IC could in principle be attributed to the BCG, a reasonable number of BCG-related ICs needs to be estimated for

instance by variance considerations (comparing the variance of the reconstructed EEG to the variance of an EEG of the same subject but recorded outside the MR scanner) to balance the losing of true EEG (if too many ICs are removed) with the amount of residual BCG artifacts if not enough ICs have been removed. As will be shown later in the Results section, two or three ICs achieve a sufficient BCG suppression. Minor residual BCG artifacts persisting after that procedure can be further reduced by an additional subtraction method as described below.

### 6.1.3 Replacing the adaptive mixing matrix by a fixed matrix to reduce the computational load

Running the MNF analysis leads to a significant computational load which roughly increases proportionally with the duration of the recorded EEG. Taking into account that in typical MR-EEG recording sessions long periods of EEG (typically 30 min) need to be processed, it is worth trying to reduce the numerical demands of MNF. Looking into the details of the algorithm, the estimation of the mixing matrix A is the most complex part of it. Therefore, the question arises, if it might be sufficient to take the mixing matrix A from the first seconds of the recorded data and subsequently apply this (fixed) matrix to process the full EEG period (as opposed to an adaptive concept which computes a new mixing matrix for each of the sequence of short term epochs constituting the signal). In this case, the MNF algorithm would be significantly speeded up.

To address this issue, a BCG identification signal (BIS) was derived from the EEG and correlated with the components derived with the two alternative concepts (i.e. adaptive mixing matrix vs. fixed mixing matrix). Components carrying BCG information (usually the last or first few ICs, see before) will exhibit a large correlation with the BIS. If the correlations of the BCG related ICs observed under the two compared regimes are similar, then the algorithm using a fixed mixing matrix will achieve the same performance regarding BCG removal as the adaptive version.

The BIS was derived as follows:

Empirically BCG artifacts are to some extent similar (although differing in amplitude and polarity) across many channels. Therefore, we defined the first channel of 10-20-system (which always showed a clear BCG artifact) as the initial BCG identification channel and added or subtracted the other 28 channels according to the sign of their correlation with the first channel. Finally, the resulting cumulated signal was normalized by the number of channels. The schematic diagram of the generation of BIS is sketched in Fig.6.3 where the modified channels are the original channels with their own signs (subtraction or addition).

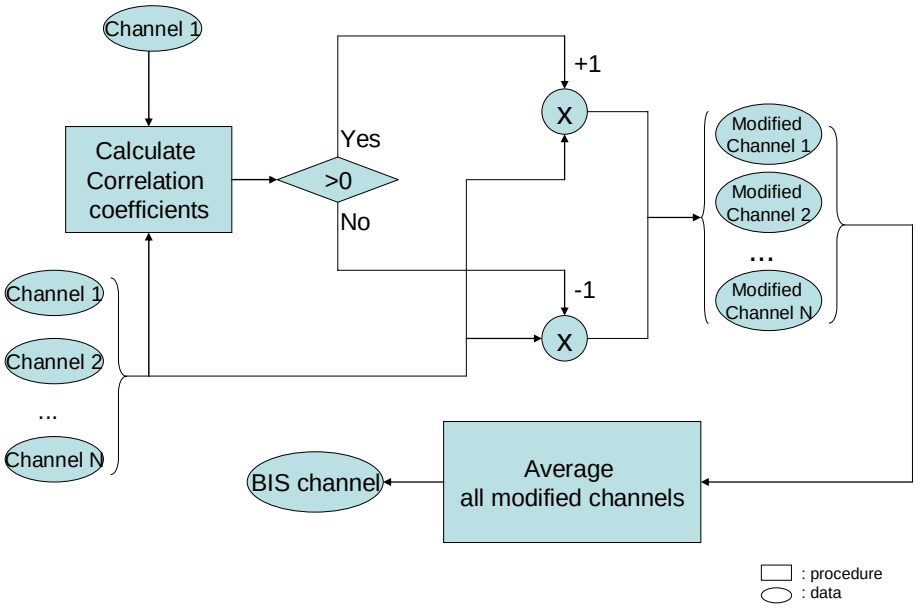


Fig.6.3 Schematic diagram of extracting the BCG identification signal (BIS).

To achieve acceptable results with a fixed rather than an adaptive mixing matrix *A* the last (or first) components (which mainly represent BCG activity) as derived with the two approaches should be equally correlated with the BIS to guarantee that the amount of BCG that can be removed by dropping these components is comparable. Therefore we calculated the correlation coefficients of each source component and the BIS of each subject's EEG for each of ten epochs of 10 sec duration. First, this was done using a fixed mixing matrix *A* for all epochs of a subject with *A* being calculated from the first epoch for each sequence. Next, we repeated the decomposition, however, this time applying the mixing matrix as derived individually for each epoch.

The epoch-wise calculated mixing matrix can be replaced by the fixed matrix if the distribution of the correlation coefficients over the source components is mainly identical in the sense that (i) the last two components (later we show, that two components are sufficient to remove the BCG) have the largest correlation of all and (ii) that the difference between these correlations obtained for the two different approaches is smaller than the standard deviation (over the subjects) of the adaptive variant. If these constraints are met the sources later being dropped to remove the artifact will carry the same fraction of artifact activity.

### 6.1.4 Separating BCG and EEG: Comparison of MNF to ICA approaches

The correlations with the BIS signal were additionally used to compare MNF to two popular ICA algorithms with respect to their capability to separate BCG from true EEG

activity. The stronger the correlations and the more the strongest correlations are focussed on a few (last) source components the greater the power of the algorithm to extract specifically BCG activity, i.e. to separate EEG and BCG.

The BIS was again derived from a 10 sec epoch selected randomly from the EEG recorded in the scanner from each of the four subjects. Next, this epoch was decomposed by MNF, fast ICA (Hyvaerinen, 1999) and JADE (Cardoso, 1998). Then, the resulting components were ordered according to their correlation with the BIS in order to allow for a comparison between the decomposition methods. These sets of correlation factors were statistically compared by means of a two-sided t-test.

## 6.2 Additional Moving Average Subtraction algorithm to remove residual BCG activity

After using MNF, it is necessary to use subtraction to suppress the residual BCG artifacts. The MNF technique can remove the BCG artifacts to a large degree but not completely. Therefore, a template subtraction method (similar to the one used for gradient artifact suppression) is applied to remove most of the residual BCG activity. Subtraction alone can also not remove BCG artifacts completely (Negishi et al., 2004; Niazy et al., 2005). Consequently – as will be demonstrated in the results chapter - the combination of the two steps is needed to achieve a sufficient BCG artifact removal.

Similar to the gradient artifact algorithm, the subtraction algorithm averages over a limited number of neighbouring BCG epochs and subtracts this average waveform from the actual BCG epoch. In this context, the precise identification of the ECG (as the origin of the BCG artifact) onset is critical for a correct alignment of the BCG epochs included in this procedure. In principle the BIS could be used for this purpose as well but the ECG is better for the following reasons: i) The peaks of the BIS are less strong. In some cases, they will be misinterpreted due to the fact that two almost equally strong peaks occur in the BIS close to each other (i.e. the one related to the R wave and a second related to the S wave of the ECG) whereas the true ECG R wave is always much higher than S wave in the real ECG. Therefore, the task of identifying the R-peak in the BIS is critical. ii) If head motions occur (especially strong movements), the BCG onsets (by BIS) will be not detected because the waveforms are corrupted by this motion. However, the ECG channels are not influenced by head motion (i.e. the signal used to identify is perfect). iii) If there is an epileptic spike in the EEG, the BCG onset may also not be detected because the spike often is the highest peak and the algorithm just uses an amplitude threshold criterion.

Here, the two ECG channels (Ecg1 and Ecg2) are summed to serve as the reference channel for this purpose. The BCG artifacts of the various EEG channels have different yet stable time delays with respect to the ECG waveform. The ECG onset is defined as the time of the maximum ECG peak which is usually the R wave of QRS complex. These ECG onsets are then defined as the BCG onsets as well. With this procedure, the delays are constant part of the channel dependent BCG waveform. Next, each individual BCG artifact's template is obtained by averaging over the BCG artifacts captured by a sliding window (rectangular profile) whose width covers 50 ECG epochs. The current individual BCG artifact is temporally located in the center of that sliding window. Finally, the average template is subtracted from the individual BCG artifact. Further details of this procedure are described below as algorithm 6.3 for ECG onset detection and as algorithm 6.5 for our subtraction. Algorithm 6.4 describes the ECG onset detection and is used in the algorithm 6.3.

Detect sequence of ECG onsets (Algorithm 6.3)

1. Identify the first ECG onset and RR interval by Algorithm 6.4. A reference ECG model with RR length is created from two ECG channels of EEG data at the first ECG onset by subtraction of the two ECG channels in order to enhance the characters of ECG (i.e. enlarge the waveforms of QRS).
2. Estimate the next onset.
   2.1 Initially, the current onset is equal to the previous onset adding RR.
   2.2 Create the current ECG model.
   2.3 Compare the two ECG models' peaks (QRS complex waves). If the distance between two peaks is not so far (less than ¼ RR), goto 2.5. Otherwise, goto 2.4.
   2.4 Relocate the current onset according to the peak position.
   The new current onset = the current onset – (model peak position – reference model peak position).
   2.5 Further adjust the current onset with correlation coefficient of the reference model and the current ECG model with different shifted offset (usually range is $\pm RR/4$, increased step is one sample). The best position is the maximum value of correlation coefficients.
3. Go to 2, until all ECG data have been processed.

ECG start onset and RR estimator (Algorithm 6.4)

1. Extract the initial 3 second ECG data which are recorded at the two ECG channels (Ecg1 and Ecg2, See section 4.3).
2. Find the ECG peaks.
   2.1 Filter the ECG data with a highpass filter to remove the bias error.
   2.2 Compute the threshold used to identify ECG peaks as 2/3 of averaged value of the local maximum values of some epochs (½ second duration for each epoch).
   2.3 Find the first onset which is larger than the threshold. For the next peak onset, the distance between this position and the previous onset must larger than ½ second.
3. Compute the RR interval by averaging the difference values between the two onsets.

Subtraction (Algorithm 6.5)

1. Detect ECG onsets with algorithm 6.3.
2. Adjust all BCG onsets: Each BCG onset is equal to the ECG onset subtracting ½ RR. Each BCG length is equal to its onset adding RR.
3. Average the closer 50 BCG artifacts. The number of averaged artifacts can be reference to the other paper about gradient artifacts removal.
4. Subtract this average from EEG.
5. Go to 3, until all BCG artifacts have been subtracted.

During the whole procedure, MNF method is firstly used to remove most of BCG artifacts and the subtraction method is a useful additional tool to remove the tiny residual BCG artifact. This combined method could be thought as a good idea to suppress the BCG artifacts with the least probability of residual BCG artifacts.

### 6.3 INPS to evaluate removal performance

To estimate the performance of the MNF method alone, the subtraction method alone and the combination of both, the improvement normalized power spectrum (INPS) ratio (introduced by Tong et al. (2001) in the context of ECG artifact removal) was applied. As specified in eq.6.18, this ratio quantifies the ratio of the cumulated power at the BCG repetition frequency (identical to the heart rate) and its harmonics before and after application of an artifact removal algorithm. First, the BCG repetition rate is determined by the RR interval as calculated from the ECG reference channel. Second, the cumulated power spectrum around this basic frequency and its harmonics below 250 Hz was calculated with 0.1 Hz bandwidth by applying the Welch power spectrum estimation method (Welch, 1967). Finally, the ratio of these cumulated values obtained before processing and after processing is estimated. The number $N$ of included harmonic frequencies in eq.6.18 is usual about 250 since the basic frequency of BCG artifact is usually about 1Hz.

$$INPS = \frac{\sum_{j=0}^{N} P_j^{before}}{\sum_{j=0}^{N} P_j^{after}} \tag{6.18}$$

Here $P_j$ is the spectral power in the 0.1-Hz window centered at the $j^{th}$ ECG harmonic frequency, the superscript ‘before’ indicates to calculate the power spectrum before applying one artifact removal method and the superscript ‘after’ indicates to calculate the power spectrum before applying one artifact removal method.

## 6.4 The schematic diagram of removing BCG artifacts

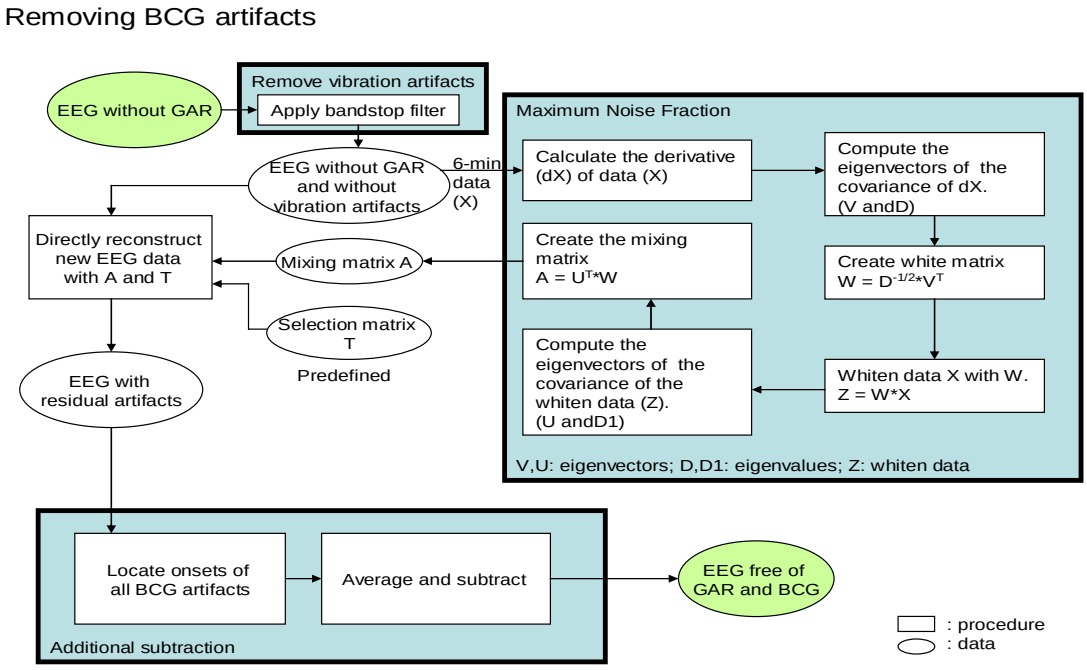


Fig.6.4 The schematic diagram of removing BCG artefacts.

As shown in Fig. 6.4, during the whole procedure of removing BCG artifacts the important parts includes the estimate of mixing matrix *A* by MNF, the direct reconstruction of EEG data, and the additional average-subtraction.

# Chapter 7 Results

## 7.1 Gradient artifacts, MAMAS-algorithm: Evaluation and Comparison with the MAS algorithm

### 7.1.1 Gradient artifact resampling

Fig.7.1A shows the average standard deviation of the differences (subsequently called 'resampling error') between the simulated reference artifact and the 30 resampled jittered templates observed at the different relative temporal resolution values δt (δt=1 representing the original sampling interval). It meets the EEG amplifier noise level of about a uV at a relative temporal resolution of approximately δt = .005 (i.e. an absolute resolution of .001 ms). Bearing in mind that even stronger artifacts cannot be ruled out around the artifact peaks, we set $\delta t_{opt}$ to .001 (corresponding to an absolute resolution of .0002 msec) for the removal algorithm. The optimized resampling algorithm needs a maximum of 30 iterations to find the optimal shift interval at this resolution. In principle this procedure is comparable to an upsampling of the gradient artifact to 5 MHz and aligning it to the reference artifact, however avoiding the boost in data volume and computational load.

Fig.7.1B shows an extreme example to illustrate in the time domain how much reduction in residual artifact activity can be achieved by replacing the *up*sampling by the *re*sampling algorithm. Visually the improvement is most prominent for high frequency components exceeding 100 Hz, but the signal's power spectrum is an average over 10 6-sec-epochs recorded at electrode position Fp1 of one subject. Fig.7.1C demonstrates an artifact reduction that extends over all harmonics of the gradient repetition frequency (10 Hz in this case).

Besides an improved artifact removal we observed a reduction of computing time by a factor of 4 and at the same time a reduction of memory usage by a factor of 10 with resampling compared to upsampling to 50 KHZ. In both cases interpolation was done by means of a cubic spline function. Since the EEG- and the fMRI-clocks were not synchronized, the amount of shifting needed leading to an optimal sampling timing (in case of re-sampling) was randomly distributed over the original sampling interval or 0.2 ms; the average number of steps to find this optimum was 15.

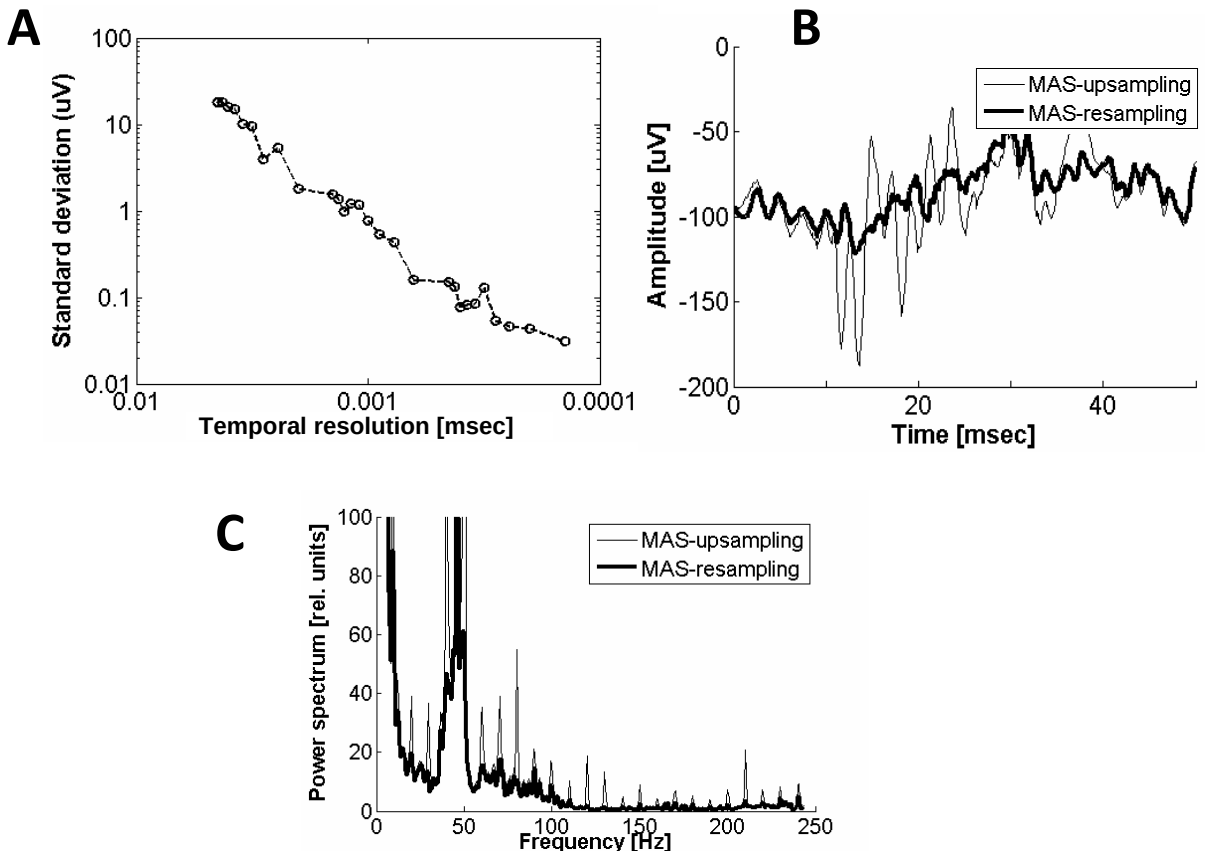


Fig.7.1 Upsampling and resampling:
A) Average standard deviation of the differences between the digitally simulated reference artifact and 30 resampled jittered variants observed at the different sampling intervals.
B) Example (real EEG) illustrating to what extent the residual artifact activity can be reduced by replacing the *up*sampling (10-fold)by the *re*sampling algorithm.
C) Same effect shown in the frequency domain. The power spectra represent the average over all subsequent 6 sec epochs of a 60 sec EEG segment recorded at electrode Fp1 in subject 1.

### 7.1.2 Head motion effect on the reduction of the gradient artifact

For the sake of testing the influence of head motion, the alignment methods (resampling and upsampling) applied in MAS and MAMAS should be identical in order to focus on the influence of head motion. Since resampling is more efficient than upsampling in the alignment of gradient artifacts, it can be used in MAS and MAMAS without any negative effect. Hence, the influence of head motion can be well observed at the level of single epochs as well as larger blocks of data. In the following, first the improvement achieved with the MAMAS method is illustrated in two representative examples showing the differences between MAS and MAMAS both on the level of a single artifact epoch (100 ms) and for a longer period of several seconds. Next, the improvement will be shown in spectral terms as averaged over all channels and subjects. Finally, the effect of the additional algorithm to reduce brief movement related artifacts will be demonstrated.

**i. Improvement as observed on a single epoch level**

Fig.7.2 presents the comparison of the results of the single epochs by applying MAS and MAMAS respectively. The only difference between the two methods is the way of selecting the gradient artifacts included in the average waveform estimation procedure. The effect of the movement guided selection is obvious for strong movements (see Fig.7.2B for an example) and less pronounced in cases of only mild movement (see Fig.7.2A for an example).

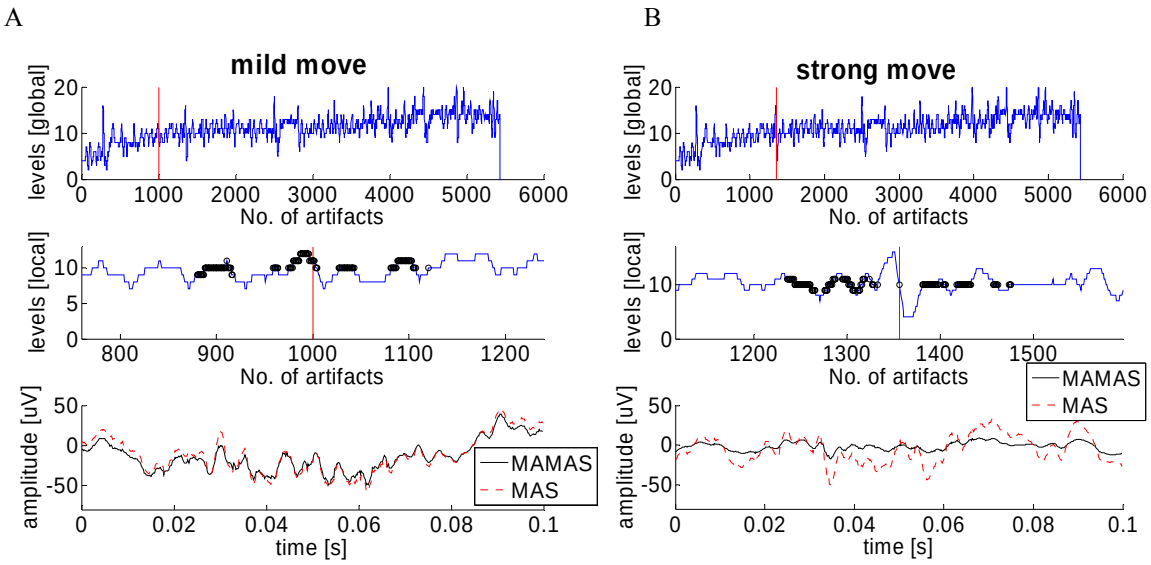


Fig.7.2 MAMAS versus MAS:
Comparison of two cases of gradient artifact removal from subject nc92. The SPM tracking data in the vicinity of this epoch are shown in two different scales in the upper and the center sub-figure. The black points reflect the selected epochs and the red line indicates the position of the current epoch. The bottom drawing shows the results obtained with the MAS and MAMAS methods.
A) One epoch observed at mild movement.
B) One epoch observed at strong movement.

**ii. Improvement observed over larger block of data.**

In the previous paragraph movement related differences between MAS and MAMAS could be tracked mainly in higher frequencies since the assessment of low frequency components was limited due the short epoch length of 100 ms. Therefore, the evaluation was extended to larger blocks of data comprising six seconds of EEG, i.e. a sequence of 60 (or 72 depending on the MR protocol) artifact epochs. They are represented with spectra in Fig.7.3 where the monitor data can be demonstrated by the SPM tracking data and the spectrum of MAMAS shows more reduction at the harmonic frequencies of gradient artifacts for the motion case.

A

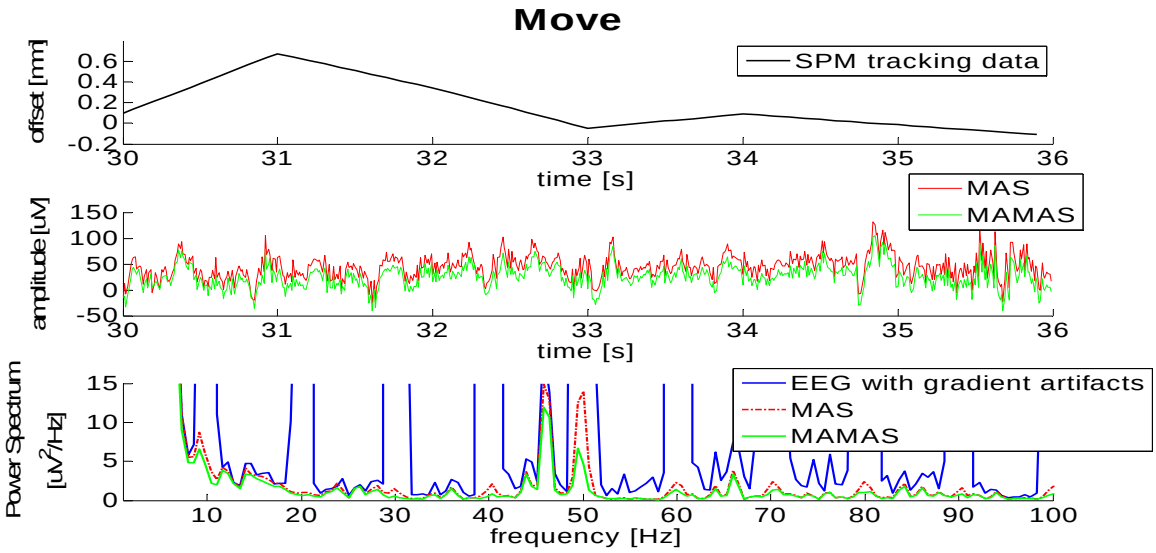


B

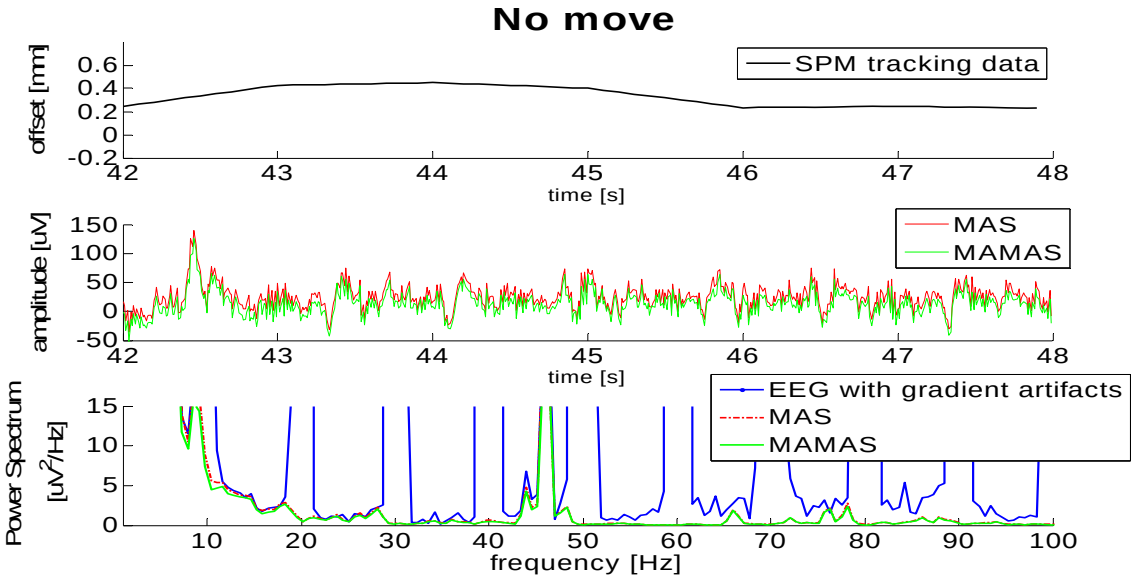


Fig.7.3 Comparison of gradient artifacts removal with MAS and MAMAS.
Per columns one 6-sec-EEG-segment of subject nc92, channel/electrode Fp1.
TR=2 sec, 20 slices, gradient repetition rate 10 Hz.
A) 'Move'-segment. B) 'No move' segment
Upper: SPM movement monitoring data.
Middle: EEG after gradient artifacts removals using MAS (red) and MAMAS (green) algorithm.
Bottom: Power spectra of the two methods.

### 7.1.3 The improved performance of using MAMAS

In this section, the performance of MAMAS and MAS is quantitatively compared depending both on the signal's frequency range and the strength of movement.

**i. Criterion to classify epochs with respect to the strength of movement as reported by the SPM displacement data**

A criterion to classify each artifact epochs into the group of 'move' epochs and 'no or mild move' epochs (this group later also called 'motionless') is needed to evaluate how much the performance differences between MAS and MAMAS depends on the presence of motion (as reported by SPM).

First, the differences (Fig.7.4B) of the y-displacement values (Fig.7.4A) provided by the SPM alignment routine are calculated to represent the actual rather than the long term change in head position. Next, the standard deviations (Fig.7.4C) of every 6 consecutive difference values are counted, each of which presenting one 6-second EEG epoch. The threshold for 'move' and 'no move' epochs was set to 0.2 mm and 0.1 mm respectively. That means that all epochs beyond 0.2 mm are classified as 'strongly moving' whereas epochs below 0.1 mm are classified as 'not or mildly moving'. All others were abandoned for the subsequent evaluation. A typical example of this classification is shown in Fig.7.5.

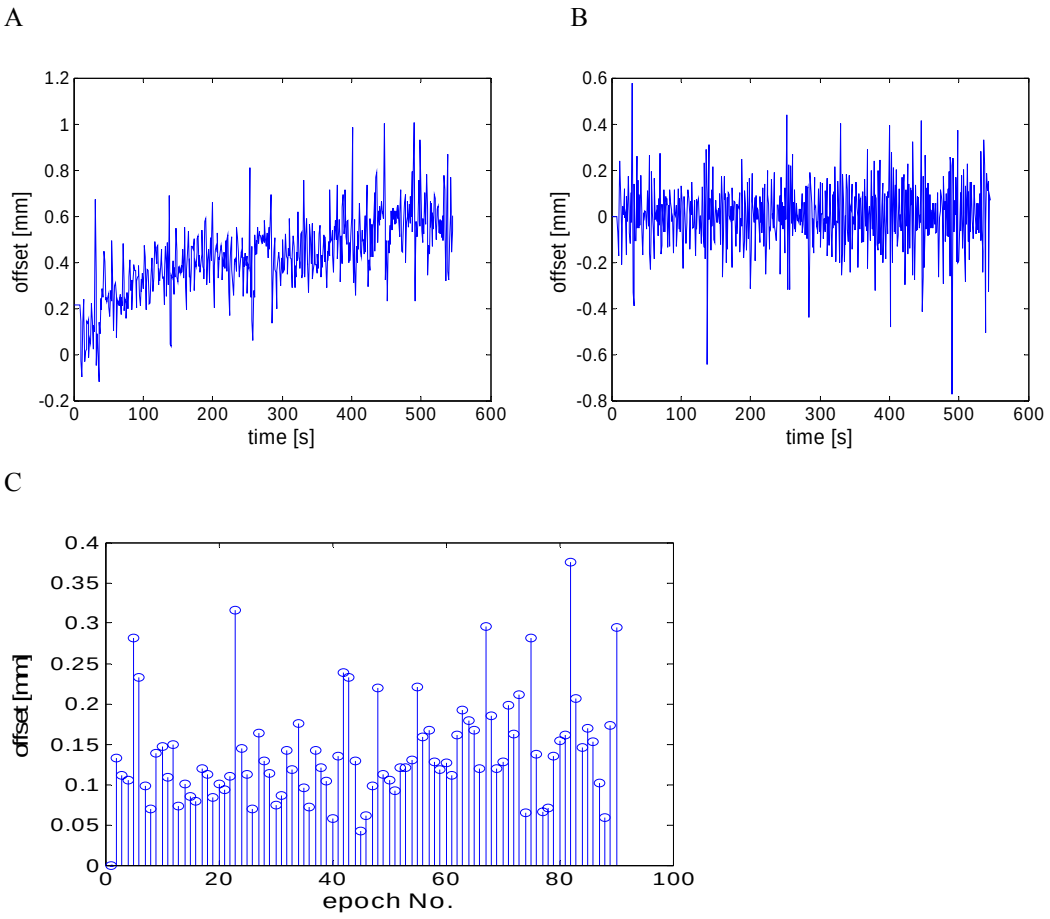


Fig.7.4 Illustration of the criterion used to select 'move' and 'no move' segments:
A) SPM monitor data (displacement in y direction) which are derived from the movement correction procedure of SPM.
B) Differences of A.
C) Time varying standard deviation (each value calculated over a 6-sec-epoch) derived from B). Epochs staying below 0.1 mm or beyond 0,2 mm are classified as 'no move' or 'move' respectively.

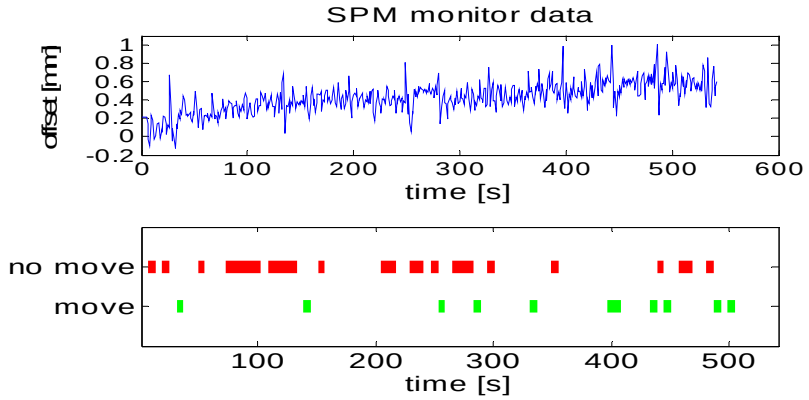


Fig.7.5 Classification of epochs according to type 'move' or 'no move' based on the temporal variation of the SPM related monitor data with 6 sec resolution.
Top : The SPM monitor data whose temporal resolution is 1 second.
Bottom: Indicate 'move' epochs (green) and 'no move' epochs(red).

## ii. The percentages of improvement (MAMAS vs. MAS)

A

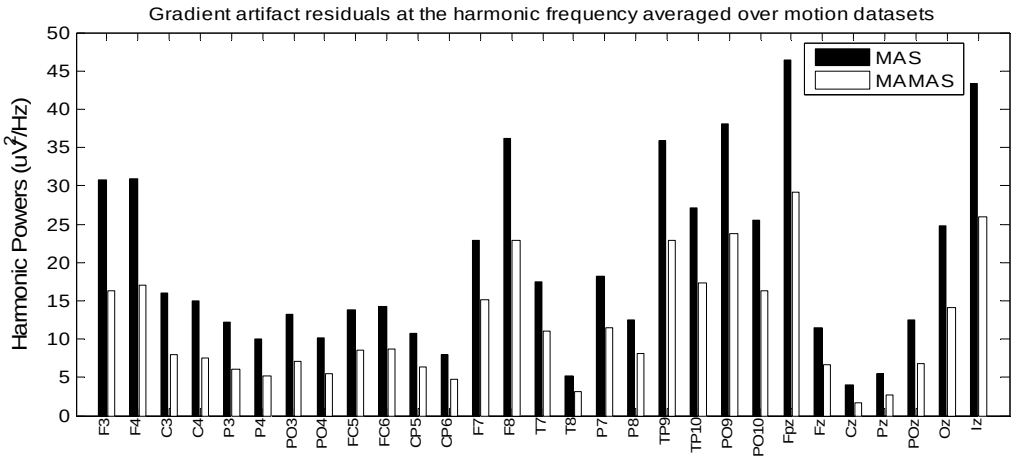


B

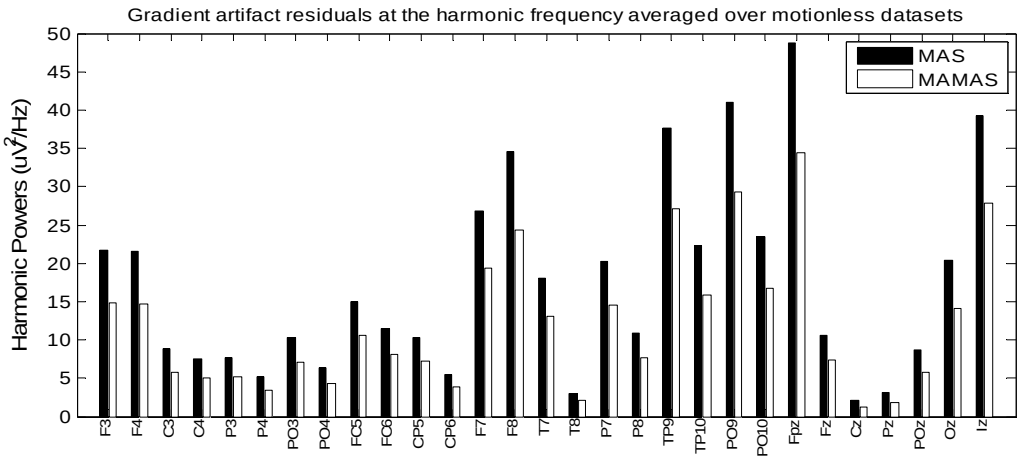


Fig.7.6 Estimation of the amount of residual gradient artifacts (MAS vs. MAMAS) at the gradient repetition rate and its harmonics for subject nc92 up to 120Hz. The underlying power spectrum was estimated according to Welch (1967) using 6-sec-segments. Each pair of bars represents the results obtained at the electrode location specified on the x-axis.
A) The harmonic powers of residual gradient artifacts averaged over 11 motion 6-sec-segments.
B) The harmonic powers of residual gradient artifacts averaged over 27 motionless 6-sec-segments.

The improvement of MAMAS was evaluated by a modified version of the 'improvement normalized power spectrum ratio' (INPS) introduced by Tong et al. (2001) in the context of removing ECG artifacts from the EEG. This measure was modified in order to quantify the relative percentage of improvement of MAMAS over the MAS algorithm by defining the following ratio:

$$RINPS = 100 * \frac{\sum_{j=N_{low}}^{N_{up}} P_j^{MAS} - \sum_{j=N_{low}}^{N_{up}} P_j^{MAMAS}}{\sum_{j=N_{low}}^{N_{up}} P_j^{MAMAS}} \quad (7.1)$$

with $P_j$ representing the spectral power at the $j^{th}$ harmonic (averaged over a 1 Hz interval) of the gradient repetition rate $g$, the superscript 'MAS' and 'MAMAS' indicating the two algorithms and the summation extending over the frequency range from $N_{low}$ *$g$ to $N_{up}$ *$g$ Hz. This measure was calculated for the following frequency bands: $g$…30 Hz, 30…100 Hz, 100…200 Hz, 200…2500 Hz by averaging over spectra estimated for representative 6-sec epochs of each of the 6 subjects. As demonstrated in Fig.7.6, the spectral power at the harmonics of the gradient repetition rate persisting after artifact removal (see Fig.7.6) exhibits substantial topographic variations. Therefore, the RINPS measure was determined individually for each electrode.

A

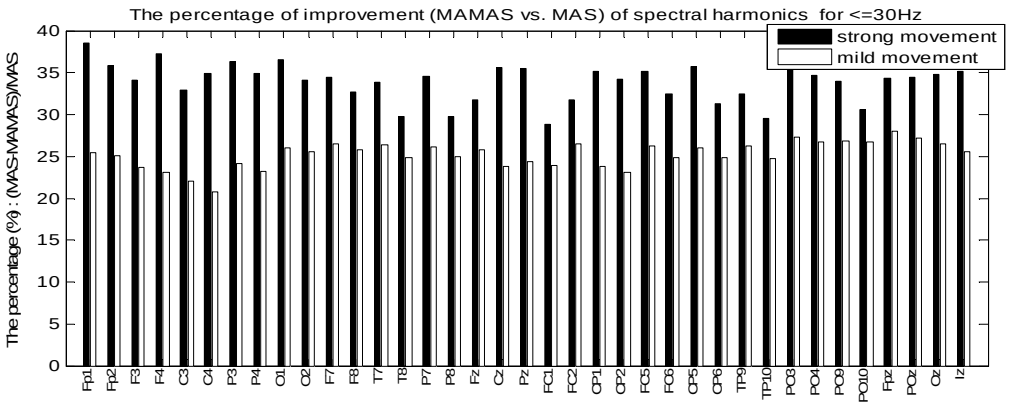


B

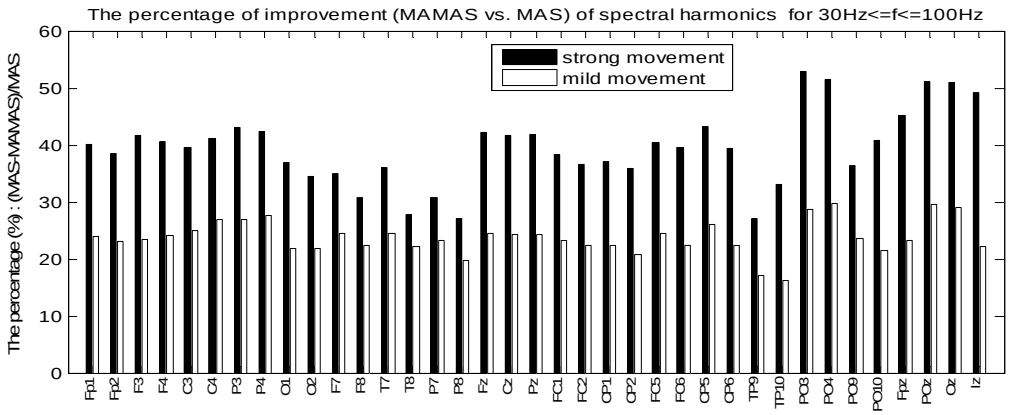

C

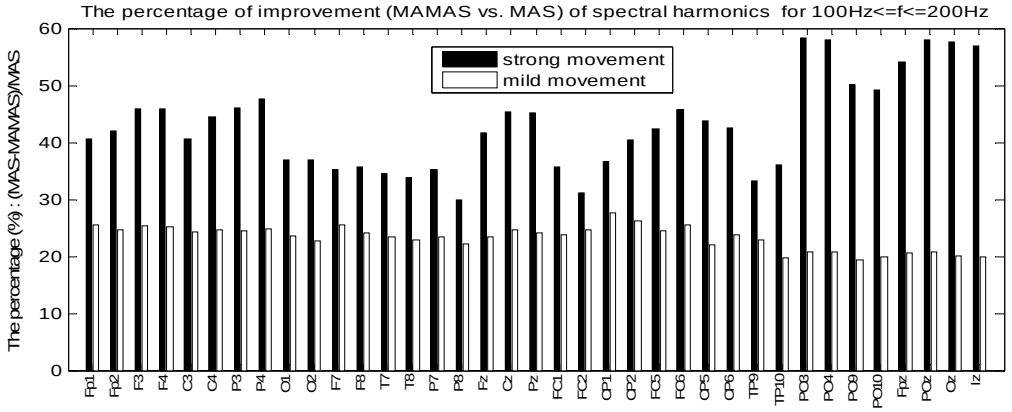


D

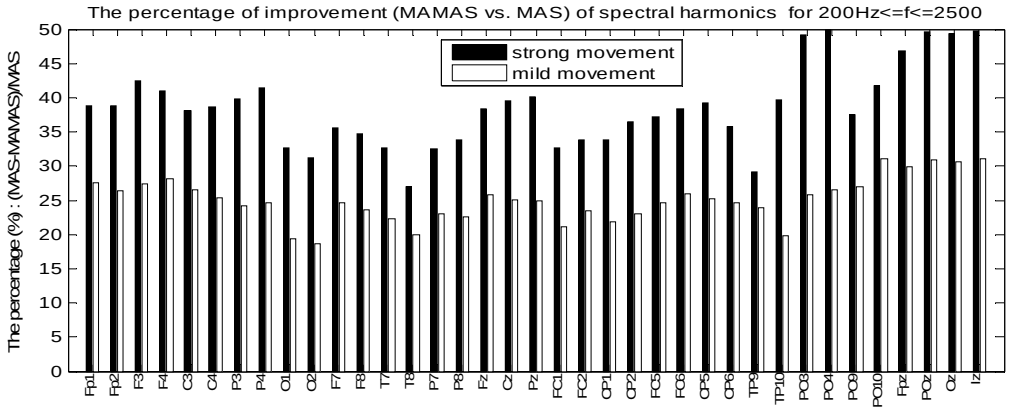


Fig.7.7 Bar diagram of cumulated spectral coefficients (RINPS-values, i.e. MAS-MAMAS/MAS ): The results of MAS and MAMAS are averaged over 87 strong movement epochs and 214 mild movement epochs of all six subjects. Each epoch is 6sec and each pair of bars represents the results obtained at the electrode location specified on the x-axis.

A) <= 30Hz,
B) 30Hz<=f<=100Hz,
C) 100Hz<=f<=200Hz,
D) 200Hz<= f <= 2500Hz.

According to eq.7.1, the percentage of improvement in different frequency ranges is shown in Fig.7.7. Obviously, throughout all frequency bands MAMAS leads to an improved reduction of artifact activity both under the 'move/strong movement' and 'no move/mild movement' conditions. In the low frequency range (10 Hz - 30 Hz) this improvement is lowest (about 25%-35% for 'mild movement'/'strong movement' segments in all channels) whereas the improvement goes up to 25%-45% in higher frequency ranges (> 30 Hz). In summary, MAMAS achieves a clearly improved artifact removal result under all conditions.

### 7.1.4 Special post processing to reduce residual artifacts caused by brief movements

Usually, if present at all, the amplitude of the residual artifact persisting after application of MAMAS is much below typical EEG artifacts of 50-100 μV peak-to-peak and can thus be neglected with respect to the clinical EEG evaluation. However, occasionally – as described

in the 5.3.4.5 section – a prominent brief movement related residual artifact occurs with peak to peak amplitudes up to 1000 µV (see Fig.7.8A and Fig.7.8C for an example) in the 3T MR scanner which massively hampers the clinical EEG interpretation. The special post processing designed to handle this kind of residual artifacts gets this artifact down to a fraction that is comparable to the usual result after MAMAS application, both in the time (Fig.7.8C) and frequency (Fig.7.8D) domain, making it thus suitable for clinical purposes.

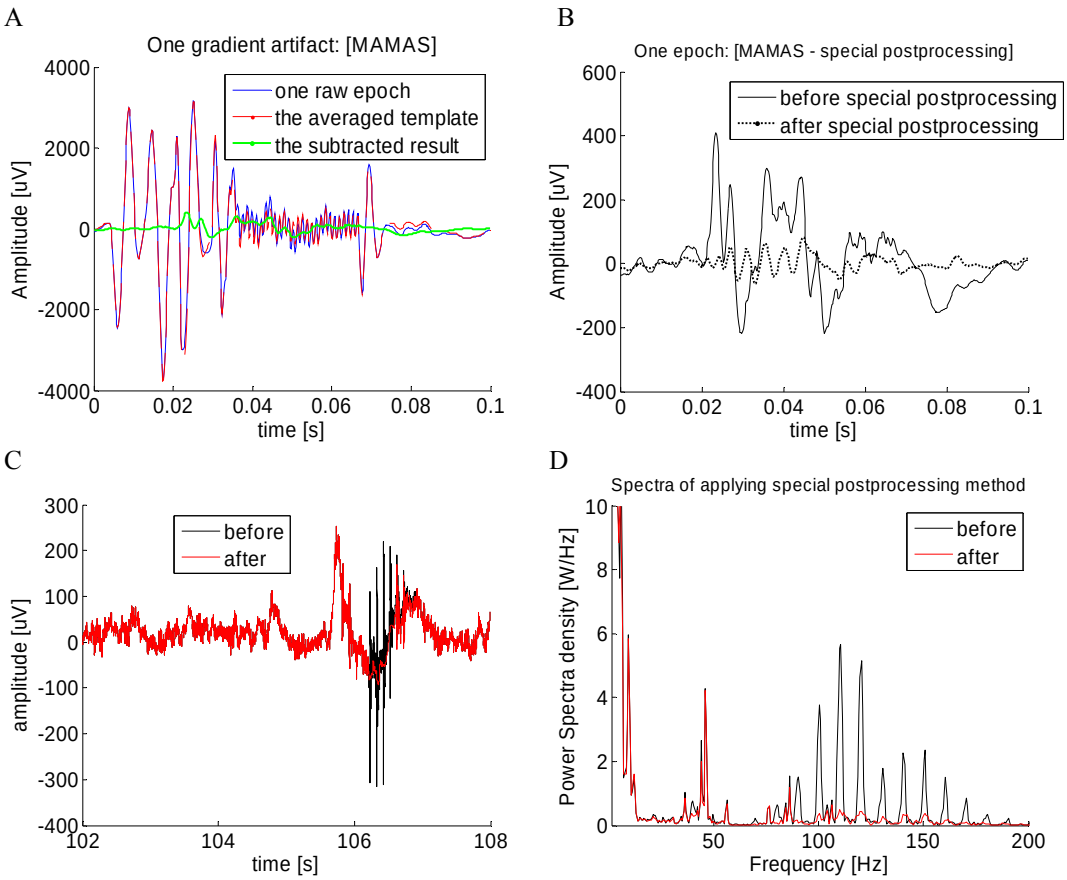


Fig.7.8 Special postprocessing:
A) One epoch of subject nc92, recorded at brief motion within only this one slice. MAMAS removes the main artifact but leaves a substantial residual.
B) Further reduction of the residual artifact amplitude after applying the special processing algorithm.
C) Results of one 6-sec-segment before and after application of the special postprocessing (Channel F3, subject tr81).
D) Spectra of C.

For further illustration, one single epoch of the raw signal before and after MAMAS application is presented in Fig.7.8A together with the large residual artifact caused by the brief motion. The effect of the removal algorithm is shown in Fig.7.8B with an adapted amplitude scale. The short epoch length cannot fully demonstrate the performance of this postprocessing, neither in the time nor in the frequency domain. Therefore, another example is presented in Fig.7.8C (time domain) and Fig.7.8D (frequency domain) before and after

artifact removal, this time using an epoch length of 6 sec. Obviously, the algorithm achieves a massive artifact reduction in both domains.

### 7.1.5 Visual evaluation of the new method and comparison with previous methods

The different steps of the new methods (MAMAS, special processing of brief movement related artifacts, vibration artifacts) are illustrated here regarding their effect of removing artifacts in the time domain. Fig.7.9 displays the results achieved both after the various steps of the new algorithm and after application of the MAS and the AAS method. Obviously, AAS both without or with upsampling comes out with significant residual artifacts thus demonstrating that a fixed averaged template for all individual artifact is not suitable even if with a higher interpolation factor. These results (Fig.7.9B and C) make clear that an additional postprocessing technique like ANC (as proposed by Allen, 2000) is necessary to yield acceptable results. In contrast, MAS and MAMAS (Fig.7.9D and E) both strongly reduce the artifact activity with MAMAS outperforming MAS regarding the residual noise especially at frequencies beyond 30 Hz which is in line with the quantitative analyses presented beforehand. The additional special postprocessing targeting brief movements related artifacts additionally contributes to the signal quality if applied subsequently MAMAS (Fig.7.9H). It is worth mentioning that the special post processing can also be applied in combination with MAS.

The final result (Fig.7.9I) included the application of the bandstop filter to suppress vibration artifacts. With respect to potential quantitative analyses of Gamma-activity (i.e. activity > 30 Hz) this may be disadvantageous since the amount of true EEG activity discarded by this procedure cannot be controlled. In such cases the vaccum pump should be switched off (which is feasible for a limited experimental time) to prevent vibration related artifacts. As expected, the only type of artifacts persisting after all these steps is the BCG activity.

A

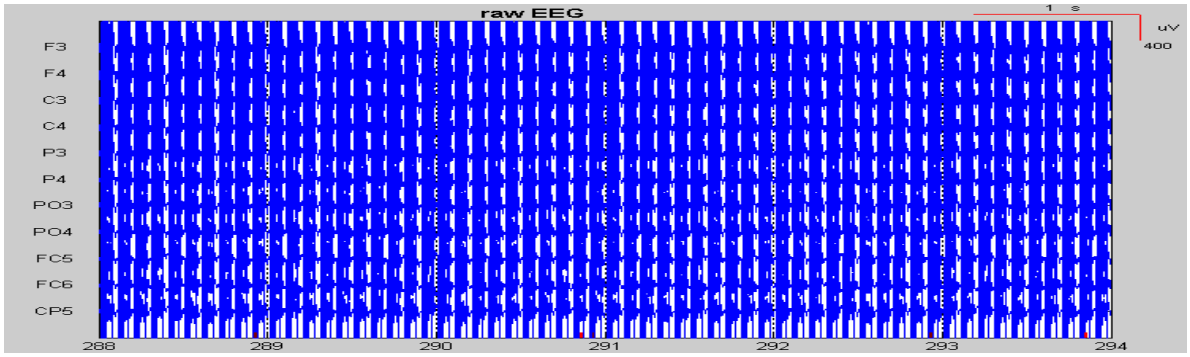
raw EEG
1 s
uV
400
F3
F4
C3
C4
P3
P4
PO3
PO4
FC5
FC6
CP5
288
289
290
291
292
293
294

B

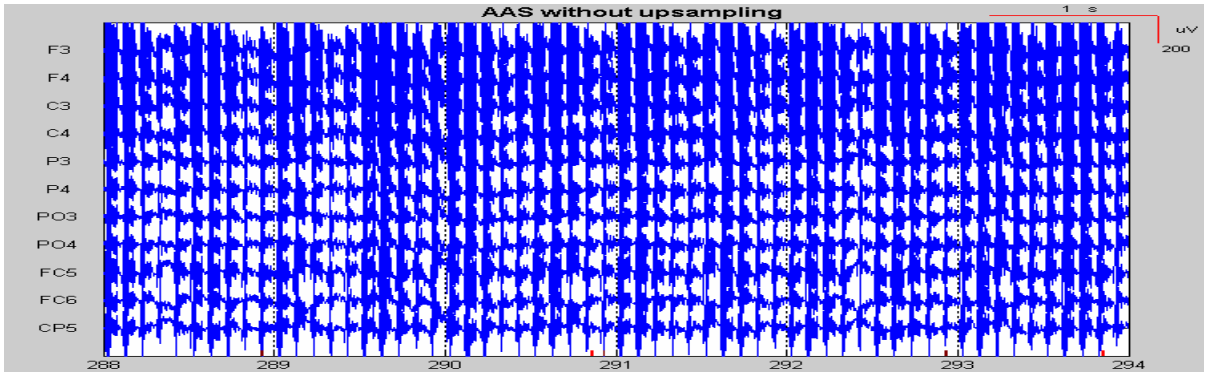
AAS without upsampling
1 s
uV
200
F3
F4
C3
C4
P3
P4
PO3
PO4
FC5
FC6
CP5
288
289
290
291
292
293
294

C

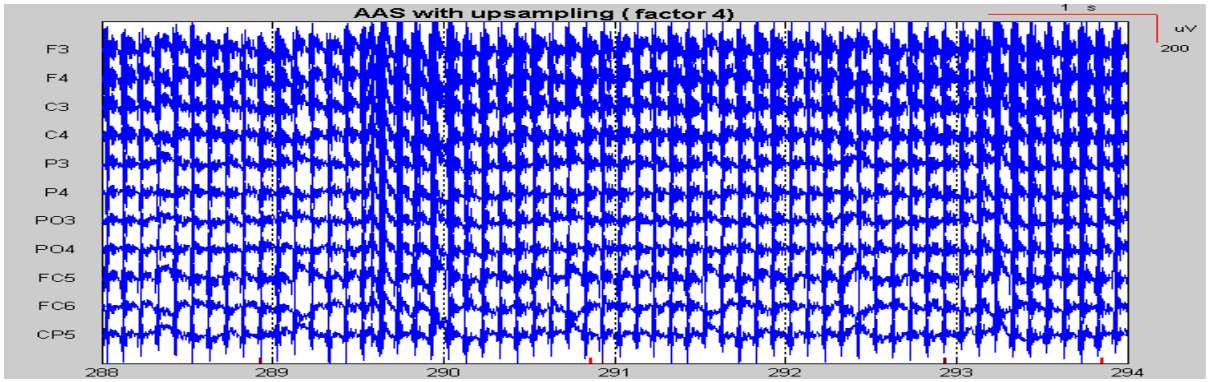
AAS with upsampling ( factor 4)
1 s
uV
200
F3
F4
C3
C4
P3
P4
PO3
PO4
FC5
FC6
CP5
288
289
290
291
292
293
294

D

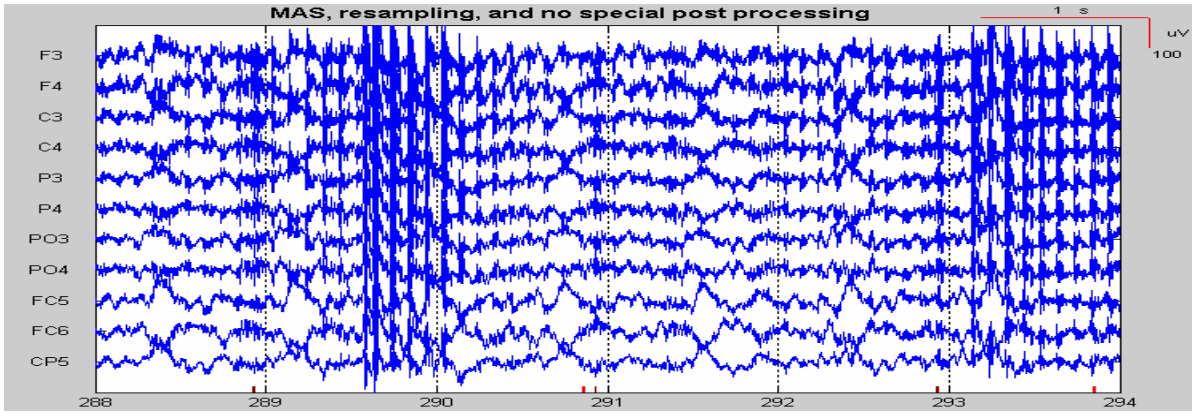
MAS, resampling, and no special post processing
1 s
uV
100
F3
F4
C3
C4
P3
P4
PO3
PO4
FC5
FC6
CP5
288
289
290
291
292
293
294

E

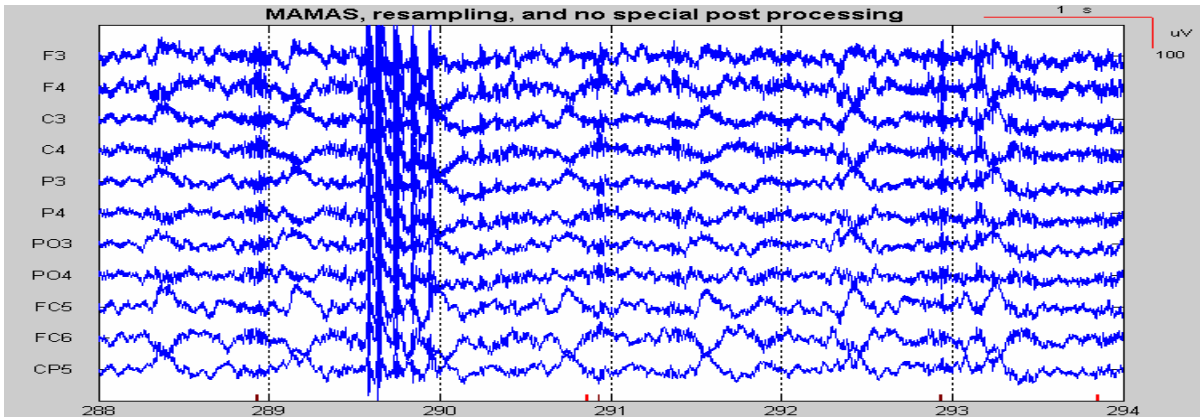
MAMAS, resampling, and no special post processing
1 s
uV
100
F3
F4
C3
C4
P3
P4
PO3
PO4
FC5
FC6
CP5
288
289
290
291
292
293
294

F

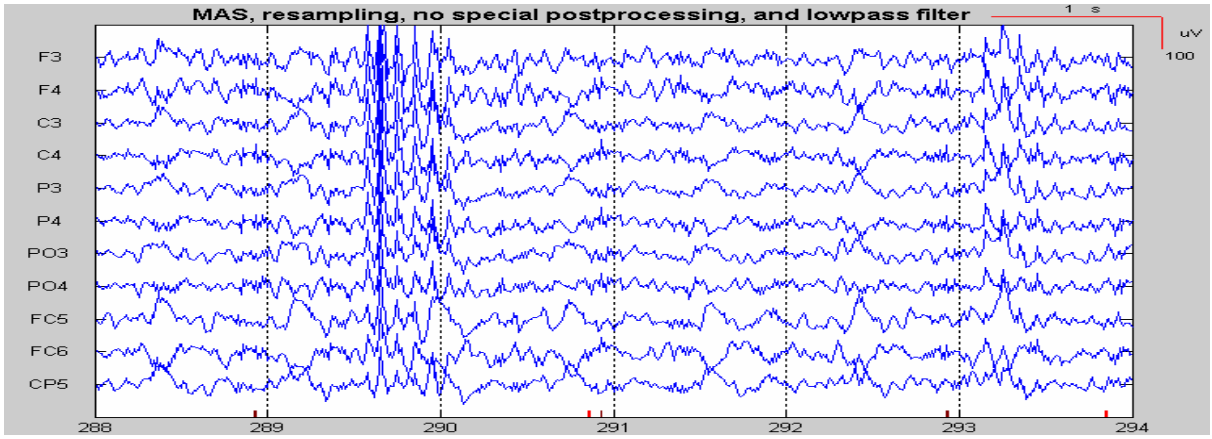
MAS, resampling, no special postprocessing, and lowpass filter
1 s
uV
100
F3
F4
C3
C4
P3
P4
PO3
PO4
FC5
FC6
CP5
288
289
290
291
292
293
294

G

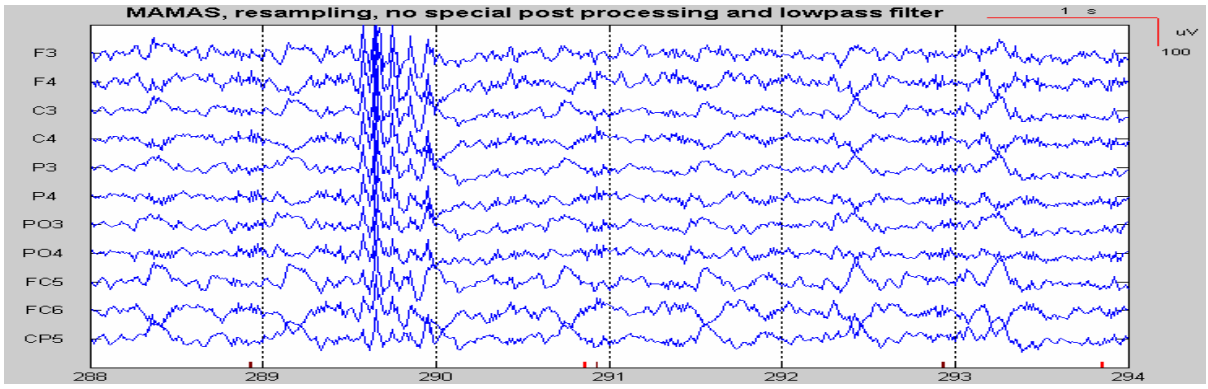
MAMAS, resampling, no special post processing and lowpass filter
1 s
uV
100
F3
F4
C3
C4
P3
P4
PO3
PO4
FC5
FC6
CP5
288
289
290
291
292
293
294

H

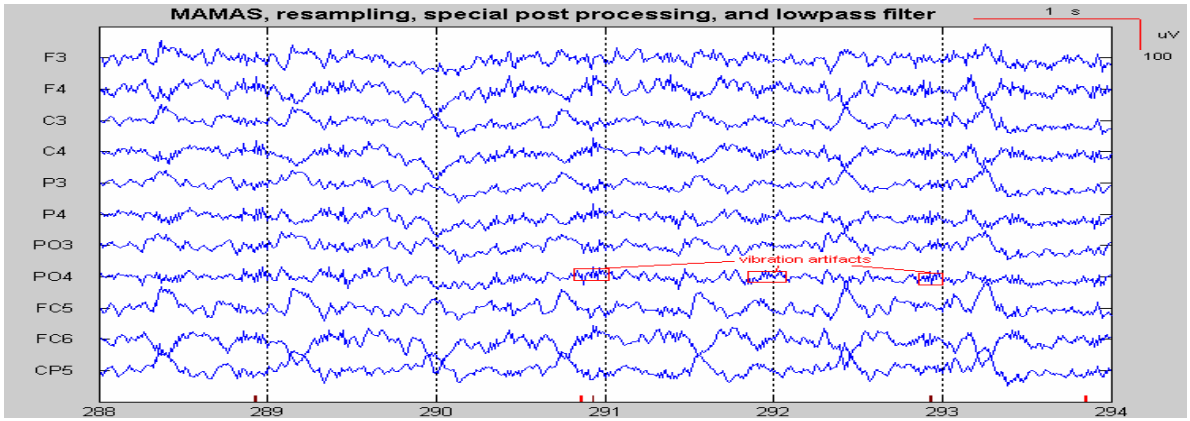
MAMAS, resampling, special post processing, and lowpass filter
1 s
uV
100
F3
F4
C3
C4
P3
P4
PO3
PO4
vibration artifacts
FC5
FC6
CP5
288
289
290
291
292
293
294

I

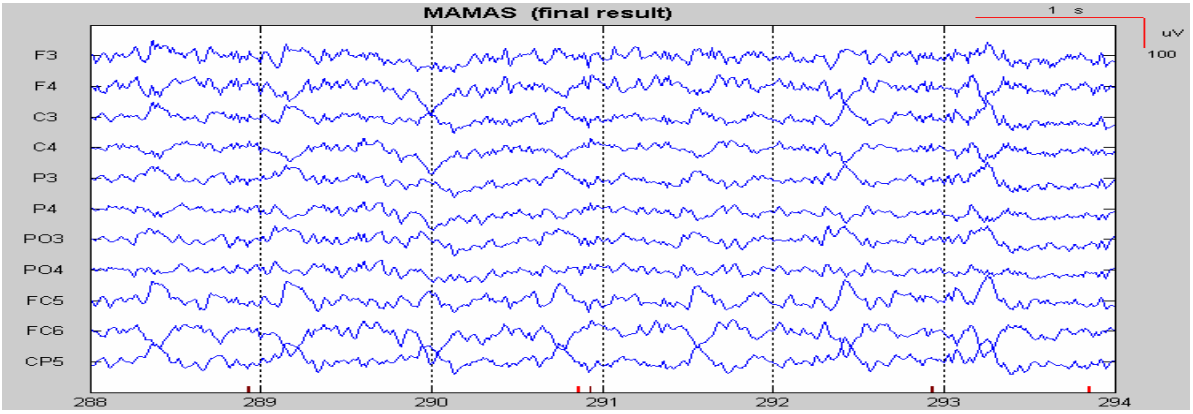


Fig.7.9 Comparison of different processing steps (as indicated) as applied to one 6-sec-EEG-segment of subject nc92.

A) Raw EEG channels (F3, F4, C3, C4, P3, P4, PO3, PO4, FC5, FC6, CP5) recorded during MR scanning.
B) AAS (Allen et. al., 2000) without upsampling.
C) AAS with upsampling (factor 4).
D) MAS with resampling, without special post processing.
E) MAMAS with resampling, without special post processing.
F) MAS with resampling, without special post processing, low pass filtering with 120 Hz cutoff frequency.
G) MAMAS with resampling, without special post processing, low pass filtering with 120 Hz cutoff frequency.
H) MAMAS with resampling, special post processing, low pass filtering with 120 Hz cutoff frequency.
I) MAMAS with resampling, special post processing, low pass filtering with 120 Hz cutoff frequency, bandstop filtering (>40Hz and <50Hz) to remove vibration artifact.

## 7.2 BCG artifacts, combined MNF and subtraction algorithm: Evaluation and Comparison

### 7.2.1 Selection of MNF-components to remove the BCG artifacts

Due to the character of MNF (i.e. ICs sorted according to the SNR), the selection of components reduces to the task to define the number of the selected components. To estimate the suitable number, the relative variance, defined as the ratio of the variance of the EEG data after BCG removal and the variance of the EEG recorded outside the scanner, was calculated individual for each subject and each channel and then averaged over all 4 subjects and 29 channels. This measure was separately determinate for the EEG resulting after processing with MNF alone and with the combined MNF and subtraction procedure. The result (Fig.7.10) shows that at a number of four removed components (i.e. the last or first four depending on the direction of ordering) would on average lead to a signal variance identical to the EEG recorded from the same subject outside the scanner room. However, looking at the standard deviation it is obvious, that in many cases the variance after removing these four components is far below the signal power observed outside the scanner indicating the risk of suppressing a fraction of true EEG. With this consideration, the removal of only two or three

components is more appropriate to preserve true EEG activity. Finally a number of two removed components were used for all further evaluation reported in the subsequent sections.

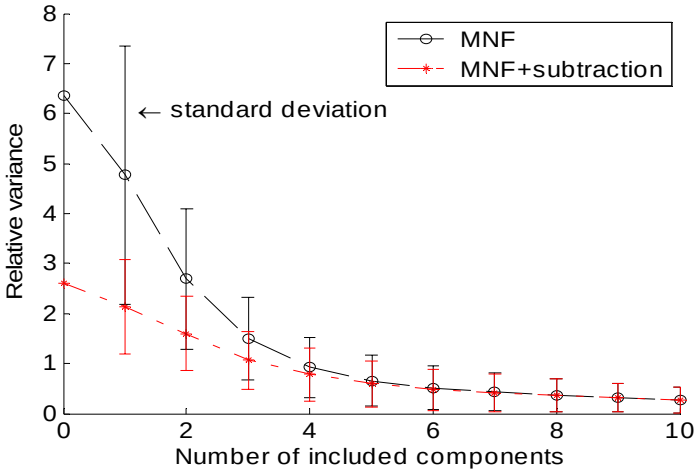


Fig.7.10 The relative variance vs. number of included components: averaged over four subjects, 29 channels.

### 7.2.2 Comparison of MNF, fastICA and JADE: Power to discriminate BCG from EEG

In order to compare the ability to separate BCG from EEG activity, each of three methods (MNF, fastICA and JADE) was applied to the same ten-second EEG segment of each subject (four subjects/four segments), where gradient artifacts and vibration artifacts had been removed before application of the three techniques. The correlation coefficients of each IC of each method with the BIS (defined in section 6.1.3) are listed in Table 7.1. By comparing the largest correlation coefficient of each method, the correlations obtained with MNF are always larger than those obtained with fastICA or JADE. As a second effect, the largest two correlations of fastICA as well as JADE are usually observed at random positions whereas in MNF they are in all cases obtained at the last positions within the sequence of components. Besides these results it is worth mentioning that fastICA usually requires long computing times to reach convergence (typically only after 1000 cycles)

Independent of the ordering feature of the three methods we analysed their specific ability to separate BCG from EEG as follows: The ten components showing the largest correlation with the BIS were selected for each subject using each of the three BSS methods (MNF, fast ICA, JADE). They were ordered by their correlation coefficient, see Fig.7.11). The error bars indicate the standard deviation over the subjects. With MNF these 10 components are the last 10 components (if ordered along their eigenvalues (i.e. their SNR)) whereas in fast ICA and JADE they are randomly distributed among the total set of 29 components. As can be seen in Fig.7.11, with the MNF method the two largest coefficients are significantly larger ($p<.005$, two-sided t-test) than the corresponding components obtained with the two other ICA solutions, whereas the components with lower coefficients with the other ICA solutions have

slightly larger values than those obtained with MNF. This means that the lower two MNF-components represent the BCG artifact in a more specific manner than the two other ICA-variants, indicating that MNF is more effective in extracting the BCG.

Table 7.1 Correlation coefficients between the BIS and the components calculated with MNF, fastICA and JADE.

| Number Of component | fv95 | | | pn48 | | | lr64 | | | be98 | | |
|---|---|---|---|---|---|---|---|---|---|---|---|---|
| | MNF | fastICA* | JADE | MNF | fastICA | JADE | MNF | fastICA* | JADE | MNF | fastICA* | JADE |
| 1 | 0,07 | 0,169 | 0,11 | 0,166 | 0,232 | 0,066 | 0,117 | 0,169 | 0,1 | 0,096 | 0,313 | 0,205 |
| 2 | 0,036 | 0,347 | 0,092 | 0,144 | 0,216 | 0,082 | 0,105 | 0,64 | 0,128 | 0,176 | 0,147 | 0,181 |
| 3 | 0,102 | 0,375 | 0,213 | 0,171 | 0,186 | 0,093 | 0,158 | 0,144 | 0,113 | 0,234 | 0,401 | 0,121 |
| 4 | 0,124 | 0,178 | 0,153 | 0,114 | 0,075 | 0,128 | 0,106 | 0,183 | 0,268 | 0,2 | 0,37 | 0,157 |
| 5 | 0,156 | 0,178 | 0,153 | 0,143 | 0,145 | 0,107 | 0,197 | 0,242 | 0,133 | 0,169 | 0,196 | 0,101 |
| 6 | 0,152 | 0,355 | 0,099 | 0,174 | 0,453 | 0,086 | 0,139 | 0,139 | 0,172 | 0,09 | 0,455 | 0,104 |
| 7 | 0,115 | 0,306 | 0,136 | 0,068 | 0,226 | 0,163 | 0,187 | 0,466 | 0,108 | 0,194 | 0,254 | 0,082 |
| 8 | 0,157 | 0,447 | 0,149 | 0,115 | 0,107 | 0,259 | 0,183 | 0,307 | 0,098 | 0,234 | 0,329 | 0,215 |
| 9 | 0,122 | 0,14 | 0,263 | 0,129 | 0,415 | 0,151 | 0,154 | 0,214 | 0,163 | 0,13 | 0,705 | 0,113 |
| 10 | 0,209 | 0,309 | 0,047 | 0,113 | 0,115 | 0,16 | 0,124 | 0,132 | 0,123 | 0,113 | 0,17 | 0,083 |
| 11 | 0,091 | 0,227 | 0,308 | 0,155 | 0,136 | 0,166 | 0,071 | 0,221 | 0,148 | 0,106 | 0,253 | 0,122 |
| 12 | 0,086 | 0,232 | 0,088 | 0,09 | 0,236 | 0,156 | 0,075 | 0,359 | 0,173 | 0,129 | 0,211 | 0,301 |
| 13 | 0,13 | 0,155 | 0,148 | 0,183 | 0,352 | 0,171 | 0,082 | 0,437 | 0,27 | 0,097 | 0,297 | 0,131 |
| 14 | 0,148 | 0,555 | 0,21 | 0,128 | 0,302 | 0,252 | 0,216 | 0,262 | 0,167 | 0,23 | 0,418 | 0,118 |
| 15 | 0,127 | 0,222 | 0,203 | 0,141 | 0,263 | 0,242 | 0,104 | 0,114 | 0,163 | 0,229 | 0,115 | 0,334 |
| 16 | 0,229 | 0,127 | 0,126 | 0,157 | 0,247 | 0,472 | 0,214 | 0,154 | 0,331 | 0,131 | 0,356 | 0,091 |
| 17 | 0,161 | 0,199 | 0,171 | 0,207 | 0,265 | 0,247 | 0,118 | 0,16 | 0,304 | 0,268 | 0,596 | 0,239 |
| 18 | 0,12 | 0,319 | 0,157 | 0,206 | 0,33 | 0,168 | 0,257 | 0,098 | 0,174 | 0,339 | 0,223 | 0,302 |
| 19 | 0,158 | 0,395 | 0,256 | 0,241 | 0,139 | 0,25 | 0,19 | 0,194 | 0,186 | 0,232 | 0,127 | 0,198 |
| 20 | 0,167 | 0,37 | 0,255 | 0,222 | 0,631 | 0,179 | 0,153 | 0,296 | 0,275 | 0,157 | 0,159 | 0,232 |
| 21 | 0,233 | 0,37 | 0,263 | 0,214 | 0,379 | 0,318 | 0,084 | 0,198 | 0,187 | 0,187 | 0,312 | 0,291 |
| 22 | 0,171 | 0,121 | 0,355 | 0,245 | 0,13 | 0,201 | 0,18 | 0,314 | 0,225 | 0,295 | 0,295 | 0,357 |
| 23 | 0,423 | 0,36 | 0,351 | 0,248 | 0,092 | 0,307 | 0,195 | 0,187 | 0,141 | 0,318 | 0,604 | 0,131 |
| 24 | 0,244 | 0,239 | 0,497 | 0,332 | 0,206 | 0,39 | 0,211 | 0,345 | 0,28 | 0,398 | 0,157 | 0,365 |
| 25 | 0,597 | 0,297 | 0,193 | 0,41 | 0,454 | 0,491 | 0,181 | 0,17 | 0,182 | 0,124 | 0,123 | 0,456 |
| 26 | 0,442 | 0,472 | 0,343 | 0,656 | 0,178 | 0,451 | 0,316 | 0,178 | 0,447 | 0,237 | 0,252 | 0,342 |
| 27 | 0,363 | 0,353 | 0,417 | 0,447 | 0,124 | 0,366 | 0,417 | 0,117 | 0,444 | 0,396 | 0,255 | 0,31 |
| 28 | 0,643 | 0,287 | 0,5 | 0,876 | 0,386 | 0,547 | 0,817 | 0,141 | 0,418 | 0,76 | 0,366 | 0,428 |
| 29 | 0,847 | 0,161 | 0,392 | 0,56 | 0,259 | 0,46 | 0,828 | 0,146 | 0,479 | 0,802 | 0,227 | 0,538 |

* : larger than 1000 cycles

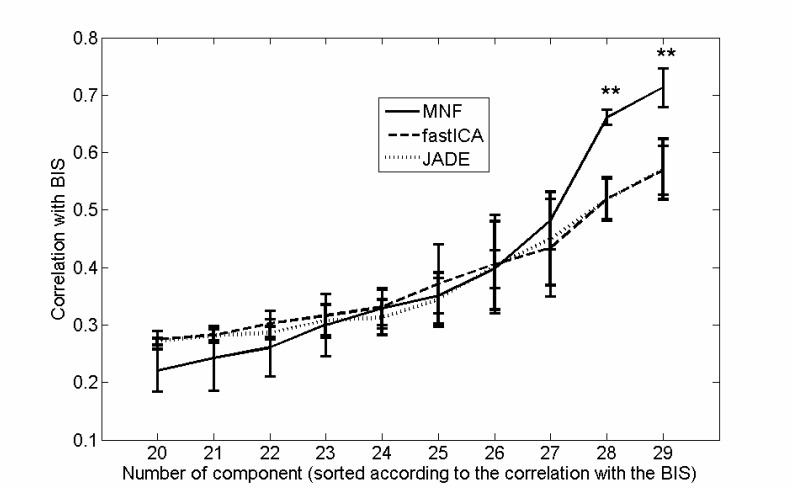


Fig.7.11 Correlations of the 10 components showing the largest correlation with the BIS.
Averaged over all four subjects. Error bars indicate the standard deviation. The correlation factors of MNF components marked by '**' are significantly higher than those observed with fastICA and JADE at a significance level p<.005 (two-sided t-test).

A

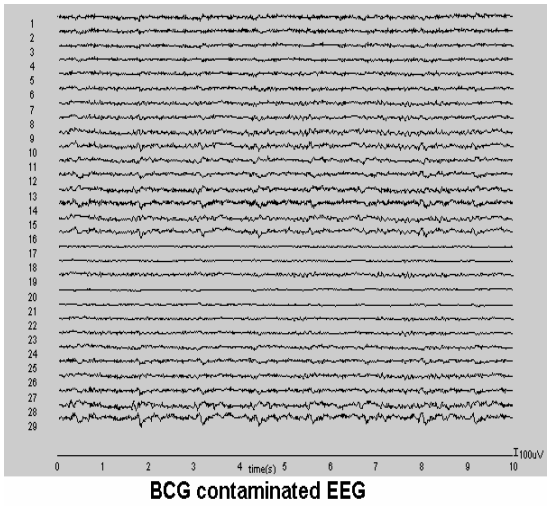


B

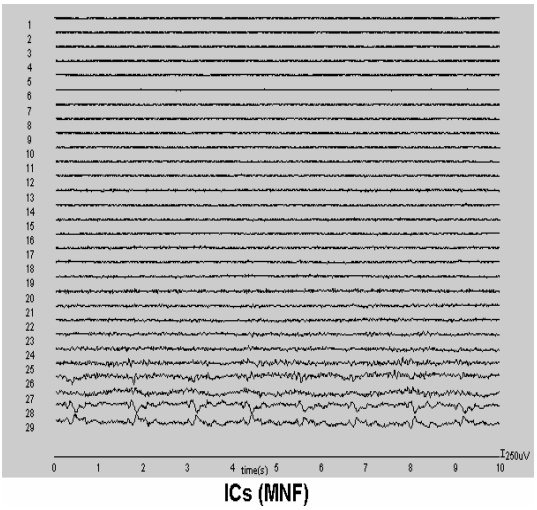


C

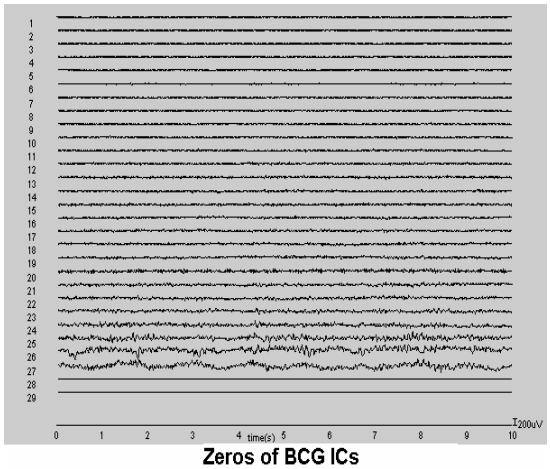


D

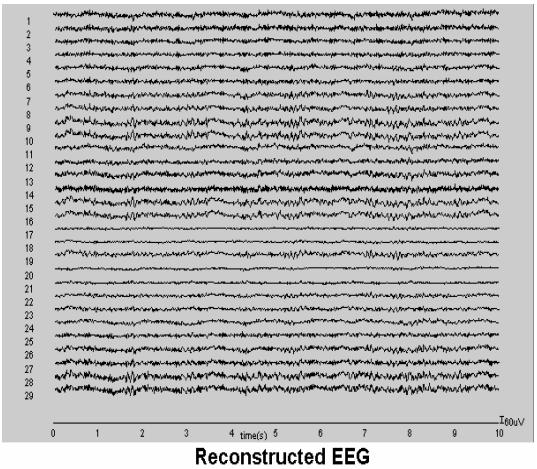

E F

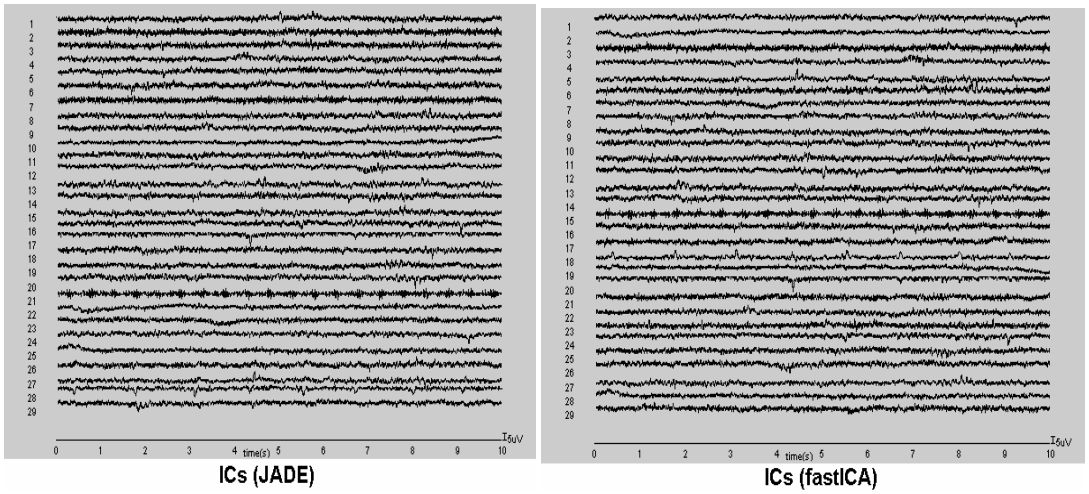


Fig.7.12 MNF- and ICA-processing of a ten-second EEG data set from subject be98.
A) EEG with BCG artifacts but without vibration artifacts.
B) Decomposed ICs using MNF.
C) Identified BCG ICs of B) are set to zeros.
D) EEG reconstructed from C).
E) Decomposed ICs using JADE.
F) Decomposed ICs using FastICA.

Fig.7.12 shows the result of the whole procedure of separation, denoising (BCG artifacts), and reconstruction. The raw BCG contaminated ten-second segment (Fig.7.12A) is separated into different ICs (Fig.7.12B) with MNF. After the last two ICs were defined as BCG ICs and replaced with zeros in Fig.7.12C, the reconstructed data is depicted in Fig.7.12D where the residual BCG is largely reduced down to the level of normal EEG (10μV-150μV). The decomposed BCG-related ICs of JADE (Fig.7.12E) and FastICA (Fig.7.12F) are obviously randomly distributed.

### 7.2.3 Reducing the computational load – Usage of a fixed mixing matrix A.

In Fig.7.13 the correlation coefficients of the source components with the BIS are shown for the adaptively derived as opposed to the fixed mixing matrix (averaged over all segments of the 4 subjects). Obviously the differences between the usage of a fixed and an adaptive mixing matrix are marginal. This indicates that a fixed (yet subject specific) mixing matrix may be used without substantial loss of performance in artifact removal but with a significant saving in computing time of about 40% (Intel Pentium4 processor running with 2.4 GHz, 512 MB RAM, Windows 2000 professional operating system). The total computing time clearly stays below the signal duration in any case (both using a fixed or adaptive mixing matrix) thus meeting the requirements of real-time processing.

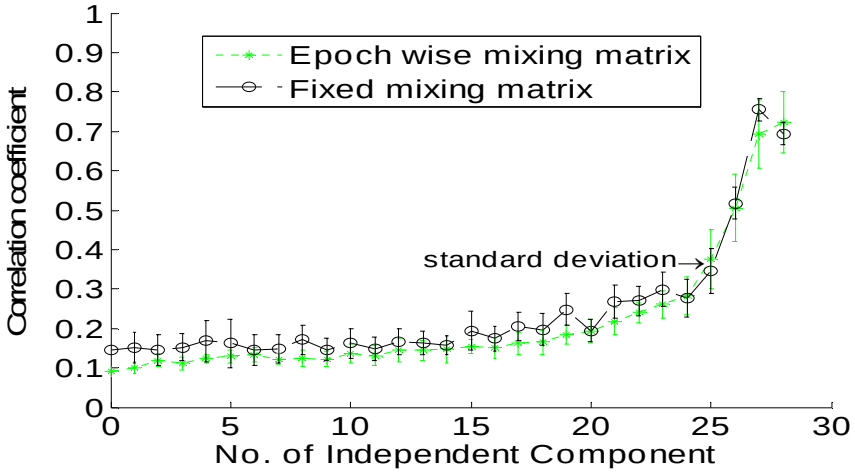


Fig.7.13 Correlation coefficients vs. number of independent components.
Each averaged over 80 segments (four subjects, 20 segments/subject, 29 channels/subject).

### 7.2.4 Evaluation in the time and frequency domain

#### 7.2.4.1 Spectral evaluation at the ECG base frequency and its harmonics

The ECG and the BCG artifacts are strictly temporally locked. Therefore, the BCG contributes to the total signal spectrum at the heart rate and its harmonics. The INPS (see chapter 6.3) measure quantifies the ratio of these cumulated power spectral components before and after processing. In Table 7.2 the total signal power and the artifact removal as reflected by INPS is presented for the signal resulting after processing with MNF alone, subtraction alone and combined MNF and subtraction. According to the INPS values MNF alone removes already the largest fraction of the BCG artifacts. Subtraction as an additional method following MNF removes a smaller fraction. Even if it is the only algorithm applied it is not as effective as MNF alone. In summary the combined method performs better than subtraction alone and MNF alone.

Table 7.2: Total Variance and INPS values of a ten-second EEG epoch (electrode O1) of each subject observed with MNF alone, combined MNF and subtraction, and subtraction alone.

| | Variance [rel. units] | | | | INPS | | |
|---|---|---|---|---|---|---|---|
| Subject | Raw signal | MNF | MNF and subtraction | Subtraction alone | MNF | MNF and subtraction | Subtraction alone |
| 1 | 141 | 22 | 9 | 37 | 6.39 | 2.54 | 3.79 |
| 2 | 586 | 75 | 27 | 101 | 7.83 | 2.81 | 5.80 |
| 3 | 33 | 7 | 4 | 23 | 4.72 | 1.83 | 1.44 |
| 4 | 68 | 15 | 9 | 45 | 4.37 | 1.64 | 1.50 |

### 7.2.4.2 Evaluation in the time domain

The quantitative analysis presented in Table 7.2 is in line with the waveforms resulting from the various processing steps as demonstrated in Fig.7.14 showing one 6 sec segment as a detailed example. Obviously, MNF alone as well as subtraction alone are worse than the combined method in suppressing the BCG. The improvement achieved with MNF is most prominent at lower frequencies below 10 Hz whereas subtraction leads to a further reduction both at lower and higher frequencies.

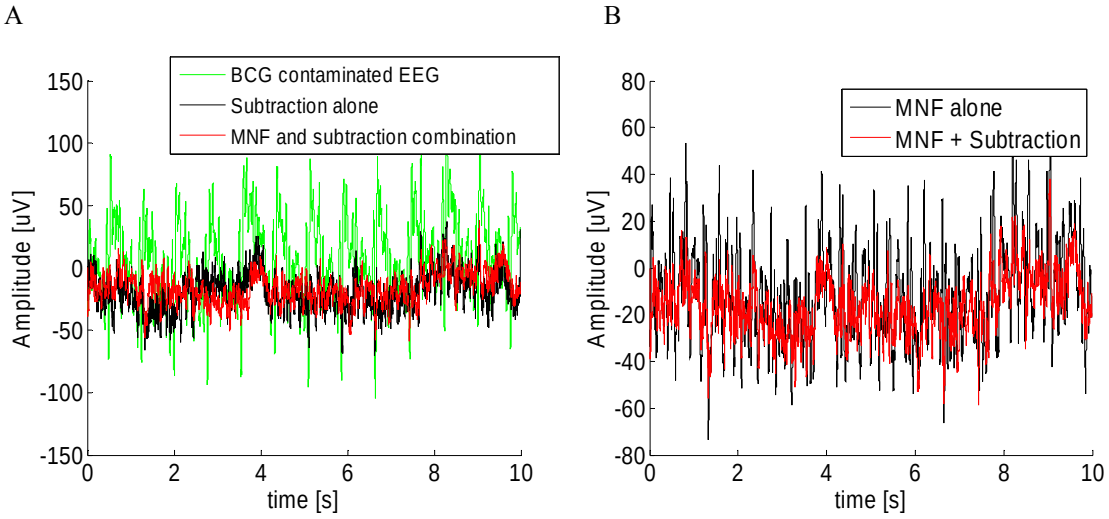


Fig.7.14 10-second BCG contaminated EEG example (electrode O1) before processing, after application of MNF alone, subtraction alone, and combined MNF and subtraction.

This impression is confirmed by another example showing a 10-sec-segment of all EEG channels after application of the three processing variants (Fig. 7.15).

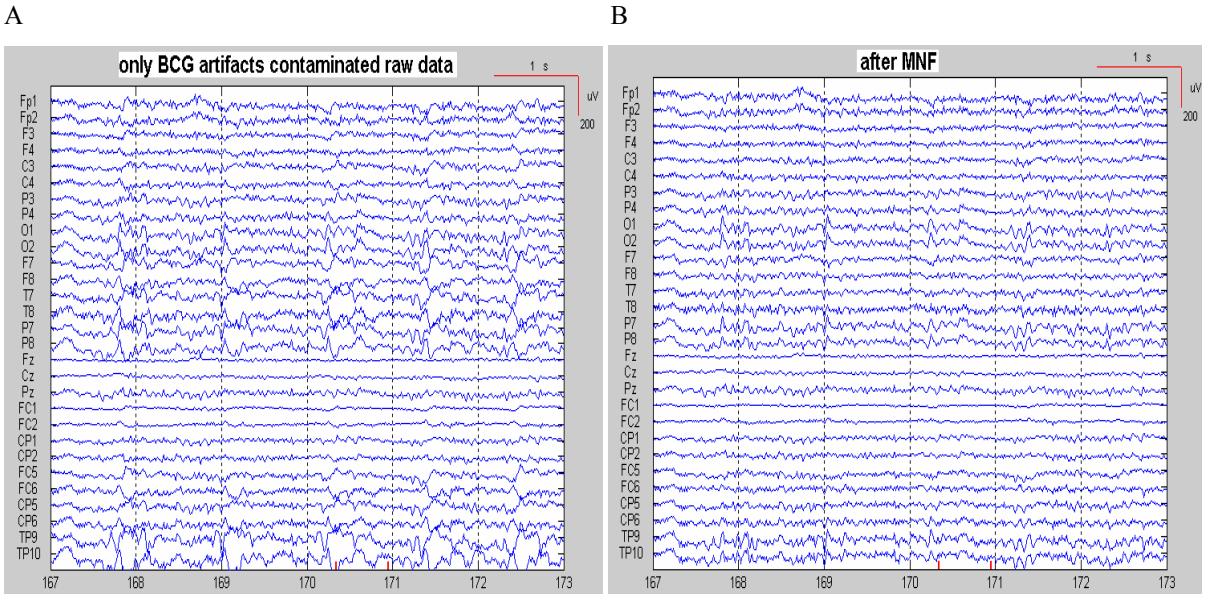

C D

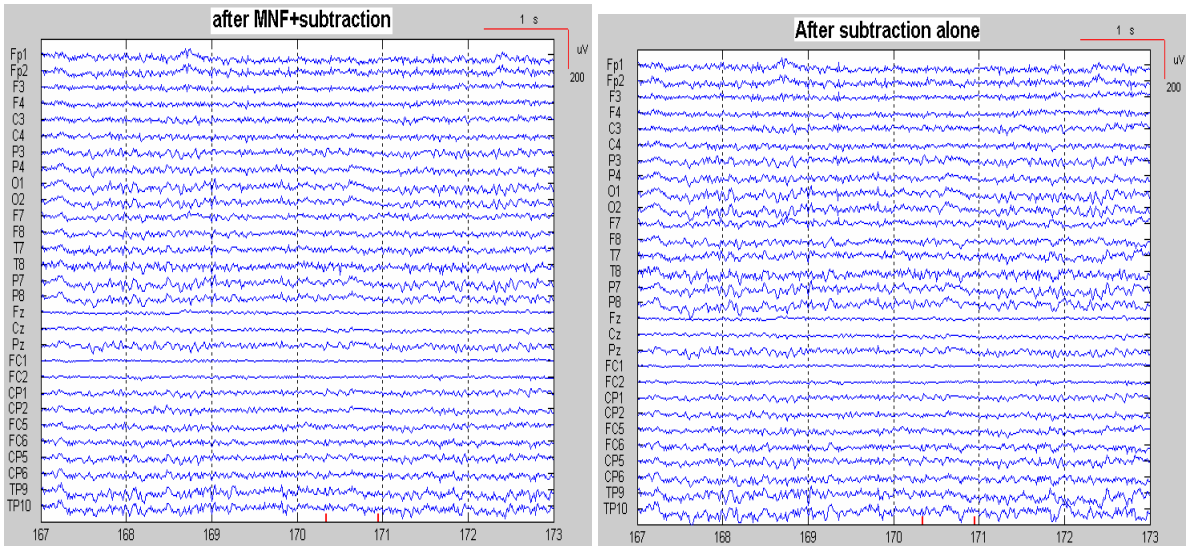


Fig.7.15 A 6 sec EEG segment of subject lr64:
A) raw EEG with superimposed BCG,
B) same signals after MNF,
C) after MNF + subtraction,
D) after subtraction alone.

### 7.2.4.3 Total spectrum

As already illustrated in the time domain evaluation, the power spectra (see Fig.7.16) averaged over all channels of all four subjects show that only a combination of the two methods leads to a signal with a spectrum close to the one observed outside the scanner. Although the recording conditions outside the scanner room differ from the situation during scanning (sitting vs. laying, quiet vs. loud etc.), the EEGs observed under the two conditions should nevertheless differ not too much, assuming a stable vigilance level (changes in vigilance significantly influence the EEG). Accordingly, the spectra of the BCG contaminated EEG after processing should roughly approach the spectrum of the EEG recorded outside the scanner. With this in mind, Fig.7.16 makes clear that only the combination of MNF and subtraction leads to an almost artifact free EEG in terms of a spectrum largely resembling the one obtained outside the scanner. Both the EEG after processing with MNF alone and subtraction alone exhibits a much larger spectrum over a wide frequency range indicating the presence of strong residual BCG activity.

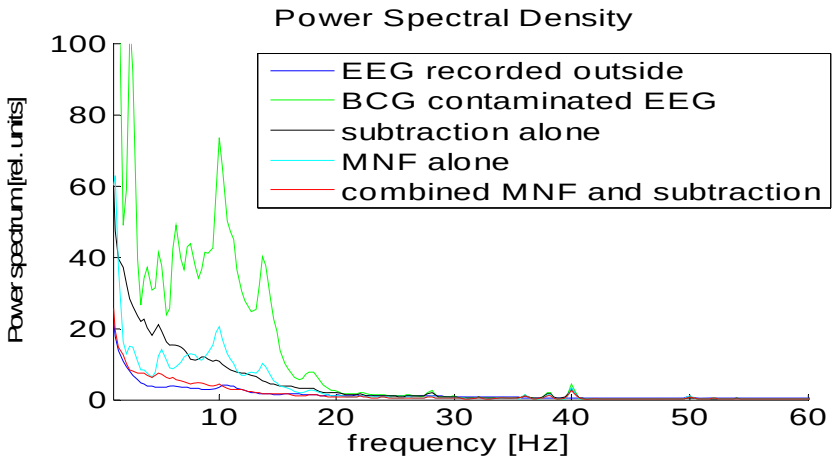


Fig.7.16 Power spectra averaged over the full 10 min recording time, all channels and all four subjects of the EEG recorded outside the scanner and of the EEG recorded inside the scanner (scanner running) after application of the two removal steps.

### 7.2.5 Evaluation with the ERPs

To verify the validity of the combined method with respect to ERP analysis, ERPs were extracted for all three conditions (outside the scanner, inside the scanner without scanning, ditto with scanning) by averaging over the 160 visual stimuli. As demonstrated in Fig.7.17 and Fig.7.18 the event related potentials only show minor temporal and topographic differences between the three different recording conditions. This underscores the efficiency of the artifact removal processing. However, it should be noted that due to the randomization of the stimulus timing, ERPs are intrinsically less susceptible to BCG artifacts than the raw EEG. The differences between the curves obtained under the three conditions are well in the range of physiological variation (Aunon and Cantor, 1977; Polich, 1997).

A B

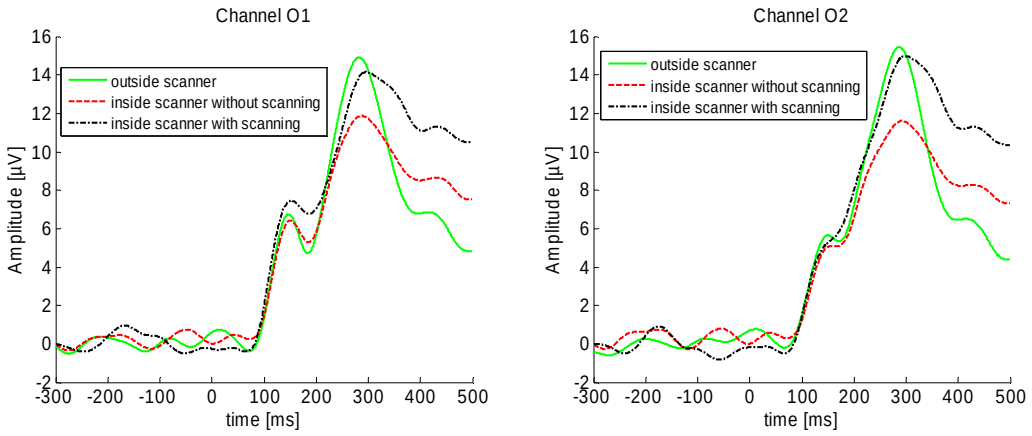


Fig.7.17 ERP averaged over four subjects separately for the three recording conditions:
A) channel O1
B)channel O2

A

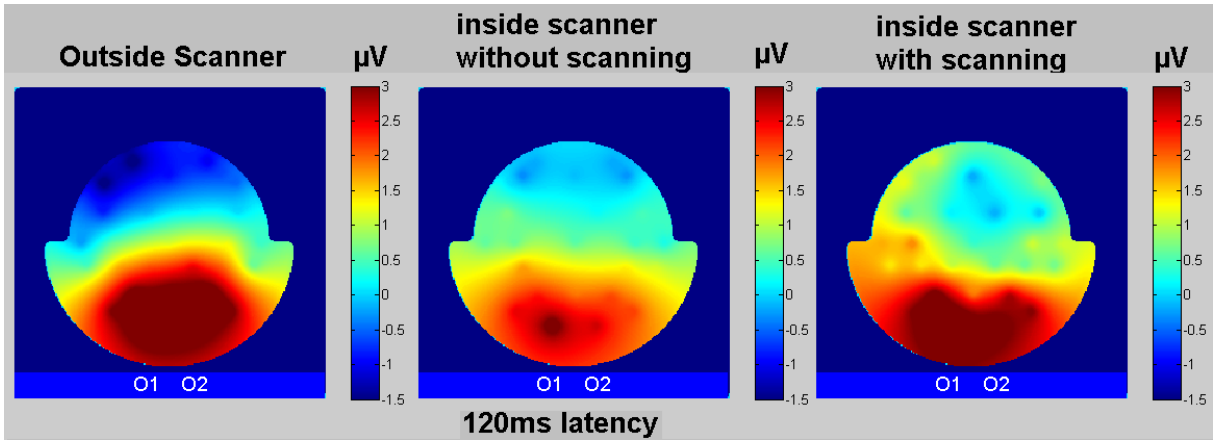


B

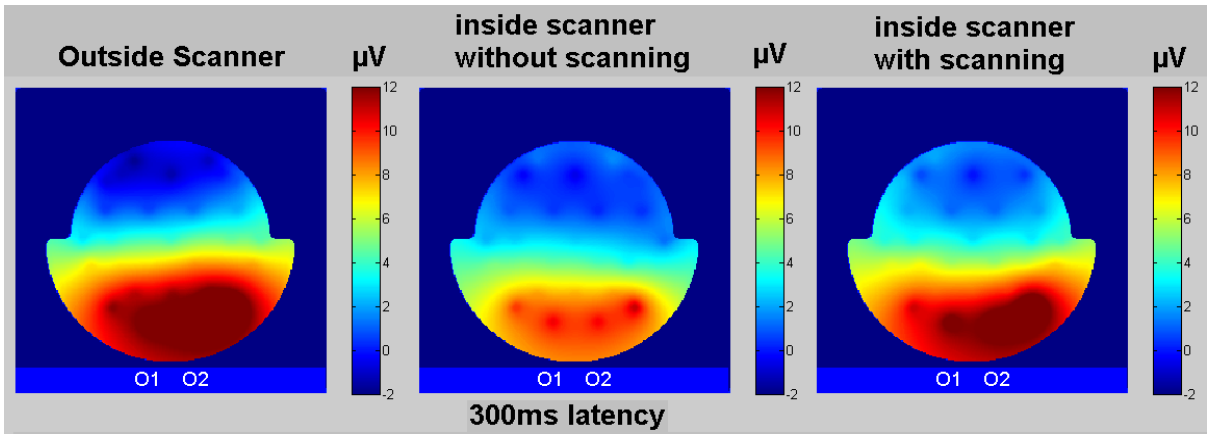


Fig.7.18 Topographic ERP amplitude maps interpolated from 29 channels (subject lr64):
A) at 120ms and B) at 300ms latency after stimulus onset:
Left: ERP recorded outside the scanner room.
Middle: ERP recorded inside the scanner room without MR scanning.
Right: ERP recorded inside the scanner room with MR scanning.

# Chapter 8 Discussion

Although there are more and more researches recording EEG and fMRI simultaneously, it is still a long way for this technique to step into the clinical application because of the main impediments, namely large gradient artifacts and BCG artifacts superimposed on the normal EEG.

In physics terms, two principles are responsible for these artifacts: (i) A changing magnetic field produces an electric field. (ii) The moving closed electrical loop (due to. subject movement)in the magnetic field induces a current.

The first artifact called ‘gradient artifact’ is caused by the changing magnetic field which is a consequence of the rapidly switched magnetic field gradients as part of the MR imaging sequence. These artifacts cannot be avoided because some kind of gradient switching is needed in any MR imaging sequence.

The second artifact comes from the regular movement of the subject, such as respiration, and blood flow. All these movements cannot be avoided. Although the breath and heart beat do not significantly influence the quality of EEG under normal recording conditions, they turn into a big problem when the EEG is recorded in the magnetic field. This ‘BCG artifact’ is largely time-locked with the heart beat but slightly varies in its waveform during recording according to the change in the subject’s position and movement. This limited reproducibility is the reason for the difficulty of separating BCG artifacts from the EEG background activity by means of a mere average subtraction technique.

The third artifact named ‘vibration artifact’ is generated due to the cryo-pump of the scanner. The pump is continuously switched on during scanning in order to avoid overheating which can lead to a dangerous situation and to a termination of the scanning. The mechanism leading to a transfer of the pump’s vibration to the EEG artifact (mechanical movement? Direct electrical coupling?) is not known, but the causal relation is obvious given that the vibration artifact does not occur if the pump is switched off. It is also worth mentioning that the artifact amplitude was clearly lower in another MR scanner with lower magnetic field strength of 1.5 Tesla (GE Signa LX).

### 8.1 Gradient artifacts

Since the first subtraction method (Allen et al., 2000) appeared, many other methods (Negishi et al., 2004; Srivastava et al., 2005; Wan et al., 2006) have already been developed. Becker(2005) has proposed an approach based on the normal subtraction method to remove

gradient artifacts with a moving weighted window. Unfortunately, these methods could not avoid the residual gradient artifacts although adaptive noise cancellation (ANC) (Allen et al., 2000), lowpass filter (Becker et al., 2005) and PCA (Niazy et al., 2005; Schmid et al., 2006) have worked on reduction of residual gradient artifacts.

One purpose of the new gradient artifacts removing method presented here was to minimize the residual gradient artifacts by optimizing the subtraction with respect to changes in the artifact template (Becker et al., 2005 and Herrmann and Debener, 2008) that may occur due to both non perfect technical stability of the EEG-MR-setting and subjects' head movements. Based on Becker's MAS method, the MAMAS approach improved the performance of artifact reduction by monitoring the change of electrodes position which causes the gradient artifacts not to be equal from slice to slice. Besides this effect the asynchronous timing of the EEG and MR measurement adds to these variations. Furthermore, tiny long term trends were observed in the artifact waveforms. For a precise analysis of the character and strength of these variations we conducted phantom measurements in order to extract the pure artifact waveform without any subject related variability. In these measurements a watermelon served as a phantom with the same type and number of electrodes as used for the human measurements. The four different mechanically fixed orientations lead to four different orientations of the electric loops (consisting of the water melon surface, the electrodes and the cables) with respect to the gradient magnetic field. In order to simulate a kind of worst case scenario the watermelon was rotated by two degrees per step which is certainly at the upper limit of realistic movements. The amplitude differences between the artifact-templates observed at different orientations were surprisingly high and reached up to 10% of the absolute artifact amplitude thus underpinning the need for taking these movements into account. However, even more surprising the shape of the artifact template changed over short periods of only a few seconds although staying clearly below the movement related fluctuations. The reported result demonstrates that gradient artifacts are different from electrode positions and time to time. The underlying technical mechanisms remain unclear. One may speculate if the warming of the gradient coils leads to very small changes in the magnetic field giving rise to tiny yet not negligible variations of the artifact shape. This observation explains the fact that among the evaluated weighting functions the efficiency in removing the artifact was most pronounced in the Becker version which has the strongest focus on those epochs positioned closest to the artifact under consideration. In general two gradient artifacts are similar (yet still slightly varying) within short intervals but are more and more different with increasing temporal distance. In summary, the gradient

artifact's waveform is not constant due to the following reasons: (i) Subject movement due to the heart beat, (ii) involuntary subject movement independent of the heart beat and (iii) a non systematic long term trend which of the reason cannot be identified. Especially the movement related fluctuations of the artifact waveform comes up to 10 % of the total amplitude and must therefore be included in the algorithm estimating a proper artifact template to be subtracted.

The aim of monitoring the head motion was to decrease the influence of motion on the gradient artifact removal. By modification of an existing eye-tracking system (Kanowski et al., 2007) a video based real time monitoring system was developed that constantly traces one fixed position of the subject's forehead with a 40 ms temporal resolution. However, since this device is not available in other MR labs it was only used to (i) test the – later used for monitoring – SPM realignment tool and (ii) to identify the reason for large residual artifacts occurring in case of very brief movements which cannot be detected by the SPM realignment routine. Compared to this high resolution monitor the temporal resolution of the movement information provided by the SPM-program is worse (half of TR (usually 1000ms)). Nevertheless this way of movement tracking was preferred to make the method usable for any MR lab having access to SPM. In general, head movements play a critical role especially in long lasting (for instance 30 min and more) fMRI experiments. In particular, strong movements can often not be avoided in patient measurements. Therefore, clinical EEG-fMRI-measurements will probably benefit most from the improvement achieved with our modified method. With respect to EEG-guided MR imaging (for instance spike triggered fMRI in epileptic patients) a real time artifact removal is required. The algorithm in its current version is non causal and thus not suitable for this purpose. However, in case of not too fast movements a non causal variant should be sufficient that relies on past epochs only. This assumption is supported by the observation that the performance of the algorithm in its current version with the position vector being temporally assigned to the center of the current half volume does not change if the same information is assigned to the end of the same half volume. As part of the so called real time movement correction most MR scanners continuously monitor head movements similar to the SPM-method and thus provide the position information needed for the artifact removal. Furthermore, a direct head movement monitor with a much better temporal precision was recently proposed by an external optical motion tracking (Speck et al., 2006). This device could be used for an improved real-time movement corrected subtraction algorithm.

Besides the head motion, another important factor influencing the artifact removal is the asynchrony between the EEG sampling and the fMRI timing. To cope with this effect, various

methods have been proposed which improve the alignment of the gradient template's slopes and peaks by a temporal adjustment of the sampling times by upsampling with different fixed sampling rates like 50KHz (Becker et al., 2005), 100KHz (Allen et al., 2000) and 20KHz (Niazy et al., 2005). However, according to the present analysis a much higher rate of about 5 MHz would be needed to keep the residual error below the noise floor due to an imperfect match. The resampling avoids this extreme boost of data and the related computational load by replacing the fixed high sampling rate by a temporally adaptive low sampling rate. The cubic spline interpolation used to calculate the new virtual samples is in this context superior to sinc interpolation and frequency domain's interpolation because both create ripple phenomena at the margins of a signal segment. Cubic splines also outperform linear interpolation regarding the reconstruction accuracy. The individual resampling with a temporal resolution of 0.1 us is capable of tracking even a tiny jitter of +/- 0.0025 ms which was observed in the slice repetition rate of the MR scanner (see below, next paragraph). Although resampling saves a lot of computation time compared to the upsampling it is still numerically demanding. To reduce the computational load one could in principle reduce the signal bandwidth by means of a digital low pass filter and subsequently decimate the sampling rate before any artifact removal processing. However, the goal of this work is to optimize the artifact removal algorithm keeping the original bandwidth and sampling rate. Recently, Goncalves et al. (2007a,b) presented an alternative approach to avoid any mismatch between the sampling grid applied to the different artifact epochs: Before any processing they precisely determined the exact inter-slice interval (ISI) in terms of the EEG sampling interval. From this they calculate the number of samples per slice plus a fraction of the EEG sampling interval defining the difference between the exact ISI and the nearest integer number of EEG samples. As shown by these authors, this approach (which largely resembles the electronic locking between the clocks of the MR- and the EEG-device presented recently by a commercial supplier) leads to a perfect temporal match of the samples representing the artifact epochs. However, this only works under the assumption of a perfectly stable ISI. In our fMRI experiments we observed a spread of about 5 usec in the ISIs observed in the slice sequence (by determining the slope onset after upsampling by means of interpolation beyond 1 MHz) which is clearly more than the critical threshold determined for our resampling scheme.

The onsets of gradient artifacts could be easily determined during the trigger supplied by many MR scanners. However, these triggers are not available in all scanners. Therefore it is preferable to have a method not depending on this information. An easy solution to this

problem is available by implementing a threshold comparator detecting the large peak to peak amplitudes within a gradient artifact period. In practice both methods are comparable both in temporal precision and computational effort.

The SPM based movement monitor allows to class each epoch into one of several position levels which is the base for estimating an individual artifact template for each artifact to be removed. The template is averaged over a limited number of the same level's epochs within a restricted period (the moving average window extending over a maximum of 8 sec) to eliminate the scanner's systematic long term trends affecting the artifact template. This limited number of epochs in the vicinity of the actual artifact conflicts with the requirement of sufficiently large number of epochs needed to keep the residual EEG of the averaged template below the noise level. As shown by the analysis of EEG signals recorded outside the scanner and taking into account the phantom related stability measurements, this constraint is clearly met by the Becker window. In further tests, we observed in cases of no or only mild movement that even an average over only 10 epochs achieves an artifact reduction that is comparable (both by eyes and by spectral measures) to the original algorithm. However, the potential distortion of the ongoing background EEG due to persisting residual EEG carried by the artifact template cannot be controlled under this condition.

In case of brief strong movements there are not enough artifact epochs available to extract the reference template because (i) the number of artifacts in the same level would be too small in the restricted period (even if the brief movement could be precisely traced with a high resolution movement monitor) and (ii) each artifact has its own shape and is less suitable for the subtraction process. Therefore after the usual template subtraction a substantial residual artifact remains to be removed by an alternative approach. This special postprocessing step was realized in terms of a second subtraction technique where the template is extracted by averaging over channels rather than over time. Thereby a clear reduction of the artifact amplitude is achieved which is sufficient for a coarse visual EEG evaluation. However, the remaining artifact residuum is still larger as compared to signal periods without strong movement. Since these special cases occur only rarely (typically in 2% of all epochs, in some subjects not at all) and each time with a different shape a more efficient way of removal seems hardly feasible.

The remaining residual gradient artifact is to about 50% restricted to frequencies beyond 100 Hz which can be suppressed by appropriate low pass filters without affecting the clinical relevant EEG frequency bands including the Gamma band. One can only speculate about the reason for the non perfect removal at all. Given the discrepancy between the almost perfect

resampling shown in the simulation and the residual amplitudes even after precisely resampling the real artifact one might speculate if tiny noise or a limited reproducibility of the gradient's time course contributes to the high frequency residuals which are most pronounced close to the steep slopes of the gradient. Second, very mild head movements which cannot be detected by the movement monitor may nevertheless cause a slight deformation of the artifact which is not captured by the average template used for subtraction. Finally, although we did not observe severe differences in the removal performance for different interpolation schemes including a sinc-interpolation, we cannot exclude that the interpolation algorithm introduces errors around the peak of the real gradient since the true gradient shape is not known.

Looking at the Gamma-EEG frequency band (i.e. beyond about 30 Hz) the question arises to what extent EEG activity at these frequencies is suitable for a valid quantitative analysis. Given that the artifacts activity (and thus the residual activity as well) is stable over some interval the residuum might be assumed to be stable as well thus adding a constant term to the total band power. If this stability cannot be assumed, only the spectral components between the harmonics of the gradient repetition rate should be included in the analysis. But even then the validity of the results would benefit from the improved removal algorithm because the lower residual harmonics lead to a lower spread of spectral power.

Given the successful application of ICA based methods to the removal of other EEG artifact types like for instance electrooculogram (EOG) or electrocardiogram (ECG) (Mantini et al., 2007; Tong et al., 2001) the question arises if blind separation methods could replace the subtraction method to remove gradient artifacts. We tried this approach but found that due to the huge artifact-to-signal ratio a large number of the independent components is affected by the dominant artifact, many of which also carrying significant EEG activity (Mantini et al., 2007). Consequently, all these components need to be discarded which leads to a loss of EEG activity at the same time. Alternatively, several groups (Niazy et al., 2005; Schmid et al., 2006; Mantini et al.,2007) have applied ICA or PCA to reduce residual artifacts after application of the subtraction method. However, all these methods need to determine the number of components to include in the artifact processing. While this task is well suitable for an interactive procedure it is less suitable for a fully automatic processing. Therefore, we renounced using this method especially since we observed only tiny improvements in our data after an interactive trial application of fastICA (Hyvaerinen, 1999) as a postprocessing tool.

## 8.2 Vibration artifacts

This type of artifact is caused by the periodic vibration of the vacuum pump of the MR scanner (‘vibration artifact’) that was observed not only in the 3T-MR device (siemens) but - to a lesser extent - also in the 1.5T-MR (GE).Due to the mechanical vibrations induced by the cold head of the magnet cooling system of the MRI scanner (Briselli et al., 2006), it exists only if the recording is conducted inside the scanner. The vibration artifacts could be completely suppressed with a simple bandstop filter because of its frequencies being restricted to (but slightly fluctuating) between about 40Hz and 50 Hz. Besides improving the visual quality of the EEG, the suppression of vibration artifacts is helpful for the separation of BCG artifacts, because the vibration bursts to some extent lead to distortions of the MNF components causing a less efficient separation of BCG and EEG. Of course, the selective suppression of the range around the frequency interval 40…50 Hz interferes with a potential analysis of the Gamma frequency band. However, frequencies below 40 Hz and beyond 50 Hz (each minus or plus the slop bandwidth) are preserved. The processing sequence, i.e. first gradient artifact removal and then vibration suppression vs. the inverse order, has no influence on the artifact removal performance.

## 8.3 BCG artifacts

Due to the fact that BCG artifacts largely depending on the heart beat and the blood flow (which are not stable for physiological reasons), only parts of BCG artifacts can be eliminated by subtracting an average template derived from the ongoing EEG. The applications of BSS methods such as PCA and ICA have been proposed by others (Srivastava et al., 2005; Briselli E et al., 2006; Nakamura et al., 2006; Mantini et al., 2007) to remove BCG artifacts. In the meantime, ICA is a kind of gold standard of EEG artifact removal including BCG removal. Comparing MNF with ICA variants such as fastICA and JADE, the main difference relates to theoptimization criterion guiding the decomposition into orthogonal or independent components. PCA derives uncorrelated variables by a linear transform that is guided by the criterion of maximizing the variance of the resulting components. ICA assumes statistically independent components and maximizes the non-gaussianity according to various criteria like maximization of kurtosis, negentropy or mutual information. MNF differs from these approaches by directly incorporating the concept of noise being superimposed on a signal as part of its optimization criterion, which is defined as SNR. As has been shown as part of the present development, MNF is superior to ICA techniques in its ability to separate BCG artifacts from true EEG (Table 7.1).

One considerable advantage of MNF is its low computational demand. A practical evaluation of this issue included the decomposition of a 10 sec 29 channel EEG epoch with fastICA, JADE and MNF. It turned out that fastICA is quite slow (about 10 minutes), JADE is a bit faster (< 4 minutes) and MNF is the fastest (about half a second). Replacing the adaptively calculated mixing matrix by a fixed – yet subject specific – matrix further speeds up the algorithm by up to 32% after taking account of the matrix multiplication operations of EEG data, which occupy the most of computational time due to the fast computation of MNF.

The second big advantage of MNF in the context of BCG removal is the intrinsic ordering of the ICs according to their SNR values. The components ordering of both fastICA and JADE are random with respect to this measure. As a consequence, only MNF allows for an easy fully automatic procedure of selecting (and subsequently discarding) components carrying artifact activity. In contrast, the two ICA techniques require additional complex detection algorithms and in some algorithms also the additional recording of an ECG signal to determine the BCG specific components (see for instance Tong et al., 2001; Be´nar et al., 2003, Joyce et al., 2004, Srivastava et al., 2005; Briselli et al., 2006).

According to the basic signal and noise concept of MNF, selecting the last few (or first few, depending on the direction of ordering) components as the ones to be discarded is successful as long as the BCG is the largest artifact occurring in the EEG. This is almost always that the BCG amplitudes are much larger than any other artifact. However, theoretically this procedure might be less effective, in cases where the BCG is accompanied by other continuous strong artifacts like for instance constant EOG and/or EMG. However, even then (i) the suppression of the last/first components will lead to a reduction of these artifacts in general and (ii) the subsequent subtraction will still remove most of the BCG. Ultimately, in an extreme case where other but BCG artifacts are clearly dominant, the EEG would hardly be evaluated since its quality is absolutely insufficient irrespectively of the BCH artifacts. This situation was never encountered in any of the recordings presented here.

The decomposed ICs of MNF are only approximately independent because MNF tries to minimize the correlation between components which not necessarily leads to statistical independence between these components. Second, the BCG artifact presumably is not completely independent from the EEG (this relation cannot be tested because the pure BCG cannot be observed). As a consequence, the BCG artifacts are distributed over more than just one MNF component. Thus setting the number of BCG ICs becomes a dilemma regarding the balance of removed BCG artifacts and suppressed true EEG. In the EEG examples of this work, the last four ICs contain the most parts of BCG artifacts, but a predefined number, two

components to discard, is a conservative strategy in order to keep as much true EEG as possible. This strategy necessarily leads to a non negligible amount of remaining residual BCG activity in many cases. Therefore, the subsequent subtraction method is necessary to further reduce these residuals.

The subtraction method used here is based on the normal subtraction method as introduced by Allen et al. (1998) but was modified by the introduction of a moving average template which is capable of tracking changes in the shape of the residual BCG. Due to the fact that BCG artifacts significantly vary over time for various reasons this adaptive procedure is more effective with respect to the ultimate residual BCG persisting after these two processing steps. The combined MNF-subtraction method removes substantially more of the BCG artifact than both of the two methods alone indicating that obviously MNF and subtraction extract different parts of the artifact complex. This conclusion is further supported by the fact that the power spectra of the signals obtained after the two individual processing steps deviate in different ways from the spectrum derived from the final EEG resulting after the two processing steps. Furthermore, the similarity between this final spectrum and the one obtained from the EEG recorded outside the scanner indicates that the BCG has been successfully removed without suppressing substantial parts of the underlying EEG. The minor differences seen between 2…10 Hz may be attributed to the very different environmental conditions during recording, which may well lead to different degrees of vigilance. In addition, the acoustic background noise in the scanner could have physiologically interfered with the ongoing EEG.

The visual perception ERP-experiment demonstrates the validity of the combined method in the caseof temporal and spatial ERP analysis. The visual ERPs calculated under the three conditions (outside the MR room, inside the MR room without scanning and inside the MR room with scanning) are comparable very much and thus proof that the removal of the gradient and BCG artifacts does not affect the ERP results.

# Chapter 9 Summary

The simultaneous recording of EEG and fMRI is a promising tool in neuroimaging research. However, three types of large artifacts dominate and completely obscure the EEG if recorded inside the scanner: (i) artifacts related to the switched MR gradients with steep slopes and extremely large amplitudes of about more than hundred times normal EEG amplitudes, (ii) vibration artifacts showing periodic burst around 40...50 Hz originating at the vaccum pump of the MR scanner and (iii) ballistocardiogram (BCG) artifacts with lower amplitudes and primarily low frequency components caused by heart rate induced tiny body movements.

With the goal of improving current gradient artifact removal techniques, a new method is presented called *movement adapted moving average subtraction* (MAMAS). It integrates an adaptive resampling technique, a gradient artifact template extraction algorithm guided by a head motion monitor and a special postprocessing tool to reduce irregular artifacts. It suppresses the residual gradient artifacts down to a level clearly below usual EEG amplitudes of about 10-100 μV. The resampling is comparable to an upsampling of the signal to an extremely high sampling but it avoids the boost of data and computational load. It greatly suppresses the error resulting from the asynchronous sampling of the EEG and the MR. Head motion monitoring was accomplished by using the SPM movement correction routine. Although the temporal resolution of SPM tracing is limited by half the TR-time of the scanning sequence, it is sufficient to guide the averaging algorithm to include only those epochs recorded at the same head position as the artifact to be removed. This technique reduces the residual artifact activity by about 50% compared to the moving average subtraction technique (MAS) as proposed by other groups. However, brief sub-second motions are not correctly represented by the SPM monitoring data thus leading to a large residual artifact after MAMAS processing. For these cases an additional special postprocessing algorithm was developed that virtually replaced the averaging of artifacts over time by averaging over channels to extract a proper template. Vibration artifacts can be easily removed by a 40-50 Hz bandstop filter, however at the cost of a loss of true EEG in the same frequency band. The only way of avoiding this artifact is halting the pump during EEG-MR-measurements.

Several ICA based approaches have been proposed to remove BCG artifacts. In the present work another blind source separation technique called maximum noise fraction (MNF) has been applied to further improve the separation between BCG artifact and EEG, substantially

reduce the computational demands and finally provide a set of components which are sorted along their signal to noise ratio thereby facilitating the development of a fully automatic removal procedure. After application of the MNF algorithm the artifact reduction is completed by appending an additional average subtraction algorithm which removes some spurious residuals existing after MNF processing. It is shown that both MNF alone and subtraction alone are not capable of providing a sufficient reduction of BCG artifact activity.

The comparison of power spectra computed from the artifact reduced EEGs with those spectra observed in EEGs recorded from the same subjects but outside the scanner room (i.e. without any MR related artifact) shows only minor differences which are most likely due to vigilance fluctuations or other physiological fluctuations. This result is confirmed by the results of ERP measurements conducted under the same conditions. Again there are only marginal temporal and topographic differences which are in the range of normal physiologic variations well known in this field of research.

# Bibliography

Allen, P.J., Polizzi, G., Krakow, K., Fish, D.R., Lemieux, L., 1998. Identification of EEG events in the MR scanner: the problem of pulse artifact and a method for its subtraction. NeuroImage 8 (3), 229–239.

Allen, P.J., Josephs, O., Turner, R., 2000. A method for removing imaging artifact from continuous EEG recorded during functional MRI. NeuroImage 12 (2), 230– 239.

Anami, K., Mori, T., Tanaka, F., Kawagoe, Y., Okamoto, J., Yarita, M., Ohnishi, T., Yumoto, M., Matsuda, H., Saitoh, O., 2003. Stepping stone sampling for retrieving artifact-free electroencephalogram during functional magnetic resonance imaging. NeuroImage 19 (2 Pt. 1), 281–295.

Anderle, M. G., and Kirby, M. J., 2001. An application of the maximum noise fraction method to filtering noisy time series, in Proc. 5th International Conference on Mathematics in Signal Processing, University of Warwick, Coventry, UK.

Aunon JI, Cantor FK., 1977. VEP and AEP variability: interlaboratory vs. intralaboratory and intersession vs. intrasession variability. Electroencephalogr Clin Neurophysiol., 42(5), 705-708

Barbati, G., Porcaro,C., Zappasodi, F., Rossini, P.M., Tecchio, F., 2004. Optimization of an independent component analysis approach for artifact identification and removal in magnetoencephalographic signals. Clinical Neurophysiology 115 (5), 1220-1232.

Becker, R., Ritter, P., Moosmann, M., Villringer A., 2005. Visual Evoked Potentials Recovered From fMRI Scan Periods. Human Brain Mapping 26, 221–230.

Bell, A.J., Sejnowski, T.J., 1995. An information-maximization approach to blind separation and blind deconvolution. Neural Computation 7, 1129-1159.

Be´nar, C., Aghakhani, Y., Wang, Y., Izenberg, A., Al-Asmi, A., Dubeau, F.,Gotman, J., 2003. Quality of EEG in simultaneous EEG–fMRI for epilepsy. Clin. Neurophysiol. 114 (3), 569– 580.

Blaschke, T., Wiskott, L., 2004, CuBICA: Independent Component Analysis by Simultaneous Third- and Fourth-Order Cumulant Diagonalization. IEEE Transactions on Signal Processing, 52 (5), 1250-1256.

Bonmassar, G., Anami, K., Ives, J., Belliveau, J.W., 1999. Visual evoked potential (VEP) measured by simultaneous 64-channel EEG and 3T fMRI. NeuroReport 10 (9), 1893–1897.

Bonmassar, G., Purdon, P.L., Jaaskelainen, I.P., Chiappa, K., Solo, V., Brown, E.N., Belliveau, J.W., 2002. Motion and ballistocardiogram artifact removal for interleaved recording of EEG and EPs during MRI. NeuroImage 16 (4), 1127–1141.

Briselli, E., Garreffa, G., Bianchi, L., Bianciardi, M., Macaluso, E., Abbafati, M., Marciani, M.G., Maraviglia, B., 2006. An independent component analysis-based approach on ballistocardiogram artifact removing. Magnetic Resonance Imaging 24, 393-400.

Comon, P., 1994. Independent Component Analysis, a new concept? Signal Processing, Elsevier, vol.36, no. 3, pp. 287-314, special issue on Higher-Order Statistics.

Cardoso, J.-F., 1989. Source separation using higher order moments. In Proc. ICASSP, pages 2109-2112.

Cardoso, J.F., 1998. Blind signal separation: statistical principles. Proceedings of the IEEE. 9, 2009-2025.

Cardoso, J.-F., 1999. High-order contrasts for independent component analysis. Neural Computation, vol. 11, no. 1, 157-192.

Cohen, M. S., Goldman, R. I., Stern, J., and Engel, Jr. J., 2001. Simultaneous EEG and fMRI made easy. NeuroImage, 13 (6 Supp.1), S6.

Comon, P., 1994. Independent Component Analysis, a new concept? Signal Processing, Elsevier, vol.36, no. 3, pp. 287-314, special issue on Higher-Order Statistics.

Chatrian, G.E., Lettich, E., Nelson, P.L., 1985. Ten percent electrode system for topographic studies of spontaneous and evoked EEG activity. Am. J. EEG Technol. 25, 83–92.

Damadian R, Goldsmith M, Minkoff L, 1977. NMR in cancer: XVI. FONAR image of the live human body. Physiol Chem Phys. 9 (1), 97-100, 108.

Debener, S., Strobel,A., Sorger,B., Peters, J., Kranczioch, C., Goebel, R., 2007. Improved quality of auditory event-related potentials recorded simultaneously with 3-T fMRI: Removal of the ballistocardiogram artifact. NeuroImage 34 (2), 587-597

De Lathauwer, L., De Moor, B., Vandewalle, J., 2000. An introduction to independent component analysis. J. Chemometrics, 14, 123-149.

Ernst Niedermeyer, Fernando Lopes da Silva, 1987. Electroencephalography: basic principles, clinical applications, and related fields (third edition).

Ellingson, M.L., Liebenthal, E., Spanaki, M.V., Prieto, T.E., Binder, J.R., Ropella, K.M., 2004. Ballistocardiogram artifact reduction in the simultaneous acquisition of auditory ERPS and fMRI. NeuroImage 22 (4), 1534– 1542.

Felblinger, J., Slotboom, J., Kreis, R., Jung, B., Boesch, C., 1999. Restoration of electrophysiological signals distorted by inductive effects of magnetic field gradients during MR sequences. Magn. Reson. Med. 41 (4), 715-721.

Flexer, A. Bauer, H., Pripfl, J., Dorffner, G., 2005. Using ICA for removal of ocular artifacts in EEG recorded from blind subjects. Neural Netw. 18 (7), 998-1005.

Foucher, J. R., Otzenberger, H., and Gounot, D., 2003. The BOLD response and the gamma oscillations respond differently than evoked potentials: an interleaved EEG-fMRI study. BMC neuroscience 4, 22.

Friston KJ, Ashburner J, Frith CD, Poline J-B, Heather JD & Frackowiak RSJ , 1995. Spatial registration and normalization of images Hum. Brain Map. 2, 165-189.

Garreffa, G., Carni, M., Gualniera, G., Ricci, G.B., Bozzao, L., De Carli, D., Morasso, P., Pantano, P., Colonnese, C., Roma, V., Maraviglia, B., 2003. Real-time MR artifacts filtering during continuous EEG/fMRI acquisition. Magn. Reson. Imaging 21 (10), 1175-1189.

Goldman, R.I., Stern, J.M., Engel, J., Cohen, M.S., 2000. Acquiring simultaneous EEG and functional MRI, Clinical Neurophysiology 111, 1974-1980

Goldman, R.I., Stern, J.M., Engel, J., Cohen, M.S., 2002. Simultaneous EEG and FMRI of the alpha rhythm. NeuroReport 13 (18), 2487-2492.

Goncalves, S.I., Pouwels, P.J., Kuijer, J.P., Heethaar, R.M., de Munck, J.C., 2007a. Artifact removal in co-registered EEG/fMRI by selective average subtraction. Clin. Neurophysiol. 118 (11), 2437-50.

Goncalves, S.I., Pouwels, P.J., Kuijer, J.P., Heethaar, R.M., de Munck, J.C., 2007b. Correction for desynchronization of EEG and fMRI clocks through data interpolation optimizes artifact reduction. Conf. Proc. IEEE Eng. Med. Biol. Soc. 1, 1590-4.

Grassberger P, Hegger R, Kanz H, Schaffrath C, Schreiber T., 1993. On noise reduction methods for chaotic data. Chaos, 3(2), 127–41.

Green, A. A., Berman, M., Switzer, P., and Craig, M. D., 1988. A transformation for ordering multispectral data in terms of image quality with implications for noise removal, IEEE Trans. Geosci. Remote Sensing, vol. 26 (1), 65–74,.

Herault, J. and Jutten, C., 1986. Space or time adaptive signal processing by neural network models. AIP Conference Proceedings, 151, 206-211.

Herrmann, C.S., Debener, S., 2008. Simultaneous recording of EEG and BOLD responses: A historical perspective. International Journal of Psychophysiology, 67, 161-168.

Hill, R.A., Chiappa, K.H., Huang-Hellinger, F., Jenkins, B.G., 1995. EEG during MR imaging: Differentiation of movement artifact from paroxysmal cortical activity. American Academy of Neurology 45, 1942-1943.

Hoffmann, A., Ja¨ger, L., Warhahn, K.J., Jaschke, M., Noachtar, S., Reiser, M., 2000. Electroencephalography during functional echo-planar imaging: detection of epileptic spikes using post-processing methods. Magn. Reson. Med. 44, 791–798.

Huettel, S.A., Song, A.W., McCarthy, G., 2003. Functional Magnetic Resonance Imaging, Sinauer Associates Inc. Publishers, Sunderland, MA, USA.

Huiskamp, G.J., 2005. Reduction of the Ballistocardiogram artifact in simultaneous EEG-fMRI using ICA. Conf Proc IEEE Eng Med Biol Soc. 4, 3691-3694.

Hundley, D., Kirby M., Anderle, M.G., 2001. A Solution Procedure for Blind Signal Separation using the Maximum Noise Fraction Approach: Algorithms and Examples, Proceedings of the Conference on Independent Component Analysis, San Diego, CA, 337–342.

Hundley, D.R., Kirby, M.J., Anderle, M., 2002. Blind source separation using the maximum signal fraction approach, Signal Processing 82, 1505-1508.

Huang-Hellinger FR, Breiter HC, McCormack G, Cohen MS, Kwong KK, Sutton JP, Savoy RL, Weisskoff RM, Davis TL, Baker JR, Belliveau JW, Rosen BR, 1995. Simultaneous functional magnetic resonance imaging and electrophysiological recording. Hum Brain Map 3, 13–23.

Hyvaerinen A., 1999 Fast and robust fixed-point algorithms for independent component analysis. IEEE Trans Neural Netw. 10 (3), 626-634.

Ives, J.R., Warach, S., Schmitt, F., Edelman, R.R., Schomer, D.L., 1993. Monitoring the patient's EEG during echo planar MRI. Electroencephalogr. Clin. Neurophysiol. 87, 417-420.

Jasper, H.H., 1958: The ten-twenty electrode system of the international federation. Electroencephal. Clin. Neurophysiology, 10, 1426-1437.

Joyce, C.A., Gorodnitsky, I.F., Kutas, M., 2004. Automatic removal of eye movement and blink artifacts from EEG data using blind component separation. Psychophysiology, 41 (2) 313-325.

Kanowski, M., Rieger, J. W., Noesselt, T., Tempelmann, C., Hinrichs, H., 2007. Endoscopic eye tracking system for MRI. J. Neurosci. Methods 160 (1), 10-15.

Kim, K.H., Yoon, H.W., Park, H.W., 2004. Improved ballistocardiac artifact removal from the electroencephalogram recorded in fMRI. J. Neurosci. Methods 135 (1– 2), 193– 203.

Kirby, M., 2001. Geometric Data Analysis: An Empirical Approach to Dimensionality Reduction and the Study of Patterns. Wiley.

Kruggel, F., Wiggins, C.J., Herrmann, C.S., von Cramon, D.Y., 2000. Recording of the event-related potentials during functional MRI at 3.0 Tesla field strength. Magn. Reson. Med. 44 (2), 277– 282.

Krakow, K., Woermann, FG., Symms, MR., Allen, PJ., Lemieux, L., Barker, GJ., Duncan JS, Fish DR., 1999. EEG-triggered functional MRI of interictal epileptiform activity in patients with partial seizures. Brain 1999 Sep, 122, 1679-1688.

Krakow, K., Messina, D., Lemieux, L., Duncan, J.S., Fish, D.R., 2001. Functional MRI activation of individual interictal epileptiform spikes. NeuroImage 13 (3), 502– 505.

Kwong K.K., Belliveau J.W., Chesler D.A., Goldberg I.E., Weisskoff R.M., Poncelet B.P., Kennedy D.N., Hoppel B.E., Cohen M.S., Turner R., et al., 1992. Dynamic magnetic resonance imaging of human brain activity during primary sensory stimulation. Proc. Natl. Acad. Sci. USA, 89 (12), 5675-5679.

Laufs, H., Kleinschmidt, A., Beyerle, A., Eger, E., Salek-Haddadi, A., Preibisch, C., Krakowa, K., 2003. EEG-correlated FMRI of human alpha activity. NeuroImage 19 (4), 1463– 1476.

Lee,T.W., Girolami, M., Sejnowski,T.J., 1999. Independent component analysis using an extended infomax algorithm for mixed sub-Gaussian and super-Gaussian sources. Neural Computation, 11, 417-441.

Lemieux, L., Allen, P. J., Franconi, F., Symms, M. R., and Fish,D. R., 1997. Recording of EEG during fMRI experiments : Patient safety. Magn. Res. Med. 38 (6), 943-952.

Lemieux, L., Salek-Haddadi, A., Josephs, O., Allen, P., Toms, N., Scott, C., Krakow, K., Turner, R., Fish, D.R., 2001. Event-related fMRI with simultaneous and continuous EEG: description of the method and initial case report. NeuroImage 14 (3), 780–787.

Liebenthal, E., Ellingson, M.L., Spanaki, M.V., Prieto, T.E., Ropella, K.M.,Binder, J.R., 2003. Simultaneous ERP and fMRI of the auditory cortex in a passive oddball paradigm. NeuroImage 19 (4), 1395–1404.

Luck, S. J., 2005. An Introduction to event-related potential technique. The MIT Press, Cambridge.

Mandelkow, H., Halder, P., Boesiger, P., Breandeis, D., 2006. Synchronization facilitates removal of MRI artifacts from concurrent EEG recordings and increases usable bandwidth. NeuroImage 32 (3), 1120–1126.

Mantini,D., Perrucci, M.G., Cugini, S., Ferretti, A., Romani, G.L., Del Gratta, C., 2007. Complete artifact removal for EEG recorded during continuous fMRI using independent component analysis. Neuroimage 34 (2), 598-607.

Masterton, R.A.J., Abbott, D.F., Fleming, S.W., Jackson, G.D., 2007. Measurement and reduction of motion and ballistocardiogram artefacts from simultaneous EEG and fMRI recordings. NeuroImage 37 (1), 202-211.

Mirsattari, S. M., Lee, D. H., Jones, D., Bihari, F., and Ives, J. R., 2004. MRI compatible EEG electrode system for routine use in the epilepsy monitoring unit and intensive care unit. Clin. Neurophysiol. 115, 2175-2180.

Moosmann, M., Ritter, P., Krastel, I., Brink, A., Thees, S., Blankenburg, F.,Taskin, B., Obrig, H., Villringer, A., 2003. Correlates of alpha rhythm in functional magnetic resonance imaging and near infrared spectroscopy. NeuroImage 20 (1), 145– 158.

Mueri, R.M., Felblinger, J., Rösler, K.M., Jung, B., Hess, C. W., Boesch, C., 1998. Recording of electrical brain activity in a magnetic resonance environment: distorting effects of the static magnetic field. Magn. Reson. Med . 39, 18-22.

Nakamura, W., Anami K., Mori T., Saitoh O., Cichocki A., Amari S., 2006. Removal of ballistocardio-gram artifacts from simultaneously recorded EEG and fMRI data using independent component analysis. IEEE Trans. Biomed. Eng. 53 (7), 1294-1308.

Negishi, M., Abildgaard, M., Nixon, T., Constable, R.T., 2004. Removal of time-varying gradient artifacts from EEG data acquired during continuous fMRI. Clin. Neurophysiol. 115 (9), 2181–2192.

Niazy, R., Iannetti, G., Brady, M., Matthews, P., Smith, S., 2004. A multisubject study of motor task modulation of EEG-alpha-rhythm/FMRI correlation. Tenth Int. Conf. on Functional Mapping of the Human Brain.

Niazy, R. K., Beckmann, C. F., Iannetti, G. D., Brady, J. M., Smith, S. M., 2005. Removal of FMRI environment artifacts from EEG data using optimal basis sets. NeuroImage 28 (3), 720-37.

Nunez P.L., 1981. Electric Fields of the Brain: The Neurophysics of EEG, Oxford University Press, NewYork.

Ogawa S., Lee T.M., Kay A.R., Tank D.W., 1990. Brain magnetic resonance imaging with contrast dependent on blood oxygenation. Proc Natl Acad Sci U S A. , 87 (24), 9868-72.

Pauling, L., Coryell, C.D., 1936. The Magnetic Properties and Structure of Hemoglobin, Oxyhemoglobin and Carbonmonoxyhemoglobin. Proc. Natl. Acad. Sci. USA, 22 (4), 210-216.

Peterson, D.A., Knight, J.N., Kirby, M.J., Anderson, C.W., and Thaut, M.H., 2005. Feature Selection and Blind Source Separation in an EEG-Based Brain-Computer Interface, Journal on Applied Signal Processing 19, 3128–3140.

Polich, J., 1997. On the relationship between EEG and P300: individual differences, aging, and ultradian rhythms. Int J Psychophysiol. 26 (1-3), 299-317.

Salek-Haddadi, A., Lemieux, L., Merschhemke, M., Diehl, b., Allen, P. J., and Fish, D. R., 2003. EEGquality during simultaneous functional MRI of interictal epileptiform discharges. Magn. Reson. Imag. 21, 1159-1166.

Schmid, M. C., Oeltermann, A., Juchem, C., Logothetis, N.K., Smirnakis, S. M., 2006. Simultaneous EEG and fMRI in the macaque monky at 4.7 Tesla. Magnetic Resonance Imaging 24, 335-342.

Schomer, D.L., Bonmassar, G., Lazeyras, F., Seeck, M., Blum, A., Anami, K., Schwartz, D., Belliveau, J. W., and Ives, J., 2000. EEG-Linked Functional Magnetic Resonance Imaging in Epilepsy and Cognitive Neurophysiology. J. Clin. Neurophysiol. 17, 43-58.

Seeck, M., Michel, C.M., Spinelli, L., Lazeyras, F., 2001. EEG mapping and functional MRI in presurgical epilepsy evaluation. Rev. Neurol. (Paris) 157 (8– 9 Pt. 1), 747– 751.

Sijbers, J., Michiels, I., Verhoye, M., Van Auderkerke, J., Van der Linden, A., and Van Dyck, D., 1999. Restoration of MR-induced artifacts in simultaneously recorded MR/EEG data. Magn. Reson. Imag. 17 (9), 1383–1391.

Sijbers, J., Van Audekerke, J., Verhoye, M., Van der Linden, A., Van Dyck, D., 2000. Reduction of ECG and gradient related artifacts in simultaneously recorded human EEG/MRI data. Magn. Reson. Imaging 18 (7), 881– 886.

Sommer, M., Meinhardt, J., and Volz, H.P., 2003. Combined Measurement of Event-Related Potentials(ERPs) and fMRI. Acta Neurobiol. Exp. 63,49-53.

Souloumiac A. and Cardoso J.-F., 1991. Comparaisons de Me´hodes de Se´paration de Sources, Xlllth Coll.GRETSI, September, 661- 664.

Souloumiac A. and Cardoso J.-F., 1996. Jacobi angles for simultaneous diagonalization. SIAM J. Matrix Anal. Appl. 17 , 161-164.

Speck, O., Hennig, J., Zaitsev, M., 2006. Prospective real-time slice-by-slice motion correction for fMRI in freely moving subjects. MAGMA 19( 2), 55-61.

Srivastava, G., Crottaz-Herbette, S., Lau, K.M., Glover, G.H., Menon, V., 2005. ICA-based procedures for removing ballistocardiogram artifacts from EEG data acquired in the MRI scanner. NeuroImage 24 (1), 50– 60.

Tong, S., Bezerianos, A., Paul, J., Zhu, Y., Thakor, N., 2001. Removal of ECG interference from the EEG recordings in small animals using independent component analysis. J. Neuroscience Methods 108 (1), 11-17.

Vincent, J.L., Larson-Prior, L.J., Zempel, J.M., Snyder, A.Z., 2007. Moving GLM ballistocardiogram artifact reduction for EEG acquired simultaneously with fMRI. Clinical Neurophysiology 118, 981-998.

Warach, S., Ives, J.R., Schlaug, G., Patel, m.D., Darby, D.G., Thangaraj, V., Edelman, R. R., and Schomer, D. L., 1996. EEG-triggered echo-planar functional MRI in epilepsy. Neurology 47, 89-93.

Wan, X., Iwata, K., Riera, J., Ozaki, T., Kitamura, M., Kawashima, R., 2006a. Artifact reduction for EEG/fMRI recording: Nonlinear reduction of ballistocardiogram artifacts. Clinical Neurophysiology 117 (3), 668–680.

Wan, X., Iwata, K., Riera, J., Kitamura, M., and Kawashima, R., 2006b. Artifact reduction for simultaneous EEG/fMRI recording: Adaptive FIR reduction of imaging artifacts. Clinical Neurophysiology 117 (3), 681–692.

Welch, P.D., 1967. The use of fast Fourier transform for the estimation of power spectra: a method based on time averaging over short, modified periodograms. IEEE Trans. Audio Electroac. AU 15, 70–73.

Zschocke, S., 2002. Klinische Elektroenzephalographie. Springer.